Study of Water Dynamics in the Soil-Plant-Atmospheric Continuum in a Water-Controlled Ecosystem

by

Xingyuan Chen

B.ENG. (Tsinghua University, Beijing, China) 2000
M.Phil. (Hong Kong University of Science and Technology) 2002
M.A. (University of California, Berkeley) 2007

A dissertation submitted in partial satisfaction of the
requirements for the degree of
Doctor of Philosophy

in

Engineering-Civil and Environmental Engineering

in the

GRADUATE DIVISION
of the
UNIVERSITY of CALIFORNIA at BERKELEY

Committee in charge:

Professor Yoram Rubin, Co-Chair
Professor Dennis D. Baldocchi, Co-Chair
Professor Mark Stacy
Professor David Brillinger

Spring 2009

The dissertation of Xingyuan Chen is approved:

Co-Chair Date

Co-Chair Date

Date

Date

University of California at Berkeley

Spring 2009

Study of Water Dynamics in the Soil-Plant-Atmospheric Continuum in a Water-Controlled Ecosystem

by

Xingyuan Chen

Abstract

Study of Water Dynamics in the Soil-Plant-Atmospheric Continuum in a Water-Controlled Ecosystem

by

Xingyuan Chen

Doctor of Philosophy in Engineering-Civil and Environmental Engineering

University of California at Berkeley

Professor Yoram Rubin, Co-Chair

Professor Dennis D. Baldocchi, Co-Chair

The study of water exchange between soil, plants, and the atmosphere in response to seasonal or periodic droughts is critical to modeling the hydrologic cycle and biogeochemical processes in water-controlled ecosystems. This dissertation consists of four essential parts of water dynamics studies in an oak Savanna ecosystem.

The first study characterizes changes in evaporation and transpiration under water stress. The influence of soil moisture on evapotranspiration at the stand scale is studied using correlations between tower-based evapotranspiration measurements and representative soil moisture obtained by aggregating point measurements. The observed pattern of this effect is found in agreement with an existing model that features a linear reduction of the evap-

otranspiration when soil moisture falls below a critical value. The model parameters are inferred using a Bayesian framework and they are found to vary from year to year due to climate variability. The comparison between various aggregations of soil moisture at the stand scale from point measurements demonstrates that the spatial variability of the soil moisture as well as the water uptake capacity limited by the root biomass need be taken into account to produce a model that is most resistant to inter-annual variability.

The second study re-evaluated the theoretical basis of sap flow measurements using heat ratio method, whose fundamental basis was built on an idealized solution to heat transport process in sapwood. An improved solution is developed to model the same process with more realistic assumptions. Extensive comparisons on the difference of calculated temperature fields by idealized solution and improved solution reveal that most significant discrepancy occurs around the early times, whereas the difference diminishes over late time window. This study also present changes in the fundamental equation of heat ratio method to account for asymmetric probe alignments in practice.

The third study is on determining probe geometry and wood thermal diffusivity for sap flow measurements using heat ratio method. A statistical framework is presented to simultaneously estimate wood thermal diffusivity and probe geometry from in-situ heat response curves collected by the implanted probes of heat ratio apparatus. Conditioned on the heat response data, the parameters are inferred using a Bayesian inversion technique with Markov chain Monte Carlo (MCMC) sampling method. This procedure not only provides a systematic yet non-destructive to estimate the crucial parameters for sap flow calculation,

it also enables direct quantification of uncertainty in estimated sap flow velocity. Experiments using synthetic data show that multiple tests on the same apparatus are essential to obtain reliable and accurate solutions, and the uncertainty in posterior distributions of the parameters is influenced by the prior knowledge on the probe geometry or heating power. When applied to field conditions, multiple tests are conducted during different seasons and automated using the existing data logging system. The seasonality of wood thermal diffusivity is obtained as a by-product of the parameter estimation process, and it is affected by both moisture content and temperature. Empirical factors are introduced to account for the influence of non-ideal probe geometry on the estimation of heat pulse velocity, and they are estimated in this study as well. The proposed methodology is ready to be applied to calibrate existing heat ratio sap flow systems at other sites. It is especially useful when alternative transpiration calibration device such as lysimeter is not available.

The fourth study investigated how an individual plant adjusts transpiration under the stressed conditions using continuous transpiration and soil moisture measurements. The objective is to appropriately calculate the potential transpiration, which is often needed in soil water dynamics models. The alternating conditional expectation (ACE) method is implemented to identify the optimal functional dependence of bulk canopy conductance on various environmental stresses including vapor pressure deficit, net radiation, and soil moisture. A multiplicative form of stress functions is found to be appropriate for the tree studied. The functional form of each individual stress is determined based on the optimal transformations identified by the ACE method, and MCMC is then implemented to estimate

the model parameters. The continuous transpiration and soil moisture data are also used to investigate the water budget on the tree over the growing season of 2007. It is found that tree transpires much more water than what is provided by the root zone soil water during dry season, which is a strong evidence of tree tapping water from deeper soil and groundwater in dry seasons. This factor need be accounted for in further soil dynamics modeling by specifying appropriate boundary conditions.

Professor Yoram Rubin
Dissertation Committee Co-Chair

Professor Dennis D. Baldocchi
Dissertation Committee Co-Chair

To my family

and

In memory of Jianzhong Guo

Contents

List of Figures

List of Tables

Acknowledgements

First and foremost, I wish to express my sincere gratitude to my advisors, Professor Yoram Rubin and Professor Dennis D. Baldocchi. They not only introduced me to the field of ecohydrology, but also have provided me with continuous guidance and encouragement. I have benefitted enormously from their expertise and enthusiasm in their distinctive fields. The discussions with them during my PHD study have inspired many great ideas, based on which I was able to win the Horton Research Grant from the American Geophysical Union to conduct field works. They have been providing invaluable feedbacks and assistances to my research and dissertation writing in time. I also thank them for always pushing me to think deep about why we are doing the work and to set clear goals. Without their support and encouragement, this dissertation would not have existed.

I would also like to thank Professor Mark Stacy and Professor David Brillinger for being on my dissertation committee. They have given me many valuable comments and constructive suggestions during our communications.

I would like to thank Ted Hehn for his numerous help on manufacturing sap flow probes and setting up the experiments in field. I also thank Mr. Russell Tonzi for providing access to his ranch for scientific research.

My thanks are due to all my colleagues, Zhangshuan Hou, Felipe Barrows, Gretchen R. Miller, Siyan Ma, Qi Chen, Jessica Osuna, and Youngryel Ryu, for their help and collaboration in data collection, and for many inspiring discussions.

I am deeply indebted to my dear friends over the years, Jianzhong He, Lili Ji, Shaonan

Wu, Qing Ji, Ran Ding, Yang Feng, Maoyi Huang, Gang Wang, Dengfeng Sun, Qingfang Wu, Peihua Jing, and many others. My PHD journey at Cal has been more enjoyable with their companion.

A special ”Thank you” belongs to my late friend, Jianzhong Guo. He was always there when I needed help, just like a big brother, even when he was fighting against cancer. His friendship and courage is my life-long treasure. Although he didn't see me finish my PHD study, I know he would feel happy for me.

Last but not least, I am deeply grateful to my family for their endless love and unconditional support. It is them who made me the person who I am today and I would like to dedicate my dissertation work to them.

Chapter 1

Introduction

1.1 Problem Overview

In water-limited ecosystems, root zone soil water availability becomes a controlling factor on water, carbon and nutrient cycles [*Rodriguez-Iturbe et al.*, 2001b; *Williams and Albertson*, 2004], and they are thus called water-controlled ecosystems. The study of water dynamics in such ecosystems is not only critical for global hydrological cycle and climate modeling, but also for assessing ecosystem functioning in response to seasonal or periodic droughts [*Knapp et al.*, 2002; *Porporato et al.*, 2004]. Such study is increasingly becoming more important as recent climate studies suggest that periodic droughts are likely to occur more frequently, due to reduced rainfall frequency resulting from global warming [*Bell et al.*, 2004; *Esterling et al.*, 2000]. In western America, the threat of droughts could be even worse due to loss of mountain snowpack in projected future climate [*Service*, 2004].

Study of water dynamics in water-controlled ecosystems requires an integrated approach that links biometeorology, biophysics, plant physiology and hydrology. The difficulties in such studies arise from insufficient understanding of the nonlinear interactions between the various processes and their scale-dependence, and from ignoring multi-scale interactions. Systematic multi-scale studies of water exchange in the soil-plant-atmospheric continuum are still at very early stages, and require coordinated efforts of modeling development and data acquisition at consistent scales [*National Research Council (NRC)*, 2008]. New technology innovations from nano-materials to airborne and spaceborne remote sensing sensors has made more variables accessible to measurements over a large range of temporal-spatial scales [*National Research Council (NRC)*, 2008]. Furthermore, the emerging monitoring networks, such as FLUXNET [*Baldocchi et al.*, 2001], have provided unique platforms for long-term multidisciplinary multi-scale study.

The purpose of this dissertation work is to develop a better understanding of water transport in the soil-plant-atmospheric continuum under drought conditions, at scales ranging from that of a plant (a few m^2) to that of a stand (a few hundreds to a few thousands m^2). The primary focus is to investigate the regulation of plant water use by water deficits and climatic conditions and its scale dependence. Models of water stress function are examined and calibrated at both plant scale and stand scale using water exchange data acquired at both scales.

The data necessary for model calibration include the spatial and temporal measurements of soil water content and water fluxes throughout the soil-plant-atmospheric continuum, as

well as climate driving forces such as net radiation, humidity and air temperature, etc. The data acquisition efforts will focus on a Mediterranean oak-savanna ecosystem, and it will be introduced in details in the next section. The site experiences dry and hot summer annually, which makes it ideal for water dynamics study in water-controlled ecosystems.

Data have been collected at the site since 2001, including meteorological variables (e.g., solar radiation, air temperature, wind speed, etc), biophysical variables (e.g., leaf area index, leaf water potential, etc), soil moisture contents, isotopes in water and CO_2 sources, as well as overstory and understory eddy fluxes of water vapor and CO_2. In addition to this on-going effort, and in support of my research goals at individual plant scale, plant-scale measurements were installed in eight trees across the footprint of the overstory eddy covariance tower. The specific measurements on an individual tree include multiple soil moisture probes to monitor soil moisture profile vertically and laterally, soil temperature probes for the purpose of energy balance and soil respiration calculations, and sap flow sensors at different tree heights for measuring tree transpiration. More detailed descriptions on the data collection activity are available in individual chapters that utilize specific data.

While the water vapor fluxes measured by the eddy covariance tower provides an estimation of water used by all the trees within the tower footprint, individual plant water use is directly measured with sap flow sensors using heat-pulse technique. The heat pulse technique uses a heat pulse as tracer and deduce the travel speed of water in porous media through the speed at which heat is transported. The heat pulse technique is known to possess advantages of low power consumption, simple instrumentation and automated data

collection [*Green et al.*, 2003]. Among all the variations of the heat pulse technique, the heat ratio method (HRM) introduced by *Burgess et al.* [1998] is chosen in this study due to its capability of detecting reverse and low flow rates and its straightforward instrumentation [*Burgess et al.*, 2001].

The theoretical basis underlying HRM is an analytical solution to the heat transport equation in tree sapwood derived by *Marshall* [1958]. The solution, however, was relied on several idealized assumptions, which are routinely violated in real applications of HRM. Therefore, an improved solution is developed to describe the heat transport process in sapwood with more realistic assumptions and modifications to the original fundamental equation of HRM is provided to account for the departure of field experimental setup from the ideal setup.

Furthermore, the successful application of HRM depends on obtaining reliable estimation of sapwood thermal diffusivity and probe geometry. The empirical estimation of wood thermal diffusivity requires information on wood moisture content and wood bulk density, which are usually obtained through intrusive core sampling. Exact spacing and geometry of the HRM apparatus cannot be guaranteed during installation due to the nature of the wood matrix, especially in hardwood species such as oak and maple. To assure the quality of the sap flow measurements acquired from the experimental site, this dissertation study also provides a systematic, non-destructive, and replicable methodology to determine wood thermal diffusivity and probe geometry for the sap flow measurements using the heat ratio apparatus. The estimation of these parameters is conditioned on the time series of tem-

perature increases, i.e., temperature response curves, monitored by the downstream and upstream temperature probes after a heat pulse is released by the central heating probe. The primary advantage of the methodology is that it relies on the information that can be obtained using the installed probes without any further disturbance to the tree.

The availability of new observations can improve our understanding of the complex mechanisms related to water dynamics and thus enables newer model development. On the other hand, it provides valuable information to model calibration. Successful model calibration based on appropriate field data through inverse modeling may prove to be an effective tool in studies of plant water uptake [*Hopmans and Bristow*, 2002; *Green et al.*, 2006]. One challenge in model calibration is to deal with uncertainties arising from various sources. A Bayesian approach is often chosen in model calibration for its strengths in dealing with uncertainties arising from various sources and in introducing assumptions and prior knowledge of the parameters through prior distributions. Another unique advantage of Bayesian approach is the availability of many powerful inference techniques [*Gelman et al.*, 1995], such as Markov chain Monte Carlo (MCMC) method, which are not available to traditional statistical approaches. The Bayesian framework with MCMC sampling methods have been successfully implemented in many areas of studies [*Clark*, 2005; *Clark and Gelfand*, 2006; *Crainiceanu et al.*, 2003; *Reis and Stedinger*, 2005; *Smith and Marshall*, 2008]. Therefore, it is adopted for model calibration in this dissertation.

1.2 Experimental Site Information

All the field experiments involved in this dissertation were conducted at Tonzi Ranch, which is an active FLUXNET site located on the lower foothill of the Sierra Nevada Mountains (see Figure 1.1), near Ione, California (latitude: 38.4311°N; longitude: 120.966°W; altitude: 177 m). The site is an oak savanna woodland with scatterings of grey pine trees. According to the meteorological records, the mean air temperature of the region is 16.6°C and the mean annual precipitation is about 559mm, most of which occurs between October and May [*Baldocchi et al.*, 2004; *Ma et al.*, 2007]. The uneven seasonal distribution of precipitation leads to a wet and cold winter and a dry and hot summer at the study site.

The ecosystem at the site is comprised of a nonuniform distribution of trees and grasses. The oak trees covers approximately 43% of the land at a scale up to 1km$\times$1km around the tall tower [*Kim et al.*, 2006] based on a high-resolution IKONOS image as shown in Figure 1.2. A recent study based on LIDAR data finds the canopy coverage to be 47% within a 200m$\times$200m area around the tower and the oak trees have heights of 9.3 ± 4.3 meters [*Chen et al.*, 2008a]. The oak trees leaf out in the spring (around day 90) and rapidly reach full photosynthetic potential until they senesce in the late autumn [*Xu and Baldocchi*, 2003]. The grasses, on the other hand, are active from late autumn to early summer and senesce when soil water is depleted during the prolonged dry summer. The trees and grasses are out of phase in their growing seasons with only a short overlap from April to early June. Their different life cycles reflect various mechanisms to survive through seasonal droughts in co-existing vegetation types.

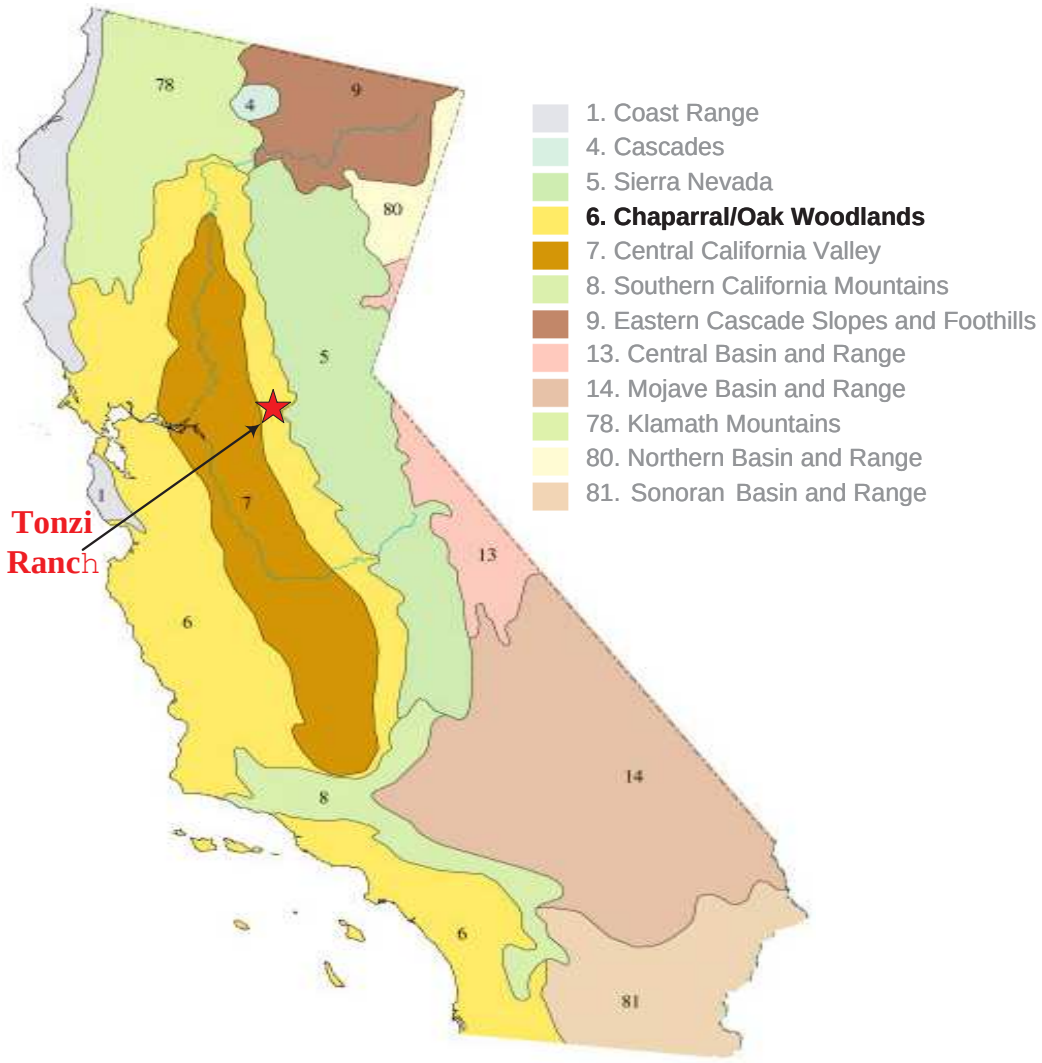

Figure 1.1: Location of experimental site overlaid on the California ecoregions map (USEPA, 2000)

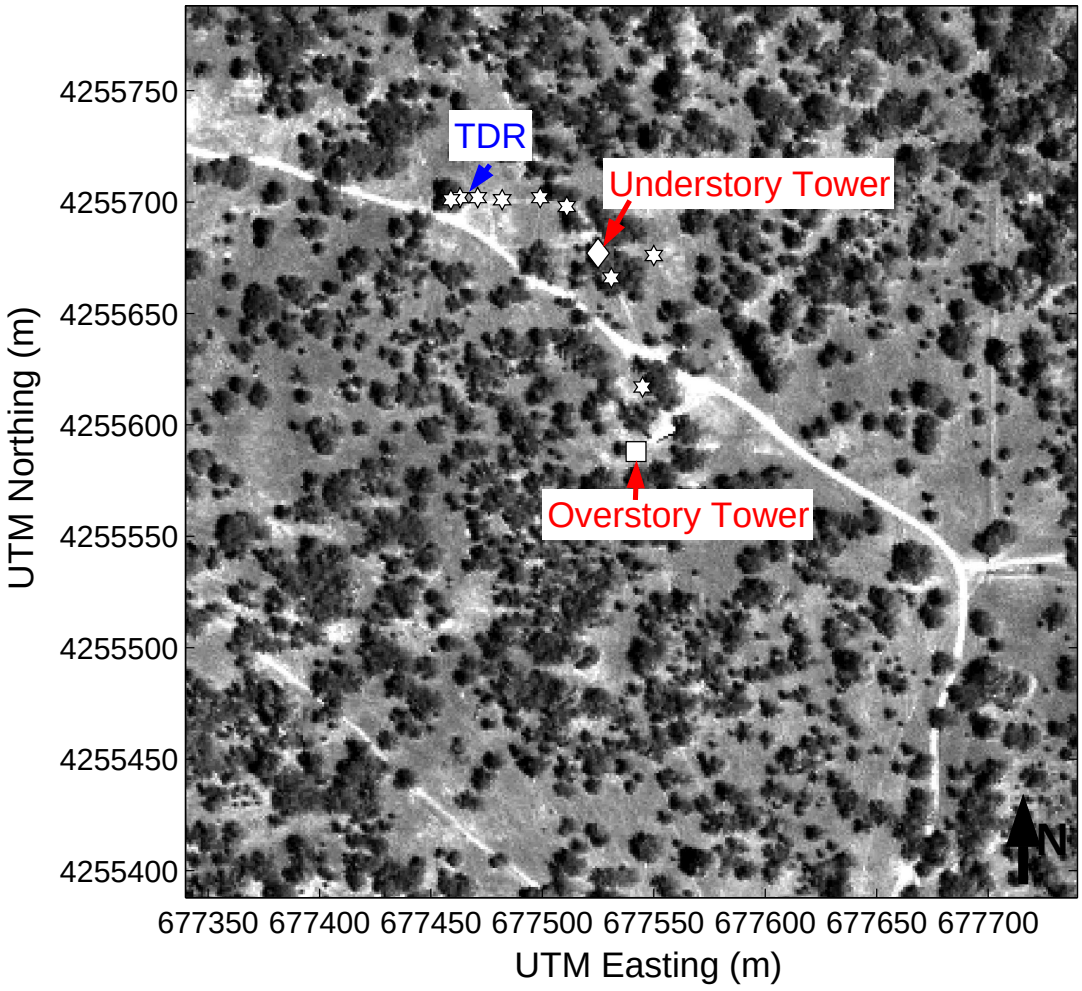

Figure 1.2: Schematic of TDR locations overlaid on IKONOS panchromatic imagery with 1m resolution

The soil at Tonzi is an Auburn very rocky silt loam [*Sketchley*, 1965]. Our survey at 49 locations over a 200 m $\times$ 200 m area found that the soil is composed of 49 *pm* 3% sand, 36 $\pm$ 2% silt and 15 $\pm$ 1% clay (soil samples analyzed at the Division of Agriculture and Natural Resources Analytical Soils Laboratory, University of California-Davis). Well logs reveal that the soil layer is about 1.0 m thick and is overlaid on fractured greenstone bedrock.

1.3 Chapter Organization

This dissertation is organized in the following way: Chapter 2 presents observations and stochastic modeling of soil moisture control on evapotranspiration in the experimental site. This study uses data collected at stand scale and discusses the controlling role of soil moisture on evapotranspiration from trees, grasses and the entire community. Chapter 3 revisits the theoretical basis of sap flow measurements using HRM and revises the fundamental equation of HRM to account for departure of field conditions from idealized ones. Chapter 4 presents a statistical technique to estimate key parameters for estimating tree transpiration from the sap flow measurements. This study is conditioned on time series data of temperature rise responding to a heat pulse. Chapter 5 studies response of whole-plant transpiration to soil and atmospheric water deficit using data collected on an individual tree. A summary is provided in Chapter 6.

Chapter 2

Observations and Stochastic Modeling of Soil Moisture Control on Evapotranspiration in a Californian Oak Savanna

[1]

[1]This chapter is based on a published article in *Water Resources Research*, Vol 44, W08409, doi: 10.1029/2007WR006646

2.1 Introduction

Oak savanna ecosystems in California are subject to soil water stress during the prolonged dry summer seasons. In such water-limited ecosystems, root zone soil water availability becomes a controlling factor on water, carbon and nutrient cycles [*Rodriguez-Iturbe et al.*, 2001b; *Williams and Albertson*, 2004]. Therefore, characterization of changes in evaporation and transpiration under water stress is essential to understand the dynamics in the soil-plant-atmosphere continuum [*Feddes et al.*, 2001; *Feddes and Raats*, 2004; *Teuling et al.*, 2006]. Eventually these processes will contribute to the studies of the hydrological cycle including the computation of water budgets [*Milly*, 1993; *Botter et al.*, 2007] and to the studies of biogeochemical processes in similar ecosystems [*Porporato et al.*, 2003; *D'Odorico et al.*, 2003].

The impacts of soil water stress on water and carbon exchange processes have been studied experimentally and have been incorporated into various modeling efforts [*Baldocchi et al.*, 2004; *Dewar*, 2002; *Feddes et al.*, 1978; *Katul et al.*, 2003"; *Rodriguez-Iturbe et al.*, 2001b; *Tuzet et al.*, 2003; *Williams and Albertson*, 2004, 2005]. A piecewise linear function of the dependence of evaporation and transpiration (ET) on soil moisture, shown in Figure 2.1, is especially appealing for its simplicity and its applicability in a range of plant functional types at leaf and stand scales [*Feddes et al.*, 1978; *Federer*, 1979; *Gollan et al.*, 1985; *Paruelo and Sala*, 1995; *Spittlehouse and Black*, 1981]. This model will be referred to as Feddes Model in the subsequent discussion. The Feddes Model has been adopted in many studies as an *a priori* assumption with the parameters selected from literature

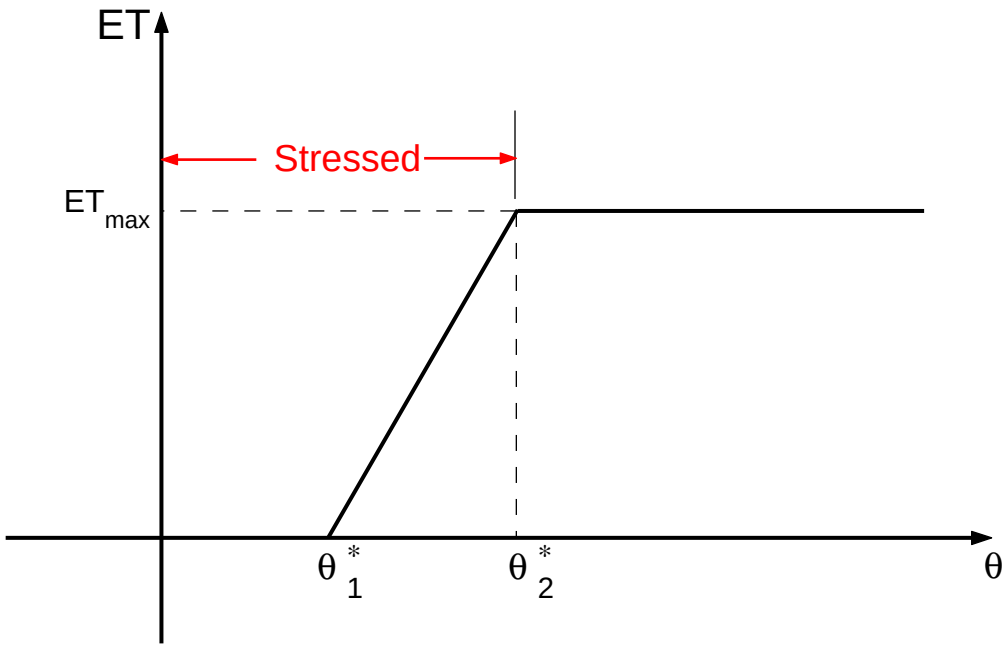

Figure 2.1: Regulation of soil moisture on ET (After *Feddes*, 1978; *Laio et al.*, 2001)

[*Guswa et al.*, 2002; *Laio et al.*, 2001; *Miller et al.*, 2007] due to the lack of concomitant observations of ET and soil moisture at matching scales.

Although the Feddes Model has been found efficient in many cases, the actual ET behavior could be different and more complex [*Lagergren and Lindroth*, 2002] due to the non-linear interactions between the soil, plants and the atmosphere and their scale-dependence. This behavior is further complicated in savannas by the coexistence of woody and herbaceous species, by their open heterogeneous canopies and their competition for the limited water resources [*Scholes and Archer*, 1997]. All these are elements which are not in line with the underlying assumptions of the Feddes Model.

There is only a limited body of research on the effects of soil moisture on ET in sa-

vannas [*Detto et al.*, 2006; *Williams and Albertson*, 2004]. Therefore, the objective of our study is to examine experimentally the applicability of the Feddes Model in a Californian oak savanna for modeling the effect of water stress on ET of single functional types and of their mixture at the stand scale, and to gain, through this investigation, a broader perspective on the myriad of related issues. Specific questions that we will address include: (1) Is the Feddes Model applicable to oak savannas with heterogeneous open canopies? This is an important question in the context of modeling water dynamics in savanna ecosystems because ET is a crucial component in water cycling and its change under water stress needs be taken into account in modeling; (2) How do trees and grasses in the oak savanna respond differently to the water stress? Heterogeneity in soil moisture in savanna is both cause and consequence of tree-grass coexistence [*Rodriguez-Iturbe*, 2000]. To capture the effects of soil moisture's spatial variability in water dynamics modeling, it is essential to investigate how trees and grasses, as individual functional types, use water under seasonal droughts; (3) Is the Feddes Model stationary in time? This is an important issue when the model characterizing soil moisture's control on ET is to be used in water dynamics modeling, because large inter-annual variability of parameters would deteriorate the predictive capabilities of models validated using historic records of undetermined duration. This specific study has not been possible until recently, when multi-year data from the FLUXNET sites became available; (4) What soil moisture data is needed for modeling water stress at the stand scale and what are the alternatives for aggregating point measurements of soil moisture to the spatial averages at the stand scale? The answer to this question will be useful for guiding

the acquisition of soil moisture field data needed for model validation and prediction.

To address these questions, the observed actual ET from eddy covariance towers will be evaluated as a function of soil moisture and potential ET. The partition of ET between woody and herbaceous species is allowed through the deployment of overstory and understory eddy flux towers. A Bayesian framework with Markov chain Monte Carlo (MCMC) method that has been applied successfully in many fields [*Clark*, 2005; *Clark and Gelfand*, 2006; *Crainiceanu et al.*, 2003; *Reis and Stedinger*, 2005] is adopted to parameterize the model that describes controlling effect of soil moisture on ET, taking into account the uncertainties in model parameters and in field measurements. The inter-annual variability in the dependence of ET on soil moisture for heterogeneous environment as well as its components is analyzed using multi-year data. The parameterized model is used for predicting the actual ET with uncertainty estimates determined using the joint distribution of the parameters derived from the Bayesian framework.

2.2 Data Acquisition

A broad suite of data types have been collected at the Tonzi Ranch since 2001, including meteorological variables (e.g., solar radiation, air temperature, wind speed, precipitation, etc), biophysical variables (e.g., leaf area index, leaf water potential, etc), soil moisture, as well as overstory and understory eddy fluxes of water vapor and CO_2 [*Baldocchi et al.*, 2004; *Xu and Baldocchi*, 2003]. The meteorological variables are needed for estimating

reference ET assuming sufficient water supply, which is called potential ET. The eddy covariance measurements of water vapor flux were taken through a 23m-high overstory tower and are viewed as representing the ET from the mixture of trees and grasses within its 300m$\times$300m fetch. In addition, eddy covariance measurements from a 2m-high understory tower were also taken, and are viewed as representing the ET from the understory grasses and soil surface. The difference in water vapor fluxes between the overstory and understory towers is a measure of transpiration by trees. All the measurements by the two towers were averaged at half an hour basis.

Soil moisture at the site has been monitored using both segmented time-domain reflectometry (TDR) probes (Moisture Point, model 917, Environmental Sensors, Inc., Victoria, British Columbia) and Theta probes (Delta-T Devices, model ML2-X, Cambridge, UK). These technologies are described in detail in *Blonquist et al.* [2005]. The TDR probes were installed at nine locations as shown in Figure 1.2, and each probe measures the average volumetric soil water content at depths between 0-15, 15-30, 30-45 and 45-60cm. Among the nine TDR probes, five were installed under tree canopies and four in the open spaces. TDR measurements were taken weekly or bi-weekly during field visits. Theta probes were installed under a tree near the tall eddy flux tower at depths of 5, 20 and 50cm, and continuous soil moisture measurements were taken at half-hour interval.

2.3 Theoretical Background

To describe the degree to which the actual ET in the ecosystem is limited by soil water availability, ET measured by the eddy covariance tower is compared to a reference ET under sufficient water supply, i.e., potential ET. The latter is approximated by the Priestley-Taylor (P-T) equation [*Priestley and Taylor*, 1972] as shown in the following equation,

$$E_p = \beta \cdot E_{eq} = \beta \cdot \frac{1}{\lambda} \frac{s(R_n - G)}{s + \gamma}, \tag{2.1}$$

where E_p is the potential ET, E_{eq} is the equilibrium ET, β is a scaling factor that depends on vegetation type and climatic conditions, R_n is the net radiation, G is the ground heat flux density, λ is the latent heat of vaporization of water, s is the derivative of the saturated vapor pressure against temperature and γ is the psychrometric constant.

The actual ET is assumed to be a fraction of the potential ET due to water deficit [*de Bruin*, 1983; *Laio et al.*, 2001; *Mahfouf et al.*, 1996; *Rana and Katerji*, 2000; *Williams and Albertson*, 2004], i.e.,

$$E_{act} = \alpha(\theta) \cdot E_p, \tag{2.2}$$

where $\alpha(\theta)$ is the reduction coefficient of ET as a function of soil moisture. The form of $\alpha(\theta)$ is not assumed as prior knowledge but will be examined and compared to the Feddes

Model using field data in our study. The analytical form of the Feddes Model is

$$\alpha(\theta) = min\left\{1, max\left\{0, \frac{\theta - \theta_1^*}{\theta_2^* - \theta_1^*}\right\}\right\} \tag{2.3}$$

where θ_1^* is normally referred to as permanent wilting point at which plants stop ET and θ_2^* is the critical soil moisture value below which ET is limited by available soil moisture.

The P-T coefficient, β of Eq. (2.1), is not directly measurable. The value of β is often taken as 1.26 for a wet surface [*Priestley and Taylor*, 1972]. However, the actual value could deviate significantly from 1.26 depending on the canopy structures and atmospheric conditions [*Baldocchi and Meyers*, 1998; *de Bruin and Keijman*, 1979; *Hikaru*, 2005; *Jones*, 1992; *McNaughton and Spriggs*, 1986]. Therefore, β is considered as an unknown constant in our study, and the form of $\alpha(\theta)$ will be evaluated through a surrogate variable, the ratio between the actual ET and the equilibrium ET, defined as

$$R(\theta) = \frac{E_{act}}{E_{eq}} = \alpha(\theta)\beta. \tag{2.4}$$

$R(\theta)$ is clearly a rescaled form of $\alpha(\theta)$ with β being the value of $R(\theta)$ under no soil water stress. All the variables required to determine $R(\theta)$ are directly measured by the eddy covariance towers. It is thus natural to extract the form of $\alpha(\theta)$ from the observations of $R(\theta)$.

To examine the form of $\alpha(\theta)$, it is also necessary to determine whether a representative

soil moisture exists at the stand scale that can be used for a stand-scale Feddes Model, and to estimate it from point measurements. The details are discussed in next section.

Once the general form of $\alpha(\theta)$ is determined from observations, the next step is to identify the model parameters. In most studies, the parameters that describe the effect of soil moisture on ET are viewed as deterministic values, although in most cases they are adopted from the past work on similar ecosystems or derived from limited field data. Uncertainties could arise from many sources in addition to their inherent variability, such as measurement errors, model errors from incomplete understanding of the underlying mechanism, and disparity in measurement scales and modeling scales. A probabilistic approach based on Bayesian concepts is adopted in this study to learn model parameters considering various uncertainties. A detailed description of the method can be found in the Appendix A.

2.4 Results and Discussions

2.4.1 Micrometeorological Observations and Soil Moisture

The data acquired between 2003 and 2005 were employed in this study. The first three plots in Figure 2.2 present time series of averaged daytime (8am-6pm) available energy ($R_n - G$), air temperature, relative humidity and daily precipitation, all of which show strong seasonal patterns. The summer is characterized by high temperature and available energy, low humidity with essentially no precipitation.

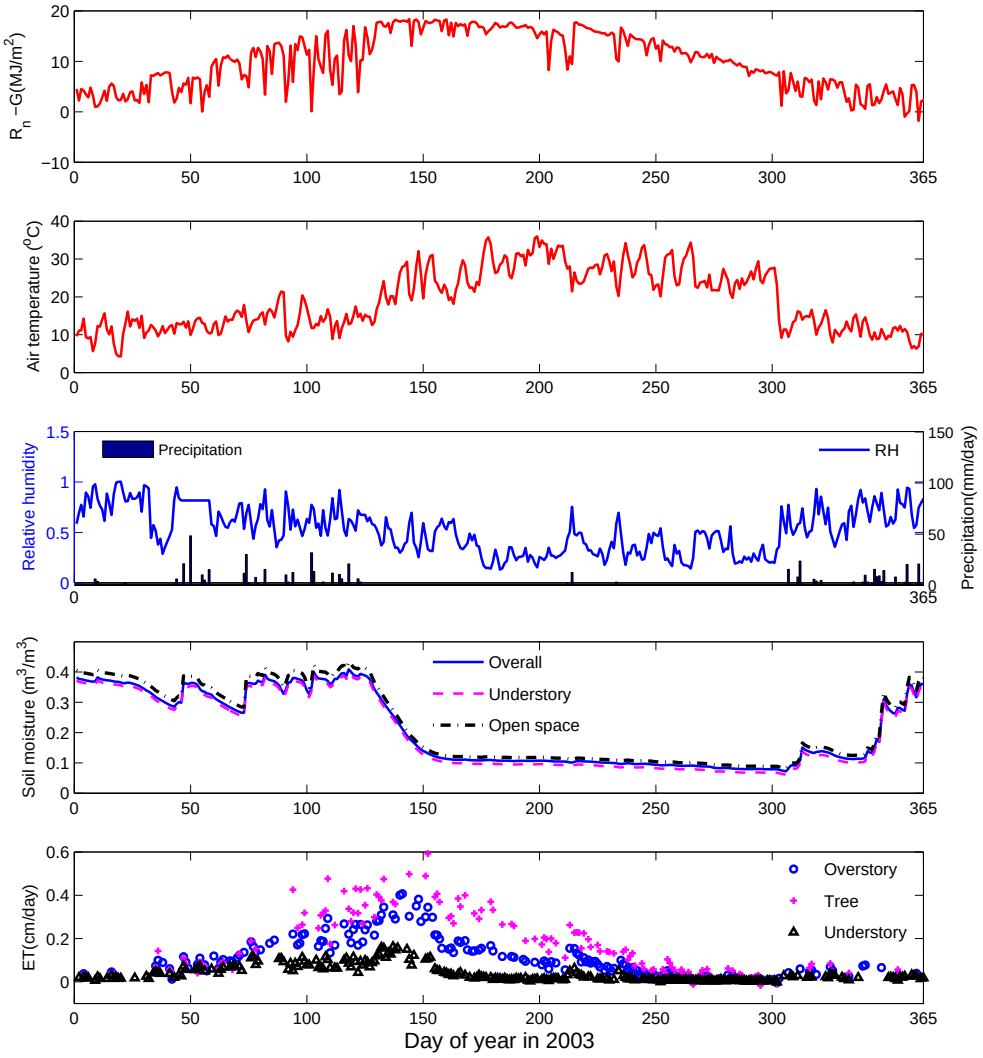

Figure 2.2: Meteorological conditions, soil moisture and measured ET at the Tonzi site. The plots from top to bottom are daytime available energy, daytime air temperature, daytime relative humidity and daily precipitation, depth-averaged soil moisture (the series labeled as overall is the averaged measurements by all TDR probes), and measured evapotranspiration

Two types of soil moisture data are available at the site: periodic TDR measurements distributed within the footprint of eddy covariance tower and continuous Theta probe measurements at a point. Recognizing their difference in temporal and spatial resolutions, the spatial averages of TDR measurements in a depth segment were regressed on the daily averages of the Theta probe measurements within the same depth range, using a robust linear approach. The resulting regression lines as shown in Figure 2.3 were used to interpolate the periodic TDR measurements to continuous ones. More regression results for years from 2003 to 2005 can be found in Appendix B. The interpolation was carried out independently for spatial averages of all TDR measurements, for those of measurements taken under tree canopies and for those taken in the open spaces. The overall averages of soil moisture measurements represent the soil water available to the entire ecosystem, while the averaged soil moisture under tree canopies and those in the open spaces are considered as the soil water available to trees and grasses, respectively. Although some tree rooting systems tend to extend beyond the edges of canopy [*Casper et al.*, 2003] and can deplete water from the intercanopy areas [*Lefever and Lejeune*, 1997; *Yokozawa et al.*, 1998; *Lejeune et al.*, 1999; *Rietkerk et al.*, 2004], there does not seem to be extensive lateral exploration of roots beyond the canopy edge at our site based on the soil respiration study [*Tang and Baldocchi*, 2005]. The soil moisture measurements at different depths for the entire area, understory area and open spaces from 2003 to 2005 are averaged vertically and are given in the third plot of Figure 2.2, which demonstrates contrasting wet and dry conditions in winter and summer. The interpolated average soil moisture values are considered to better capture

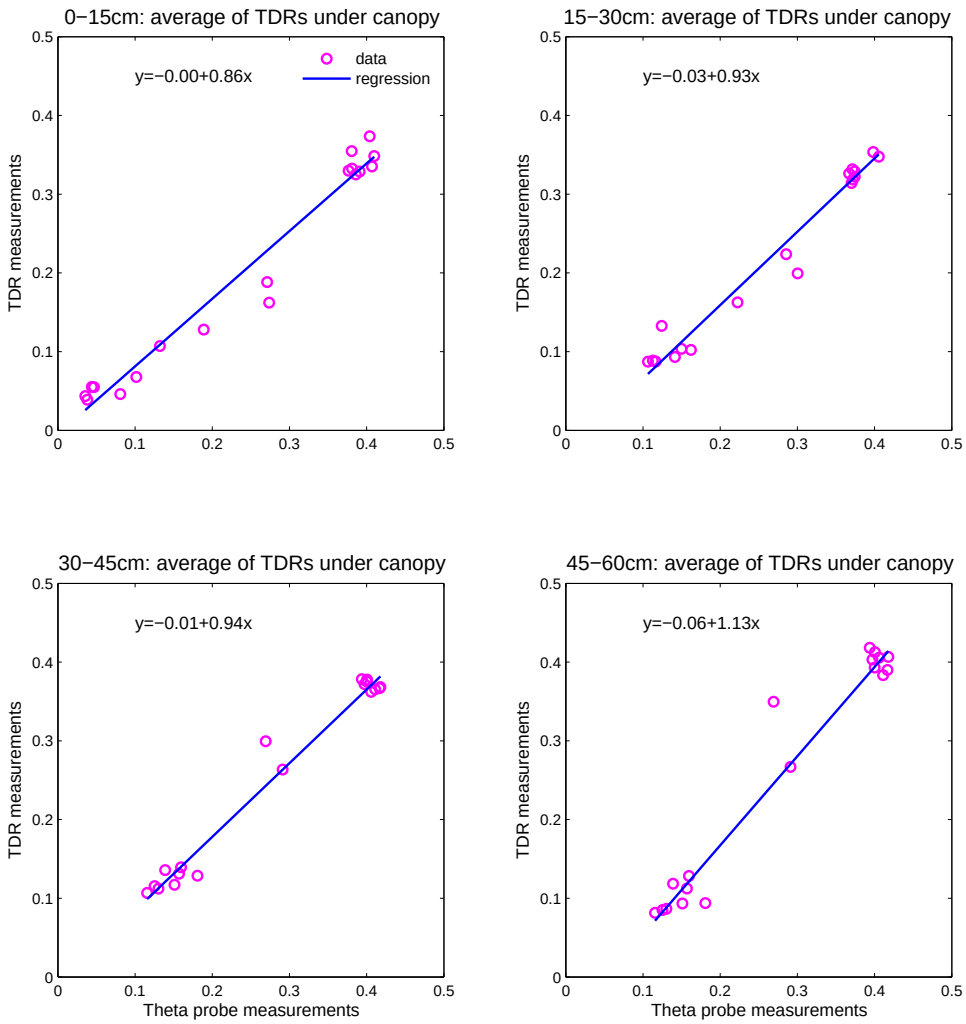

Figure 2.3: Regression of TDR measurements under canopy on the Theta probe measurements in 2005. Theta probe measurements are daily averages calculated from continuous data on half-hour basis. TDR measurements are averages calculated from TDRs located under tree canopies. The regression equations are shown along with the regression lines.

the spatial and temporal variability at the stand scale, and this will be demonstrated in the further analysis of this study.

Figure 2.2 also presents the observed ET time series for trees, the understory layer and

the overstory layer within the footprint of the overstory eddy covariance tower. The understory's ET includes ET from the grasses under tree canopies and in the open spaces, as well as evaporation from the soil surface, whereas the overstory's ET contains ET from the understory layer as well as ET from the trees. Although the fetch of the understory eddy covariance tower is smaller than that of the overstory tower [*Baldocchi*, 1997], the observations by the understory tower are assumed to be representative of the entire understory layer within the fetch of the overstory tower. The ET of trees is higher than the overstory's ET because it was calculated as the difference between the overstory's ET and understory's ET, normalized by tree canopy coverage (taken as 40%).

The plots are enlarged for 2003 in Figure 2.4 to better demonstrate their seasonal patterns within the year. The seasonality of ET is controlled by the available soil moisture, plant physiology and the atmospheric demand [*Baldocchi and Xu*, 2007]. It can be observed from Figure 2.4 that the ET from the ecosystem follows an upward trend as the atmospheric demand increases until the soil water supply can no longer meet the demand, which is the point when soil moisture starts to limit ET. The understory's ET stops earlier than the tree's ET due to the shallow root profile of grasses. The tree's ET, on the other hand, is observed to continue while the soil moisture at the top 60cm barely changes, which indicates that trees may tap deeper water sources [e.g., *Lewis and Burgy*, 1964]. We also found in Figures 2.2 and 2.4 that scattered summer rains trigger pulses in ET measured by both towers without visible change in soil moisture, which implies that summer rains are mostly intercepted by the tree or grass canopies and are evaporated to the atmosphere.

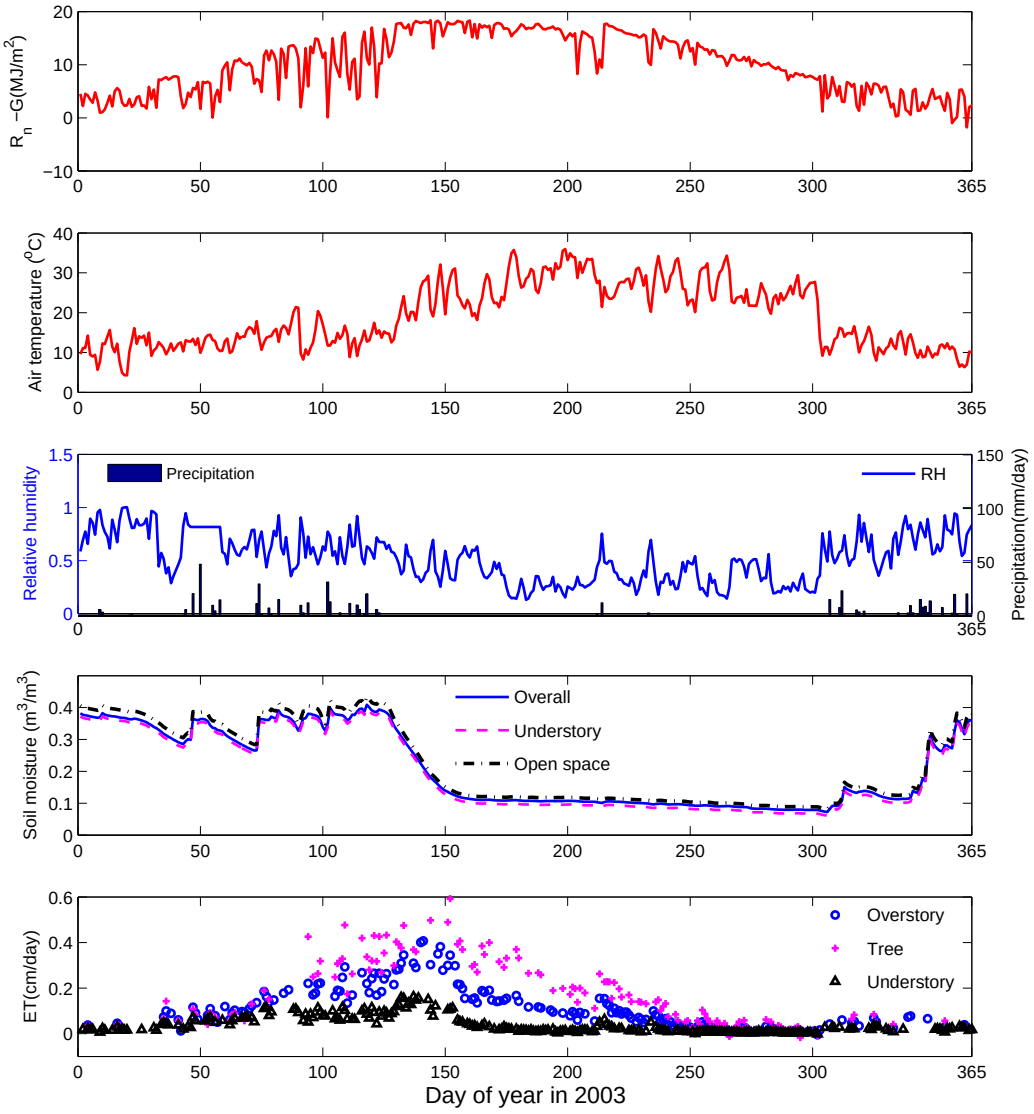

Figure 2.4: Meteorological conditions, soil moisture and measured ET at the Tonzi site in 2003. The plots from top to bottom are daytime available energy, daytime air temperature, daytime relative humidity and daily precipitation, depth-averaged soil moisture (the series labeled as overall is the averaged measurements by all TDR probes), and measured evapotranspiration

2.4.2 Soil Moisture Effects on ET

Calculated E_{act}/E_{eq}

The ratio, $R(\theta) = E_{act}/E_{eq}$, was calculated from the meteorological and ET observations following equations (2.1), (2.2) and (2.4) for the understory layer, for the overstory layer and for the trees, and the corresponding results are provided in Figure 2.5. Only daytime ratios were taken into the analysis, excluding rainy and cloudy days that are not covered by the potential ET model or by the eddy covariance technology. The small values of E_{act}/E_{eq} for the trees and for the overstory layer in winter and early spring are primarily due to the underdevelopment of tree foliage that are not taken into account in the Priestley-Taylor equation to determine the potential ET and the insufficient available energy because of the low solar radiation. Therefore, the estimation of $\alpha(\theta)$ used only the observations between the last spring rain and the first winter rain in the same year, during which soil moisture can be considered as the dominating limiting factor. These periods are highlighted in Figure 2.5 by the double arrows on top of the scatters.

Influence of representative soil moisture

Soil moisture at the site varies horizontally between canopy and inter-canopy patches as a result of the open nature of the canopy. It is recognized that trees and grasses use different amount of water under the same atmospheric condition and trees obtain moisture from deeper soil storage than grasses do. These two facts lead to the vertical heterogeneity of soil moisture in addition to its horizontal heterogeneity. To obtain a representative soil

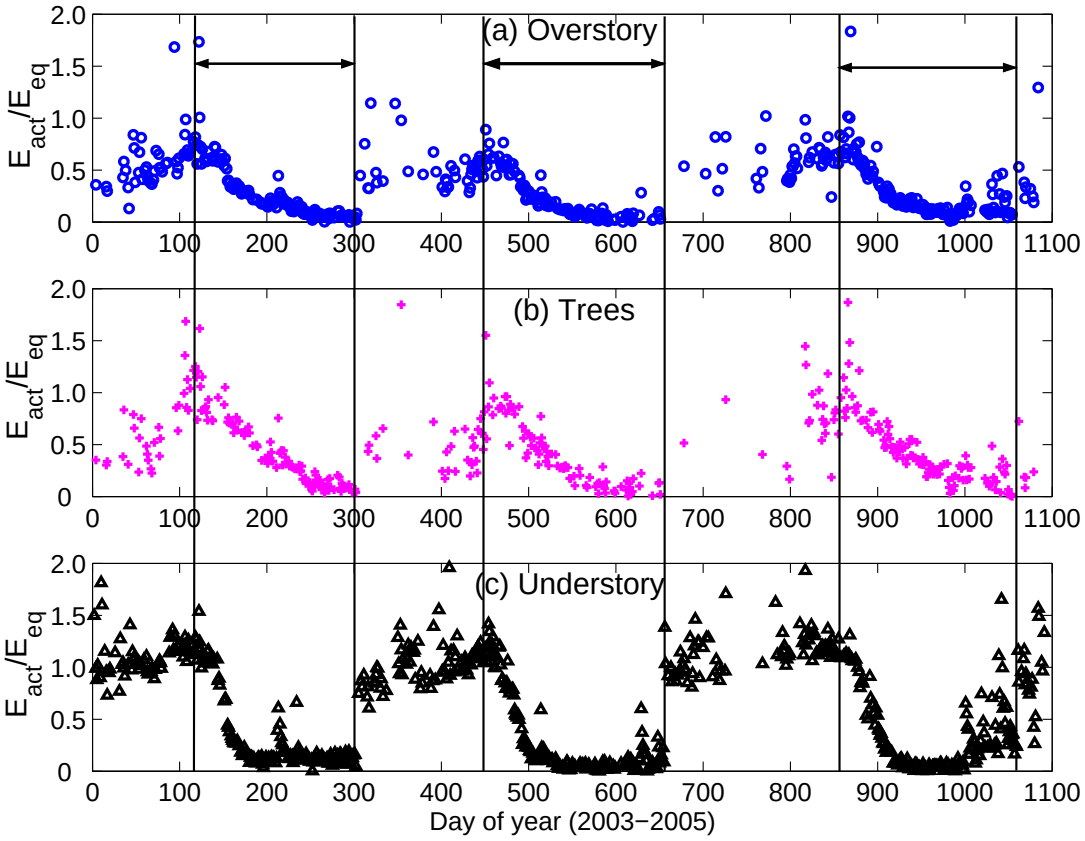

Figure 2.5: Time series plots of E_{act}/E_{eq} for (a) overstory, (b) trees and (c) understory

moisture value at the stand scale from the point measurements, the aggregation strategies in horizontal and vertical directions have impacts on accounting for contributions of point soil moisture to the overall stand-scale soil moisture. We examined in this study various averaging techniques to compute the representative soil moisture values as well as their effectiveness in describing soil moisture control on stand-scale ET.

We first assumed that only the soil moisture data measured by the Theta probes were available, and the arithmetic averages of measurements at three depths were adopted as the representative soil moisture values. The plots of E_{act}/E_{eq} against this representative soil moisture as shown in Figure 2.6 display considerable variations from year to year, yet with each year following a pattern remarkably similar to the Feddes Model. Some large values of E_{act}/E_{eq} under very dry soil moisture conditions are due to scattered summer rainfall events, which were intercepted by the tree and grass canopies and evaporated into the atmosphere soon after.

Secondly, the representative soil moisture was taken as the vertical arithmetic average of spatially distributed TDR measurements. The dependence of E_{act}/E_{eq} on this representative soil moisture is depicted in Figure 2.7, which shows much less inter-annual variability compared to Figure 2.6, especially for trees. The trend of each single year again follows similar pattern as the Feddes Model.

It is observed in Figure 2.7 that in the understory layer the dependence of E_{act}/E_{eq} on soil moisture in 2005 deviates considerably from those in 2003 and 2004. This discrepancy is possibly caused by the unusually large amount of precipitation occurring prior to the

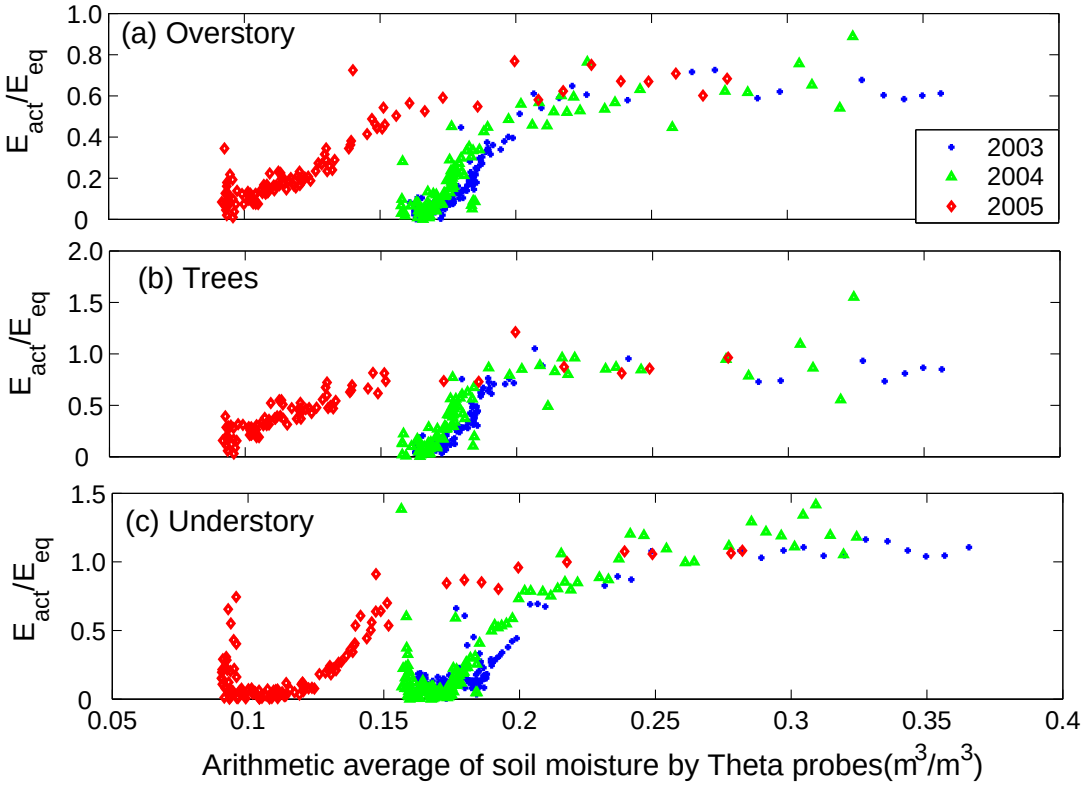

Figure 2.6: Dependence of E_{act}/E_{eq} on soil moisture measured by the Theta probes

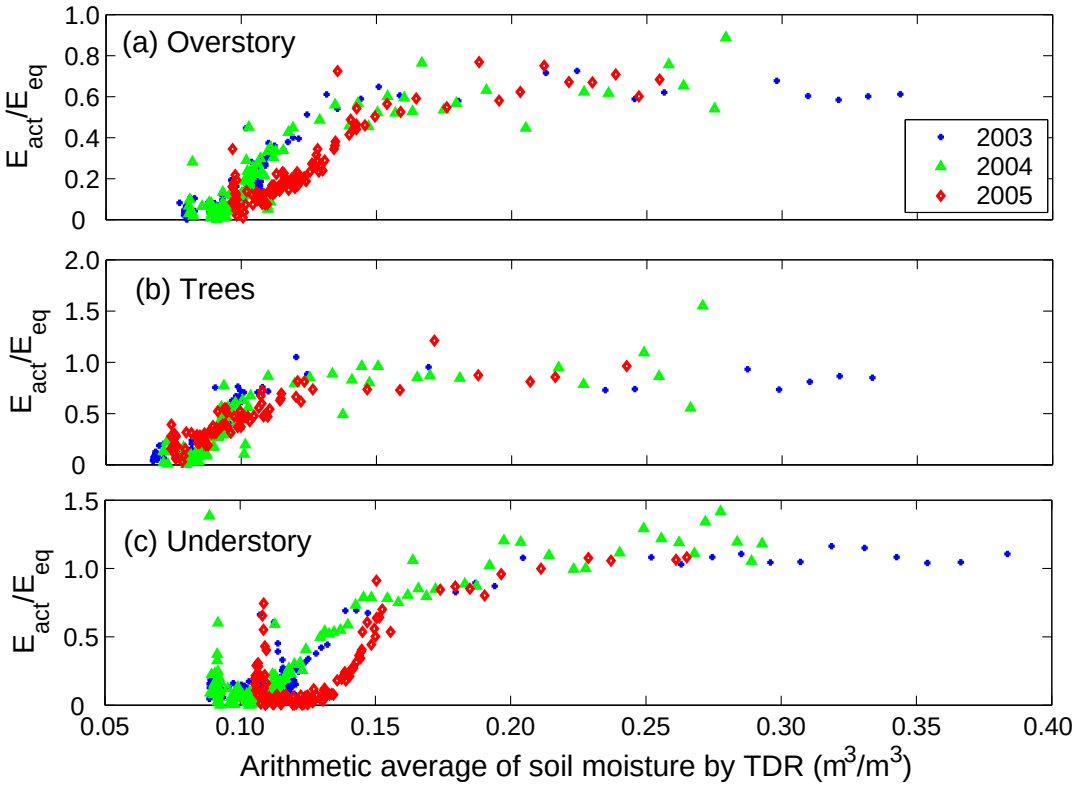

Figure 2.7: Dependence of E_{act}/E_{eq} on interpolated soil moisture measured by the TDR probes

summer drought in 2005 as demonstrated in Figure 2.2. The frequent spring rainfall events allow the percolation of water to deeper soils that is not accessible to grasses. The open space soil moisture at depths between 30 and 60cm in the summer of 2005 is found to be significantly higher compared to the summers of 2003 and 2004, while the soil moisture at the top 30cm shows more consistent pattern of behavior over time. By taking an arithmetic average of soil moisture at four depths up to 60cm, the soil water available to the grasses was overestimated. In other words, an effective representation of soil water available to the plants should account for the vertical variation in water uptake capacity limited by the rooting depth.

An alternative to arithmetic averaging of vertical soil moisture profile is to weigh the soil moisture at various depths by the fractions of roots present in the corresponding depths [*Baldocchi et al.*, 2004], i.e.,

$$\langle \theta \rangle = \frac{\int_0^z \theta(z)\, dP(z)}{\int_0^z dP(z)}, \tag{2.5}$$

where $P(z)$ is the cumulative distribution of root biomass from the surface to depth z (in centimeters) and an exponential model based on extensive field surveys [*Jackson et al.*, 1996], $P(z)=1-\beta^z$, was assumed for oak trees and grasses at the Tonzi site. The β value of the grasses was chosen to be 0.94 based on the data provided in *Jackson et al.* [1996], which yields 84% of roots in the top 30cm and 13% in 30-60cm. For the oak trees, β value of 0.976 is inferred from the finding that 70% of excavated root biomass of a blue oak tree is located above 0.5 m on average [*Ishikawa and Bledsoe*, 2000].

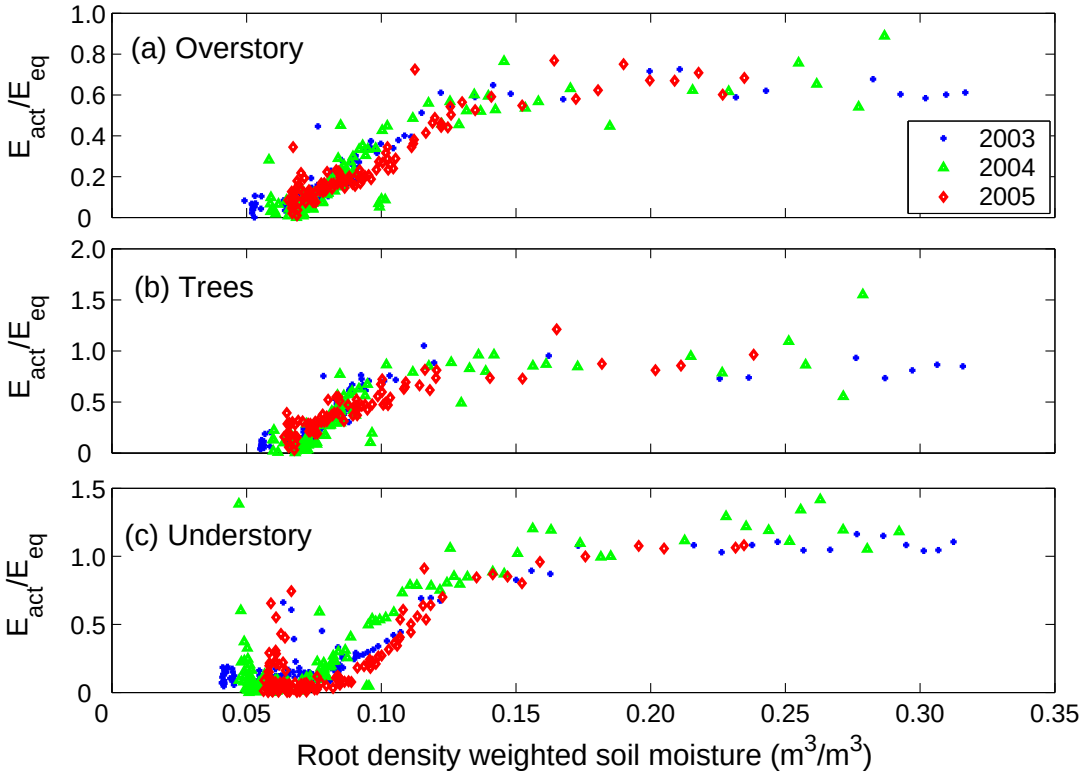

Figure 2.8: Dependence of E_{act}/E_{eq} on root density weighted soil moisture measured by the TDR probes

The relationship between E_{act}/E_{eq} and root density weighted representative soil moisture is provided in Figure 2.8, where the pattern of the understory layer shows less inter-annual variability compared to the cases when the arithmetic averages of soil moisture at various depths were used. Linear decay patterns are visible for the understory and overstory layers and for the trees. The Feddes Model can thus be applied to generalize the impact of soil water availability on ET at the Tonzi site.

The comparisons among various representations of soil moisture at the stand scale found that the least inter-annual variability of soil moisture effects on ET was yielded when the root density weighted average of distributed TDR measurements were taken as the rep-

resentative soil moisture. This result suggests that a single-point soil moisture measurement is not sufficient to represent the soil moisture status at a stand scale because it is not able to capture the heterogeneity of soil moisture field. *Settin et al.* [2007] reports similar findings through numerical studies. For this reason, spatially distributed soil moisture data collection is preferred at the stand scale. Furthermore, root biomass distribution profile plays an important role in causing the vertical variation in water uptake capacity of the plants, and its influence ought to be taken into account in averaging the vertical soil moisture profile.

2.4.3 Parameterization Results and Discussions

As the applicability of the Feddes Model to characterize the effects of soil moisture on ET appears suitable for the understory and overstory layers and for the trees in the oak savanna ecosystem, we proceed here by identifying its parameters using WINBUGS [*Lunn et al.*, 2000].

In applying the WINBUGS software for inference, multiple chains of the parameters were simulated in parallel and the modified Gelman-Rubin convergence diagnostic statistics [*Brooks and Gelman*, 1998] were used to test the effective convergence of the samples. Each chain had a sample size of 100,000 parameter sets with the first 50,000 realizations discarded to obtain a stationary distribution. One sample out of every 20 samples was selected to assure the independence among samples. The resulting pool of samples was considered being drawn from the joint posterior distribution of the parameters. The marginal distribution of each parameter can be approximated from the joint posterior samples by

using the kernel density estimator [*Venables and Ripley*, 2003].

The marginal distributions of the parameters in the Feddes Model, β, θ_1^* and θ_2^* (see Figure 2.1 and equations (2.1), (2.2), and (2.3), conditioned on the root density weighted soil moisture are given in Figure 2.9 for the overstory's, understory's and trees' ET in years 2003, 2004 and 2005. Compared to the uniform prior distributions assigned to the parameters as shown in the Appendix, the posterior distributions are bounded by narrower ranges with well-defined peak densities, which implies a reduction in uncertainty. Some of the parameters, for instance, θ_2^* for the understory layer in 2005, have multi-modal posterior distributions, which is an advantage of the MCMC method over most traditional parameter estimation methods.

In Figure 2.9, the inter-annual variability of the inferred parameters is evident from the differences in their marginal distributions from year to year. In addition to the natural variability, the inter-annual variations of model parameters could arise from the variations in seasonal precipitation distribution patterns, because the timing and amount of a rainfall event strongly affect how it will be partitioned, and different functional types use the available water in different ways depending on how stressed they are prior to the rainfall event [*Burgess*, 2006; *Rodriguez-Iturbe*, 2000]. The precipitation time series given in Figure 2.2 demonstrated that 2005 has much longer raining season compared to 2003 and 2004, and the precipitation amounts prior to the summer droughts in 2003 through 2005 are 395mm, 409mm and 717mm, respectively. It is noted that the understory layer experiences larger variability than the trees, possibly because the grasses are less able to tackle the change in

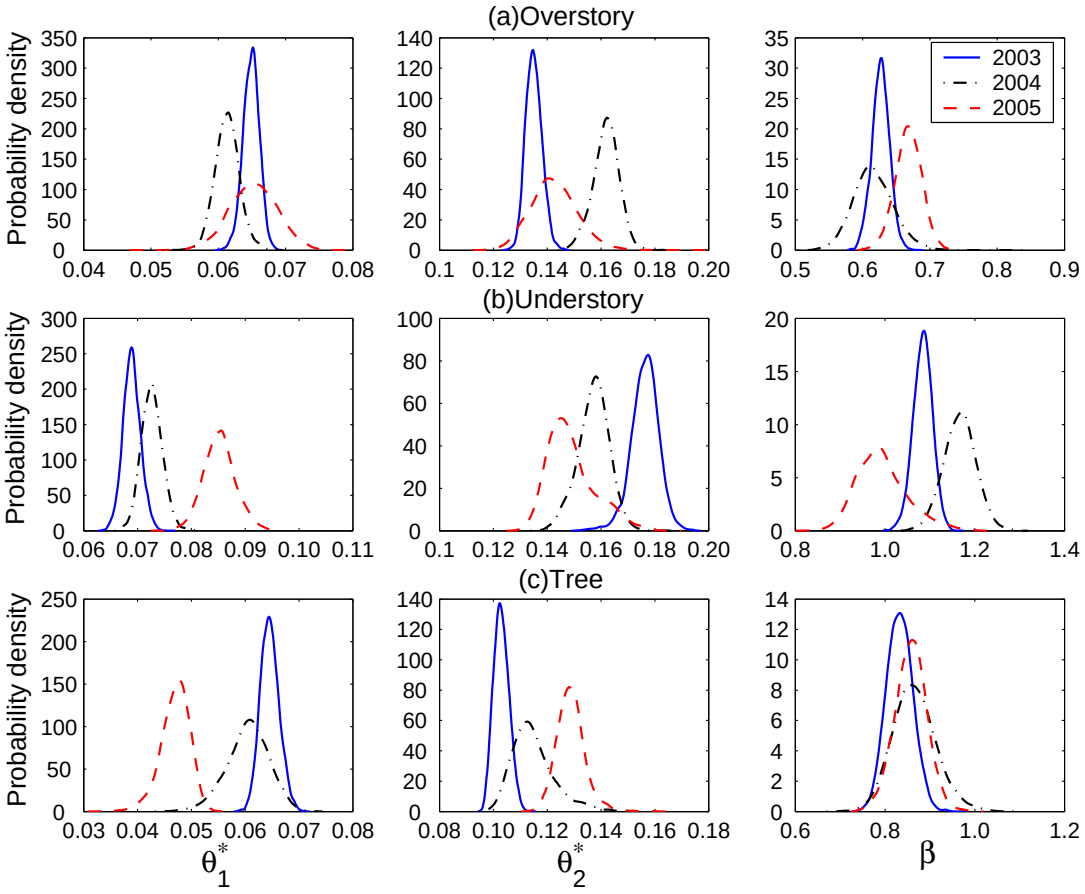

Figure 2.9: Posterior marginal distributions of the Feddes Model parameters

the ambient environment, such as change in the frequency and amount of precipitation, due to their shallow rooting depth.

It is interesting to note that from 2003 to 2005, θ_1^* and θ_2^* of the understory layer were moving closer to each other, whereas those of trees were moving in the opposite direction. This might indicate that grasses and trees respond differently to changes in water availability. Grasses tend to rapidly use up the available water resources, reflected by lower θ_2^* and higher θ_1^*, during wetter years. However, trees adopt a more conservative strategy. They started to control ET under moister soil during wetter years so that their ET can persist into drier soil conditions. This finding is in agreement with *Rodriguez-Iturbe et al.* [2001a]. The rapid depletion of water for the grasses is partly due to the fact that the superficial soil water in the grassland evaporates and grasses have very little control over it. However, the trees have more control over transpiration through their physiological structure. For example, their xylem can impose hydraulic conductance limitations during period of higher water availability to avoid dysfunction during drought [*Eamus et al.*, 2000], which is also known as safety-efficiency trade-off [*Tyree et al.*, 1994]. Trees can also control water loss through the opening and closing of their stomata, which is observed on the oak trees at our site [*Xu and Baldocchi*, 2003]. It is also possible that the variation in seasonal precipitation alters the fine root distribution of the grasses and trees [*Wan et al.*, 2002], and the effect could be very different on trees and grasses as they compete for the same water resources. The weighting factors used to aggregate point soil moisture to stand-level average might be adjusted to cope with the inter-annual variability of the Feddes Model parameters. Further

experimental evidence is needed to address the effects of precipitation distribution pattern on the plant responses to seasonal droughts in oak savanna.

2.4.4 Predicting ET with Calibrated Model

Each set of the sampled parameters from the MCMC method represents a realization of the Feddes Model fitted to the data. The inclusion of all realizations produced by the algorithm defines the variability in the parameterized model, as demonstrated in Figure 2.10. Rather than identifying an optimal fit of the model, the Bayesian inversion technique with the MCMC sampling scheme yields a range of possible models, which can then be used for statistical interpretation of the observations.

For instance, the realizations of the fitted model as shown in Figure 2.10 can be used to predict the actual ET with known meteorological variables and soil moisture. For given conditions, each realization of the Feddes Model leads to a realization of predicted ET, and consequently, a complete distribution of the predictions can be determined using a large number of realizations. As an example, the model calibrated using data in 2003 is used to predict the overstory's, understory's and trees' ET between the last spring/early summer rain and the first winter rain in 2004 and 2005. The results are presented in Figure 2.11. The comparisons between the predictions and the observed ET by the eddy covariance towers reveal that the model predicts the actual ET during the dry seasons fairly well, with the mean values being around the one-to-one line. Part of the misfit is due to the inter-annual variability of the parameters.

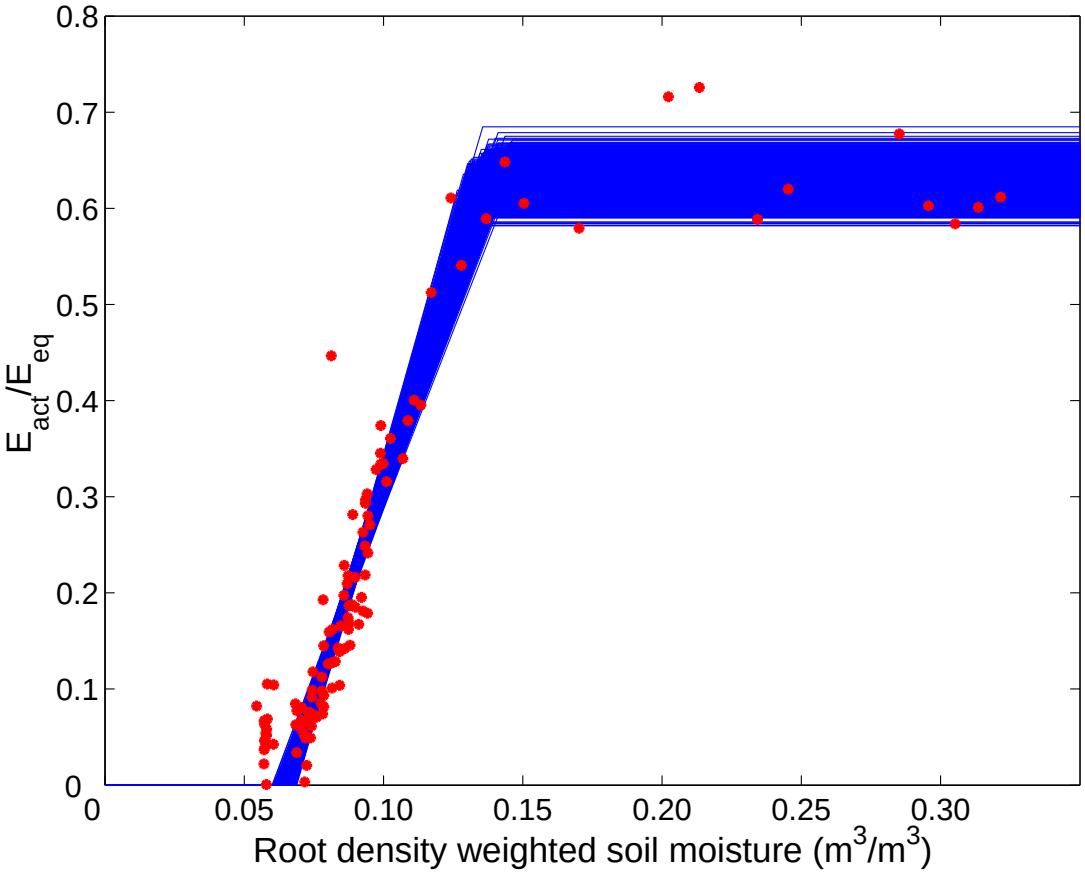

Figure 2.10: Realizations of the Feddes Model compared to the data for the overstory's ET in 2003 (Scatters are the data and lines are the realizations of the Feddes Model)

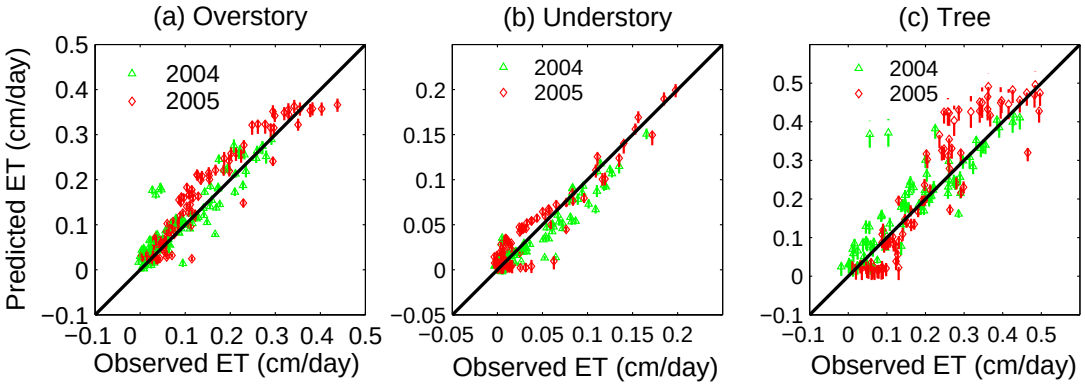

Figure 2.11: Prediction of ET in 2004 and 2005 with model calibrated using data in 2003 (Scatters are the mean values of the predictions and the dashed lines delineate the range within two standard deviations from the means)

2.5 Conclusions

We discussed in this chapter how soil moisture controls actual evapotranspiration in a water-limited oak savanna ecosystem located in California, and examined the applicability of the Feddes Model for describing the effects of water stress on ET of the heterogeneous environment as well as its components, using multi-year field observations at the daily, stand scale.

The influence of soil moisture on actual ET was investigated through the dependence of the ratio between ET, as measured by the eddy covariance towers, and the potential ET, as approximated by the Priestley-Taylor equation, on representative soil moisture. The observed relationship was compared to the pattern suggested by the Feddes Model in order to evaluate its applicability in the oak savanna ecosystem. Various representations of soil moisture at the stand scale, obtained from point measurements at various locations and depths were investigated. The model parameters were inferred using a Bayesian framework with the MCMC sampling method and their inter-annual variability was studied based on the difference in posterior marginal distributions from year to year. Finally, the parameterized model was used for predicting actual ET with uncertainty estimates determined using the joint distribution of the parameters derived from the Bayesian framework.

The Feddes Model was found to be in agreement with the observed patterns of soil moisture effects on ET regardless of whether the heterogeneous environment of trees and grasses was homogenized or treated as the sum of its individual components. However, the parameters of the Feddes Model varied with time. Grasses have lower θ_2^* and higher

θ_1^* during wetter years, whereas trees have the opposite trend, i.e., they start to control ET under moister soil (higher θ_2^*) during wetter years so that their ET persists into drier soil conditions (i.e., lower θ_1^*). This inter-annual variability is primarily driven by variations in the seasonal precipitation distribution pattern from year to year, as well as the responses of various plant functional types to changes in soil water availability. Grasses tend to rapidly use up the available water resources during the wetter years because they have little control over the evaporation, whereas trees are able to control water loss by limiting the xylem hydraulic conductance and by controlling their stomata. This difference in responses can also be a result of change in fine root distributions due to water availability in early seasons.

The selection of representative soil moisture leads to considerable difference in the inter-annual variability of model parameters. Among the various averaging schemes tried in this study, including (1) the arithmetic average of soil moisture measurements at different depths obtained at one location, (2) the arithmetic average of the spatially distributed soil moisture measurements at different depths and (3) the root density weighted average of the distributed soil moisture measurements at different depths, the last scheme yielded the most consistent behavior of the Feddes Model over time. The study demonstrates that distributed sampling of soil moisture is necessary to study the effects of soil moisture availability on ET in open canopy ecosystems. Furthermore, the soil water availability at different depths has a different influence on the total ET depending on the fraction of root biomass present at the corresponding depths. This difference can be accounted for by using the root density weighted average of the vertical soil moisture profile to produce representative soil

moisture.

The inter-annual variability of climate brings inherent variability to model parameters in addition to parameter uncertainties arising from measurement errors and an incomplete understanding of the underlying physical mechanisms. It is thus insufficient to assign deterministic values to model parameters without identifying the associated uncertainties. The parameter estimation methodology presented in this study, a Bayesian framework based on the MCMC sampling method, provides a systematic tool to quantify the parameter uncertainties conditioned on field observations and to directly estimate the prediction uncertainties using the model parameterized in this way. We calibrated the Feddes Model using data from 2003 and predicted the actual ET in 2004 and 2005 with quantified uncertainty. The comparison between the predicted and measured ET showed good agreement. The calibrated Feddes Model can be incorporated into the water balance equation to study water dynamics at the stand scale and eventually to better understand the water cycle in a heterogeneous environment.

This study developed a methodology to model the changes in ecosystem ET under drought conditions and to statistically parameterize the model using field data. The successful application of the methodology in the complex oak savanna ecosystem inspires its employment in other water-limited ecosystems.

Chapter 3

Theoretical Analysis for Sap Flow Measurements using Heat Ratio Method

3.1 Introduction

Heat pulse method is widely employed to measure water use by trees [*Cohen et al.*, 1981; *Granier*, 1985; *Swanson*, 1994; *Smith and Allen*, 1996; *Green et al.*, 2003]. It works by deducing sap flow rate from the speed at which a short heat pulse is propagated through the porous medium. The heat pulse technique has the advantages of simple instrumentation and lower power consumption. Among the numerous variations of the heat pulse technique, heat ratio method (HRM) introduced by *Burgess et al.* [1998] has been widely applied in various fields due to its ability to detect reverse and low flow rates and its straightforward instrumentation [*Burgess et al.*, 2001]. The apparatus for the HRM consists of a pair of

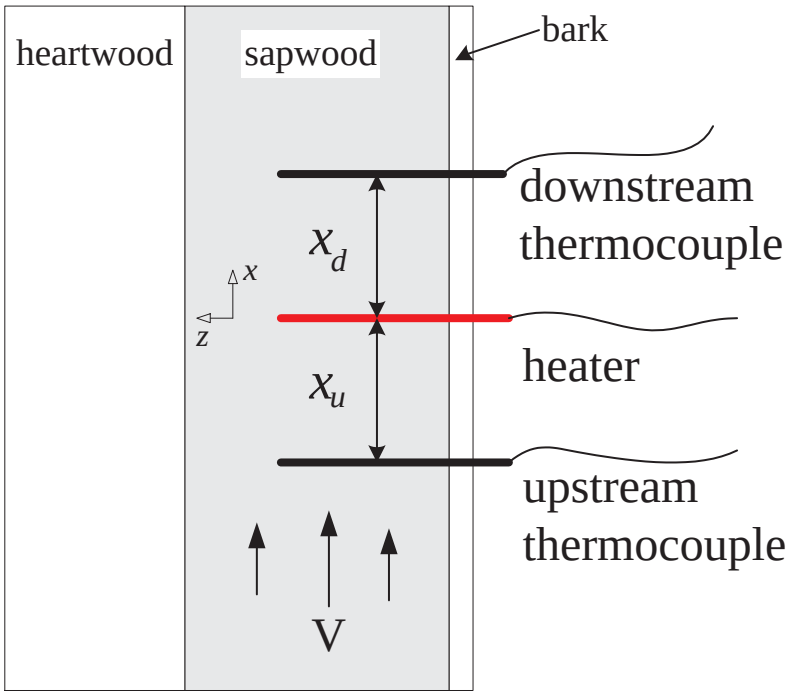

Figure 3.1: Diagram of heat ratio apparatus

thermocouple probes located equidistantly upstream and downstream from a heating element as depicted in Figure 3.1. The probes are parallel and aligned in a common plane.

The heat pulse velocity in HRM is deduced from the ratio of temperature increases recorded at downstream and upstream temperature probes, following the release of a heat pulse by the central heating element. The theoretical basis underlying HRM is an analytical solution to the heat transport equation developed by *Marshall* [1958], which is derived under idealized assumptions. For instance, the porous medium is assumed unbounded and homogeneous, and heat is instantaneously released from an infinite line source. However, these assumptions are routinely violated in real applications of HRM, e.g., tree sapwood and heating element are of finite dimension rather than being infinite, and heat is not re-

leased instantaneously but over a duration of time. The departure of the real conditions from the ideal assumptions may result in different temperature field around the heating element, and consequently affect the theoretical basis of HRM.

The objectives of this study are to (1) develop a solution to the heat transport process in tree sapwood with more realistic assumptions, (2) compare the difference in temperature fields approximated by Marshall's idealized solution and our more realistic solution, and (3) provide modifications if necessary to the fundamental equation of HRM based on improved understanding of the heat transport process.

3.2 Theory

3.2.1 Heat transport equation in sapwood

Wood is considered as a porous medium composed of cellulose, a solid fraction forming the vessel walls, and sap, a liquid filling the void space. The heat released from the central heating element is transported away by conduction and convection. Assuming sap water is moving uniformly in the $x-$direction and wood is thermally homogeneous and isotropic, the heat transfer process can be described as [*Carslaw and Jaeger*, 1959; *Gribben*, 1999]

$$\frac{\partial T}{\partial t} = \kappa \left(\frac{\partial^2 T}{\partial x^2} + \frac{\partial^2 T}{\partial y^2} + \frac{\partial^2 T}{\partial z^2} \right) - v_h \frac{\partial T}{\partial x} + Q\delta(x)\,\delta(y)\,\delta(z)\,\delta(t) \tag{3.1}$$

where T is temperature rise, t is time, κ is the thermal diffusivity of the wood matrix, and x, y, and z are space coordinates, Q represents the heat source term, and $\delta(\cdot)$ is the Dirac

function. The heat pulse velocity, v_h, is related to sap velocity, v_s, by the following equation defined by *Marshall* [1958],

$$av_s = \frac{\rho_w c_w}{\rho_s c_s} v_h \tag{3.2}$$

where a is the fraction of the cross-sectional area of conducting sapwood occupied by moving sap streams and ρ and c are density and specific heat capacity, with the subscript s referring to sap and w referring to wood matrix. The volumetric sap flux density per unit cross-sectional area of sapwood is given by $J_s = av_s$.

3.2.2 Marshall's solution

Marshall [1958] derives an analytical solution to Eq. (3.1) considering instantaneous heat released from an infinite line source normal to the $x-y$ plane and passes through the point $(x,y) = (0,0)$, in an infinite medium at uniform initial temperature, which is

$$T(x,y,t) = \frac{q}{4\pi\rho c\kappa t} \exp\left[-\frac{(x-v_h t)^2 + y^2}{4\kappa t}\right] \tag{3.3}$$

where q is the quantity of heat released per unit length.

If temperature increase is measured at points equidistant downstream and upstream from the line source, the heat pulse velocity can be derived from Eq. (3.3) as

$$v_h = \frac{\kappa}{x} \ln \frac{T_d}{T_u} \tag{3.4}$$

where x is the distance between the heater and either temperature probe, T_d and T_u are temperature increases measured at x cm downstream and upstream from the heater, respec-

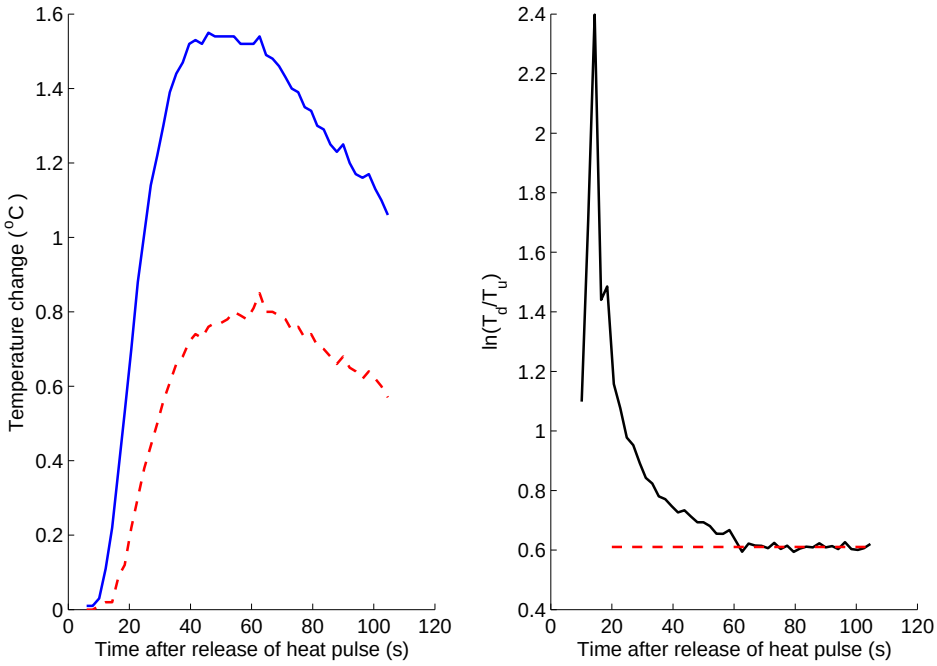

Figure 3.2: Example of heat response curves taken downstream and upstream from the heater probe and the corresponding time series of log-ratio of temperature increases. The dashed line in the right panel is the log-ratio calculated from average temperature rise over t=60-100s following the heat pulse.

tively. Eq. (3.4) is the theoretical basis of HRM [*Burgess et al.*, 2001]. An example of temperature increases measured using the HRM apparatus and the calculated temperature increase ratios is shown in Figure 3.2.

3.2.3 Improved solutions

Ren et al. [2000] present another solution for Eq. (3.1) based on the same assumptions as Marshall's except that the instantaneous heating is replaced by a heat pulse lasting from 0 to t_0, which is a better representation of the heat source in practice. Their solution is

$$T(x,y,t) = \frac{q'}{4\pi\rho c\kappa}\int_{t-t_0}^{t} s^{-1}\exp\left[-\frac{(x-v_h s)^2+y^2}{4\kappa s}\right]ds \tag{3.5}$$

where q' is the quantity of heat released per unit length per unit time and t_0 is the duration of heat pulse. This solution is for $t > t_0$.

It is further studied in *Wang et al.* [2002] that Eq.(3.5) can also lead to eq. (3.4) when the temperature probes are aligned symmetrically about the heater probe. If asymmetry occurs, Eq. (3.4) asymptotically approaches the heat pulse velocity using average distance between the probes as x. Therefore, it is recommended that the ratios of temperature increases should be calculated at a time when its value has reached a constant.

However, the assumptions of an infinite medium and an infinite line source corresponding to Marshll's and Ren's solutions are not satisfied in sap flow applications. To account for the finite width of the sapwood, *Gribben* [1999] developed a solution for the temperature increases following an instantaneous heat release from a linear line source as

$$T(x,y,z,t) = \frac{q}{\pi\rho c\kappa t}\exp\left[-\frac{(x-v_h s)^2+y^2}{4\kappa t}\right]\sum_{n=1}^{\infty}\frac{\sin(b_n L)\cos(b_n z)}{2b_n L+\sin(2b_n L)}\exp\left(-\kappa {b_n}^2 t\right) \tag{3.6}$$

where L is the depth of the sapwood and the line source is assumed to extend through the entire sapwood depth, and b_n is obtained by solving the equation, $\tan(bL) = K/b$, with $(n-1)\pi/L < b_n < (2n-1)\pi/(2L)$.

In deriving Eq. (3.6), it is assumed that geometry in the vicinity of the heating element is flat since length of heating element is much smaller than the tree radius, and no heat flow boundary and Newton's Law of Cooling are applied at the bark $(z = 0)$ and at the boundary

between sapwood and heartwood ($z = L$), respectively, i.e.,

$$\frac{\partial T}{\partial z} = 0 \qquad \text{at} \quad z = 0 \tag{3.7}$$

$$\frac{\partial T}{\partial z} + KT = 0 \qquad \text{at} \quad z = L \tag{3.8}$$

where K is the parameter describes how fast the surface cools and it is not expected to be known because the solution is not sensitive to its values [*Gribben*, 1999].

Based on Gribben's solution, we further replace the instantaneous heat source with a pulsed one, and add the flexibility that the length of line source can be shorter than the sapwood depth. Skipping the evolving steps, our final solution based on the realistic assumptions is obtained as follows,

$$T(x,y,z,t) = \frac{q'}{\pi\rho c\kappa} \sum_{n=1}^{\infty} \frac{\sin(b_n a)\cos(b_n z)}{2b_n L + \sin(2b_n L)} \int_{t-t_0}^{t} s^{-1} \exp\left[-\frac{(x - v_h s)^2 + y^2}{4\kappa s} - \kappa {b_n}^2 s \right] ds \tag{3.9}$$

where a is the length of line source. To ensure the no heat flow boundary at the tree bark, it is recommended to insulate the tree bark around the sap flow apparatus in field.

In all the solutions presented here, sap is assumed to flow uniformly through the porous medium that is at uniform initial temperature. In addition, the flow deformation caused by the implanted probes is not considered, assuming that the size of the probes is infinitesimally small compared to the tree size.

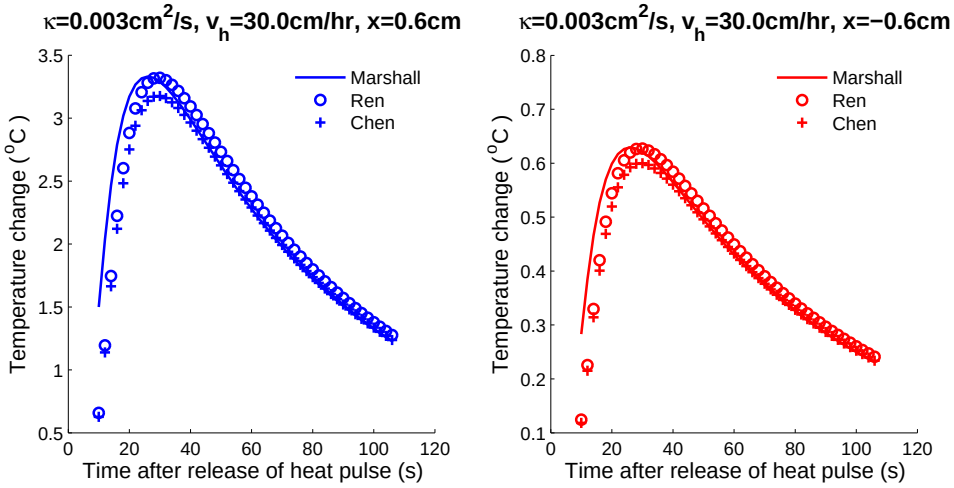

Figure 3.3: The temperature increases calculated from various theoretical models. Our solution is labeled as Chen's

3.3 Results and Discussions

3.3.1 Comparison of calculated temperature fields

It is demonstrated in the previous section that the various solutions to heat transport process differ in their fundamental assumptions, which may consequently lead to differences in their calculated temperature fields around the line source. Figure 3.3 shows an example of temperature rises calculated from various theoretical models at 0.6 cm downstream (x = 0.6 cm) and upstream (x = -0.6 cm) from the line source assuming κ = 0.0030 cm^2/s, v_h = 30 cm/hr, y = 0.0 cm, z = 1.0 cm, L = 7.0 cm, a = 3.0 cm, and t_0 = 6 s. It is evident from this example that significant differences among the solutions mostly occur at early times, say, before the arrival of peak, while the differences at late times are negligible.

However, the differences among these solutions may vary with probe geometry, wood thermal diffusivity, heat pulse velocity as well as the sapwood depth. Therefore, an in-depth

investigation is conducted on how the aforementioned parameters affect the difference in calculated temperature rises caused by the theoretical models. As the largest difference is anticipated between the Marshall's solution and our solution, the comparisons are focused on these two models, and their relative difference is calculated as $|\left(T^{Marshall} - T^{Chen}\right)/T^{Chen}|$.

Influence of vertical probe distance (x)) and heat pulse velocity (v_h)

Assuming values of κ, y and z are fixed at 0.0030 cm^2/s, 0.0 cm and 1.0 cm, respectively, the change of relative difference in temperature rise in sapwood with a depth of 7 cm is shown in Figure 3.4 as a function of time and x-locations. The difference is found to be symmetric about the x values. Therefore, only results for positive x values are provided here. It is observed that most of the significant differences occur in the early times for all the cases represented in the plots. In addition, the early-time difference is observed to increase with probe spacing in x-direction. Nevertheless, this trend can be reversed around the time approaching the minimum difference, which is dependent on both the probe spacing and heat pulse velocity.

It is evident in Figure 3.4 that, at a fixed location, the heat pulse velocity affects the decreasing rate of difference in the early times, the time for the difference to reach its asymptotic value, as well as the magnitude of the asymptotic difference. The example shown in Figure 3.5, extracted from Figure 3.4 for x = 0.6 cm, exhibits that the difference decreases with heat pulse velocity in early times, whereas the asymptotic difference increases with the heat pulse velocity. It is noticed that, for t >40 s, the difference corresponding to any

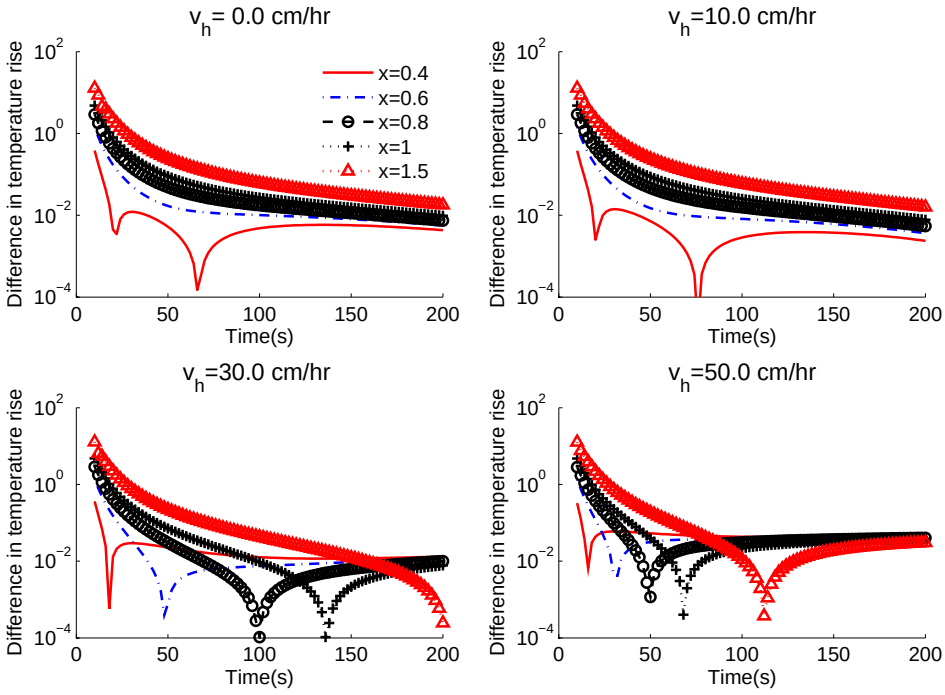

Figure 3.4: Difference in temperature rise between Marshall's solution and our solution as affected by $x-$location and heat pulse velocity for $L = 7$ cm, $\kappa = 0.0030$ cm^2/s, $y = 0$ cm, and $z = 1.0$ cm. The difference is calculated as $\left| \left(T^{Marshall} - T^{Chen} \right) / T^{Chen} \right|$.

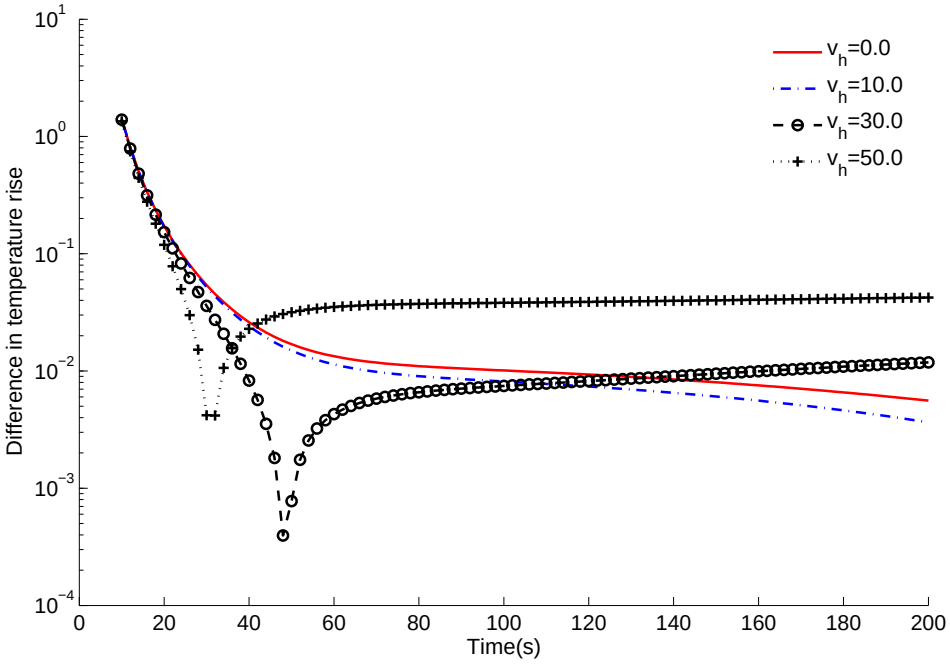

Figure 3.5: Difference in temperature rise between Marshall's solution and our solution as affected by heat pulse velocity for $L = 7$ cm, $\kappa = 0.0030$ cm^2/s, $x = 0.6$ cm, $z = 1.0$ cm, and $v_h = 30$ cm/hr. The difference is calculated as $\left| \left(T^{Marshall} - T^{Chen} \right) / T^{Chen} \right|$.

heat pulse velocity is less than 3%, which may be considered negligible.

In addition, it is noted that the minimum differences in the plots are not the exact ones, which should be zero ($-\infty$ in log-scale) when two solutions meet. Nevertheless, the time corresponding to the minimum difference is close to the true ones. Except for these cases corresponding to small values of x and v_h, the solutions of Marshall's model and our model meet only once after the arrival of peak.

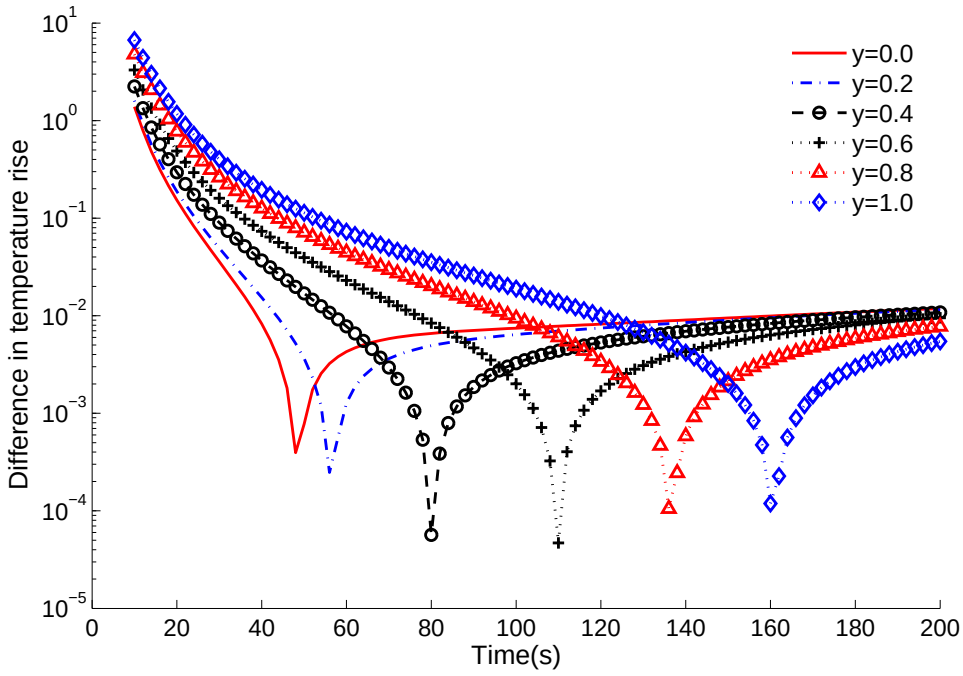

Figure 3.6: Difference in temperature rise between Marshall's solution and our solution as affected by y-coordinate for L = 7 cm, κ = 0.0030 cm^2/s, x = 0.6 cm, z = 1.0 cm, and v_h = 30 cm/hr.The difference is calculated as $\left|\left(T^{Marshall} - T^{Chen}\right)/T^{Chen}\right|$.

Influence of lateral position (y)

In both Marshall's solution and our solution, y-coordinate of the measurement point is a necessary component to derive its temperature rise. As revealed in Figure 3.6, the difference of temperature rise between two solutions is influenced by values of y. With the other parameters being fixed, the difference at early times increases with the y value, while same asymptotic value will be reached when elapsed time is sufficiently long. At t >60 s, the difference is within 2% and 10%, respectively, for $y \leq 0.6$ cm or otherwise.

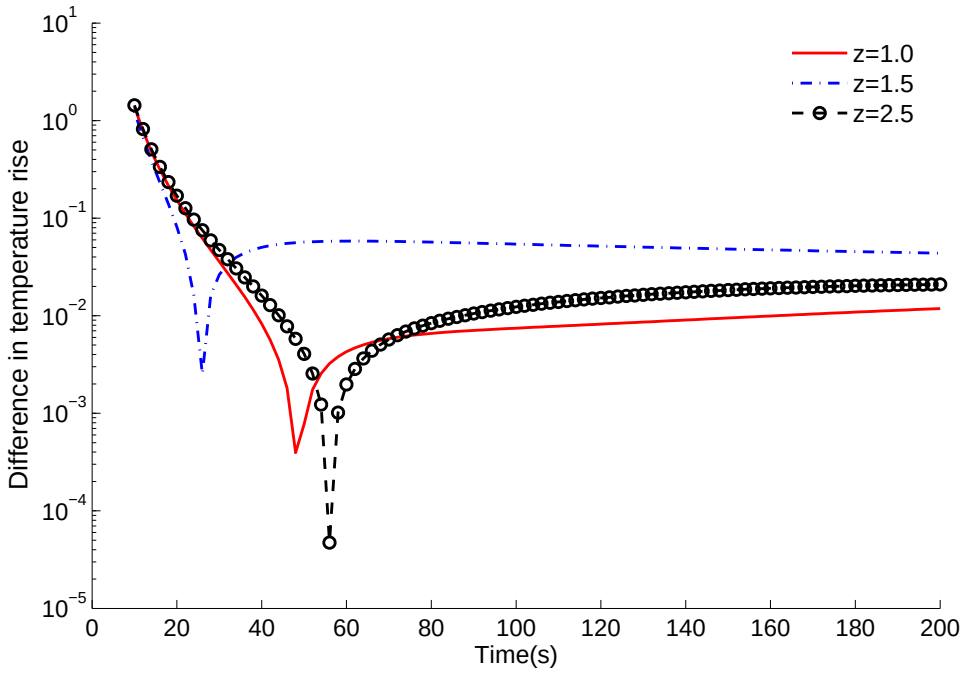

Figure 3.7: Difference in temperature rise between Marshall's solution and our solution as affected by y-coordinate for L = 7 cm, κ = 0.0030 cm^2/s, x = 0.6 cm, y = 0.0 cm, and v_h = 30 cm/hr.The difference is calculated as $\left|\left(T^{Marshall} - T^{Chen}\right)/T^{Chen}\right|$.

Influence of radial depth (z)

One of the key differences between two solutions is that Marshall's solution is two-dimensional, while ours is three-dimensional. The coordinate along z-direction represents the relative position to finite line source and the distance to boundaries. Therefore, the impact of z on the difference of two solutions may be more complex than x and y due to the interacting effects of boundary conditions and finite length of line source. The example provided in Figure 3.7 proves that there is no clear trend of the difference against z. The largest difference is yielded at the mid-point of the line source at z = 1.5 cm when $t > 40$ s, whereas the difference in the same time frame for other z values is smaller.

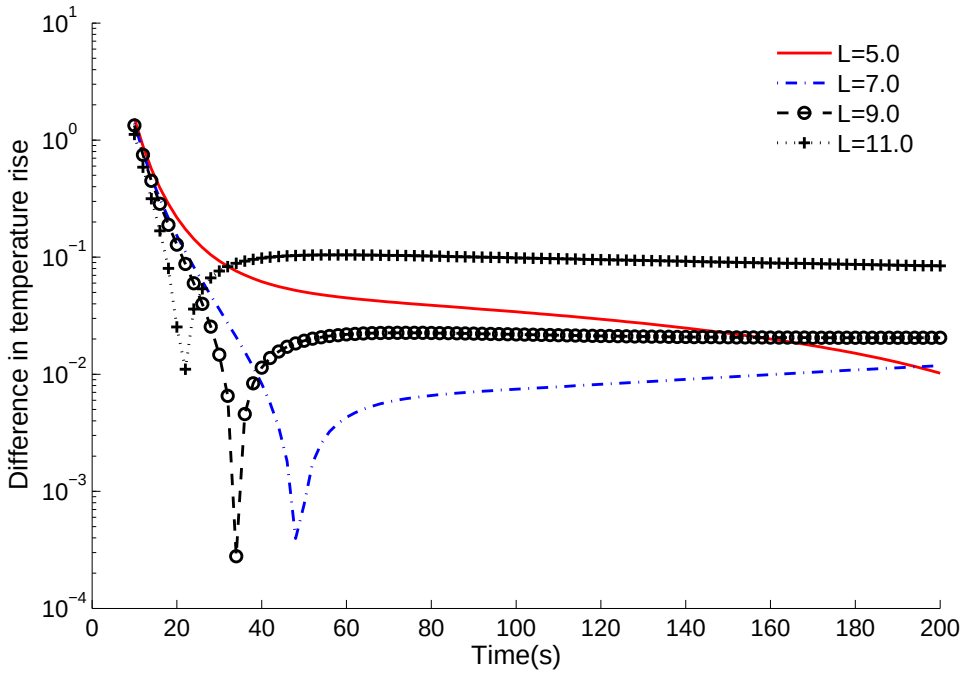

Figure 3.8: Difference in temperature rise between Marshall's solution and our solution as affected by the sapwood depth for $\kappa = 0.0030$ cm^2/s, $x = 0.6$ cm, $y = 0.0$ cm, $z = 1.0$ cm, and $v_h = 30$ cm/hr. The difference is calculated as $\left| \left(T^{Marshall} - T^{Chen} \right) / T^{Chen} \right|$.

Influence of sapwood depth (L)

The influence of sapwood depth on the solution difference is related to the assumptions of infinite medium and infinite line source in Marshall's solution. For a typical range of sapwood depth from 5 cm to 11 cm, the example presented in Figure 3.8 illustrates that the asymptotic difference at $t > 60$ s increases with sapwood depth, while the decay of difference with time is very slow for small sapwood depth, e.g., $L = 5.0$ cm, compared to the other depths considered. The reason may be that boundary effects is more dominant in small sapwood depth, whereas the inappropriate assumption of infinite line source plays a more significant role in medium to large sapwood depths.

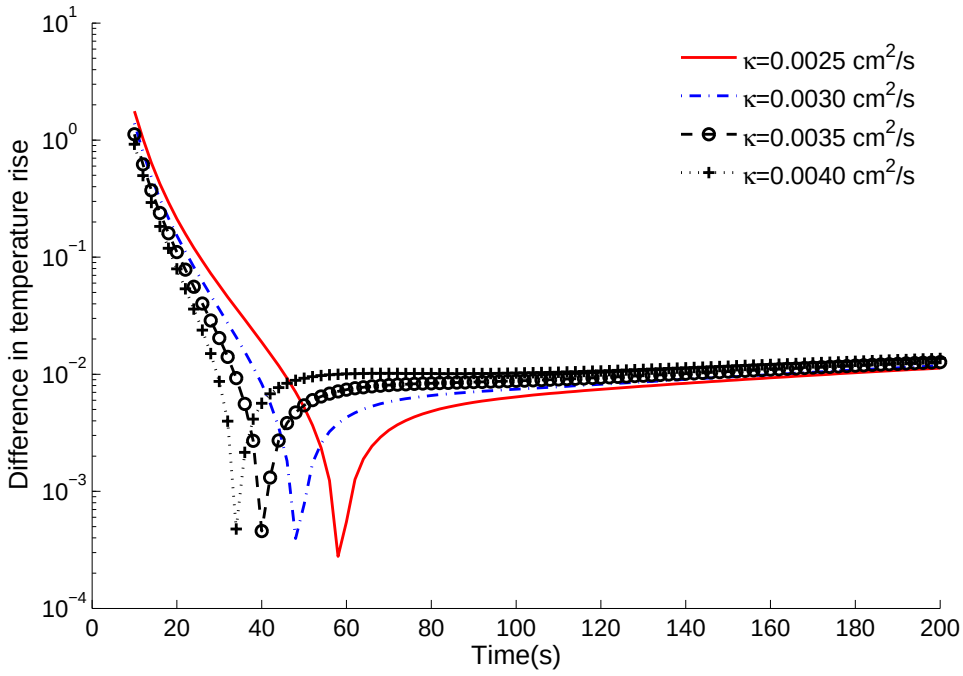

Figure 3.9: Difference in temperature rise between Marshall's solution and our solution as affected by the sapwood depth for $L = 7$ cm, $x = 0.6$ cm, $y = 0.0$ cm, $z = 1.0$ cm, and $v_h = 30$ cm/hr. The difference is calculated as $\left| \left(T^{Marshall} - T^{Chen} \right) / T^{Chen} \right|$.

Influence of thermal diffusivity (κ)

An example showing the impact of κ on solution difference is given in Figure 3.9. The range of κ value is chosen based on the calculation provided in Appendix D, which shows that the wood thermal diffusivity at the site may vary between 0.0025 and 0.004 cm^2/s in response to various wood densities and moisture conditions. Larger difference is observed in Figure 3.9 for smaller κ value in early times. However, the trend is reversed for $t > 50$ s, and at the same time, the difference caused by varying κ value is diminishing with time.

3.3.2 Impacts on HRM

It is of interest to investigate whether the estimation of the heat pulse velocity based on our improved solution differs from that based on Marshall's solution. As presented in the previous section, the difference between two solutions is normally negligible at late times. It can be expected that Eq. (3.4) is still valid for symmetric probe alignment if the temperature increase are recorded at late times, say over 60-100s following the heat pulse. It is confirmed true using the extensive data for comparing solution difference in the preceding section.

Nevertheless,the probe geometry in practice can depart from the ideal alignment assumed to derive Eq. (3.4): the probe spacing may not be symmetric in x-direction and the three probes outlined in Figure 3.1 may not lie in the same plane in y-direction. In order to examine the applicability of Eq. (3.4) under arbitrary probe alignments, the data in the previous section are used to create numerous combinations of probe geometry and the heat pulse velocity is found to be linearly related to $\frac{\kappa}{x}\ln\frac{T_d}{T_u}$, i.e.,

$$v_h = B_0 + B_1\frac{\kappa}{x}\ln\frac{T_d}{T_u} \tag{3.10}$$

where B_0 and B_1 are empirical factors, x is the average distance of downstream and upstream temperature probes from the line source, and T_d and T_u are average temperature increases over $60s \leq t \leq 100s$ measured by the downstream and upstream temperature probes, respectively. The average temperature increase is used to calculate the ratio in the consideration that temperature increase is usually small for $t > 60$s, especially at the up-

stream probe. As a result, random noise in individual temperature measurement may lead to unreliable result of ratio.

Further study shows that B_0 and B_1 are mainly controlled by the geometry asymmetry, while the other parameters, including κ, L, and z, have no significant impact. The contour plots in Figure 3.10 demonstrate that B_0 and B_1 are nearly linearly related to $x_d - x_u$ and $y_u^2 - y_d^2$, while there is no noticeable difference caused by varying z values. It is also noted from the plots that B_1 only varies slightly around 1, whereas B_0 can be as large as 30 cm/hr.

Linear regression of B_0 and B_1 on probe geometry along with κ, L, and z confirms that κ, L, and z are not significant factors, and the regression equations are obtained as

$$\begin{aligned} B_0 = &-0.031 + 22.35x_d - 21.91x_u - 44.77\left(y_u^2 - y_d^2\right) - 0.42x_d x_u \\ &+ 26.55x_d\left(y_u^2 - y_d^2\right) + 27.39x_u\left(y_u^2 - y_d^2\right) - 19.77x_d x_u\left(y_u^2 - y_d^2\right) \end{aligned} \tag{3.11}$$

$$\begin{aligned} B_1 = &\left[100 + 1.32x_d - 1.30x_u - 2.66\left(y_u^2 - y_d^2\right) - 2.10x_d x_u\right. \\ &\left.+1.58x_d\left(y_u^2 - y_d^2\right) + 1.63x_u\left(y_u^2 - y_d^2\right) - 1.18x_d x_u\left(y_u^2 - y_d^2\right)\right] \times 10^{-2} \end{aligned} \tag{3.12}$$

where x_d and x_u are both taken as their absolute values. Both equations yield R^2 value of 0.999, which is a sign of good fitting to the data.

3.4 Conclusions

This study re-evaluated the theoretical basis of sap flow measurements using HRM. The fundamental equation of HRM was originally derived from Marshall's solution to heat

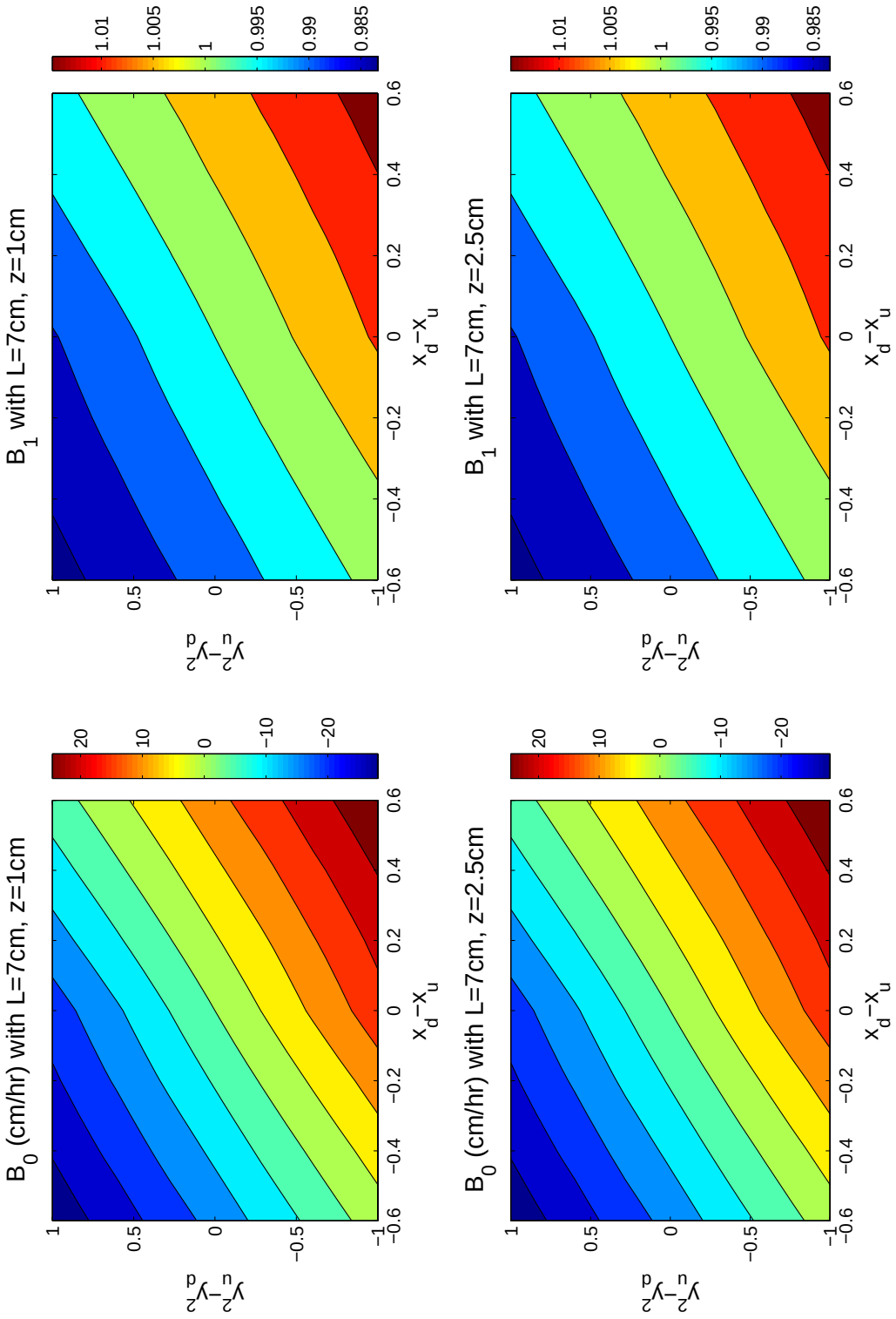

Figure 3.10: Contours of empirical factors versus spacing asymmetry in x- and y-directions.

transport process in sapwood with idealized assumptions. we developed an improved solution to the same process with more realistic assumptions. More specifically, the sapwood was considered bounded porous medium, the line source had finite length, which may or may not extend through the entire sapwood depth, and the heat was released from the line source over a duration. Extensive comparisons on the difference of calculated temperature fields by Marshall's solution and our solution revealed that most significant discrepancy occurs around the early times, whereas the difference is negligible at later times, say $t >$ 60 s. It is therefore recommended that when employing HRM the temperature increases should be measured in this late time window.

Furthermore, the fundamental equation of HRM was derived on the basis of symmetric probe alignment. In practice, however, the probes can be misaligned during the installation process, even if the probes were carefully installed with a drilling guide. Due to this practical consideration, this study also investigated whether the fundamental equation of HRM was changed under asymmetric probe alignments. With the numerical data generated from our solution, which cover a wide range of possible sapwood properties and probe alignments, a significant shift from the true heat pulse velocity may be resulted from the asymmetric alignment if the heat pulse velocity is estimated by the HRM equation for symmetric probe alignment. Therefore, the fundamental equation of HRM can be slightly changed to include an interception (B_0) and slope (B_1) to account for this asymmetry. Linear regression of B_0 and B_1 on sapwood properties and probe alignment found that B_0 and B_1 can be accurately determined by probe geometry in x- and y- directions. The implementation of

this revised HRM equation is shown in next chapter.

This study not only improves our understanding of the underlying principles of HRM, but also provides sounding evidence that the fundamental equation of HRM can only be slightly adjusted to account for the departure of real conditions from the idealized one. These findings are the solid base for our choice of HRM in monitoring tree transpiration.

Chapter 4

On Determining Wood Thermal Diffusivity and Probe Geometry Using In-Situ Heat Response Curves for Sap Flow Measurements

4.1 Introduction

The sap flow method has long been used to measure transpiration by individual plants [*Barrett et al.*, 1995; *Burgess et al.*, 2001; *Cermak et al.*, 1973; *Chandra et al.*, 1994; *Kluitenberg and Ham*, 2004; *Marshall*, 1958; *Swanson and Lee*, 1966], and has a history of applications in hydrology, forestry, ecology, agriculture, and horticulture [*Cohen et al.*,

1988; *Cohen and Li*, 1996; *Eastham and Gray*, 1998; *Fernandez et al.*, 2001; *Wilson et al.*, 2001]. The transpiration measurement at individual tree by the sap flow technique not only provides sounding evidence to study the plant response to ambient stresses or disturbances such as drought and irrigation [*Cermak et al.*, 1993; *Duursma et al.*, 2008; *Dye*, 1996; *Oren et al.*, 1999; *Poyatos et al.*, 2008; *West et al.*, 2008], it can also be upscaled to areal transpiration [*Cermak et al.*, 2004; *Cienciala et al.*, 1999; *Crosbie et al.*, 2007; *Granier et al.*, 1996; *Saugier et al.*, 1997; *Whitley et al.*, 2008]. The sap flow method has contributed significantly to studies of nighttime transpiration [*Dawson et al.*, 2007; *Fisher et al.*, 2007] and hydraulic redistribution in root zone [*Burgess et al.*, 2000; *Kurz-Besson et al.*, 2006; *Nadezhdina et al.*, 2006; *Scott et al.*, 2008], both of which are important to understanding plant water use in semiarid regions. A recent special issue in *Plant and Soil* [*Burgess*, 2008] provides a comprehensive review of new developments and applications of the sap flow method.

In general, there are three major thermometric techniques used to measure sap flow: heat pulse, heat balance, and heat dissipation. In all the three techniques heat is used as a tracer but in different ways: With the heat pulse technique, sap flow rate is measured by determining the speed at which a short heat pulse is propagated through the porous medium; With the heat balance technique, sap flow rate is determined from the vertical heat loss by convection, which is calculated from the balance of heat fluxes into and out of the heated stem section. Heat can either be externally applied to the entire circumference of the trunk or be internally applied to a segment of the trunk on large trees. Finally, with the thermal

dissipation technique, which is often known as the Granier method [*Granier*, 1985], an empirical equation is used to relate the sap flow rate and temperature difference between two thermocouple probes that are about 10 cm apart, and constant power is applied to the heater that is put together with the thermocouple probe on the top. We refer readers to the work of *Smith and Allen* [1996] for a review of the underlying theories of these techniques and to *Swanson* [1994] for a review of the history of their use.

This study focuses on the heat pulse technique, which has advantages of low power consumption, simple instrumentation and automated data collection. *Green et al.* [2003] provide a detailed review of its theory and practical applications. Among the variations of the heat pulse technique, the heat ratio method introduced by *Burgess et al.* [1998] has been widely applied due to its ability to detect reverse and low flow rates and its straightforward instrumentation [*Burgess et al.*, 2001]. The apparatus for the heat ratio method consists of a pair of thermocouple probes located equidistantly upstream and downstream from a heating element as shown in Figure 3.1.

When measuring the sap velocity using the heat ratio method, it is critical to know the thermal diffusivity of the wood matrix and the distance of the thermocouple probes from the heater probe. While thermal diffusivity may be estimated from the core samples of the sapwood [e.g., *Scott et al.*, 2008] or calculated from measurements of stem water content and sapwood density [e.g., *Burgess et al.*, 2001], many studies do not report how thermal diffusivity values are chosen. Given the exact probe spacing, the wood thermal diffusivity can be estimated using the methodology developed by the soil science community to

determine soil heat properties using the heat pulse technique [*Bristow et al.*, 2001, 1994; *Campbell et al.*, 1991]. Nevertheless, the exact spacing and geometry of the probes cannot be guaranteed in practice even when the probes are carefully installed, due to the nature of the wood matrix. This problem is especially prevalent in hardwood species such as oak and maple. Considering the fact that the estimation of sap flow rates is sensitive to the probe spacing, e.g., a 1-mm error in probe spacing can cause more than 10% difference in the estimated sap flow rates, *Burgess et al.* [2001] suggest a correction procedure for the probe misalignment. However, it is dependent on obtaining zero-flow conditions, which is either assumed to happen at night or is achieved by cutting down trees. Therefore, there is a need for in-situ and non-destructive approach to determine both the wood thermal properties and probe geometry, in order to improve the accuracy of the sap flow measurements with the heat ratio method.

The objective of our study is to provide a systematic, non-destructive, and replicable methodology to determine wood thermal diffusivity and probe geometry for the sap flow measurements using the heat ratio apparatus. The estimation of these parameters is conditioned on the time series of temperature increases, i.e., temperature response curves, monitored by the downstream and upstream temperature probes after a heat pulse is released by the heater probe. The temperature response curves are controlled by the combination of thermal diffusivity, probe geometry, and convective velocity, which is in turn a function of wood thermal diffusivity, probe geometry, and the ratio of temperature increases detected by the downstream and upstream probes. Thus the wood thermal diffusivity and probe

geometry may be inversely estimated provided the temperature response curves taken at downstream and upstream locations from the heater probe. The primary advantage of the methodology is that it relies on the information that can be obtained using the installed probes without any further disturbance to the tree.

The difficulties in parameter estimation procedure may arise from various sources, among which the most important one is the uncertainties rooted in the measurement error of the temperatures and the inadequacy of selected model to approximate the heat transport process in wood stem. Therefore, a Bayesian inversion framework with Markov Chain Monte Carlo (MCMC) sampling scheme is chosen for its strengths in dealing with uncertainties arising from various sources and in combining prior knowledge of the parameters to be estimated [*Clark*, 2005; *Clark and Gelfand*, 2006]. Empirical factors are adopted to account for the departure of the field conditions from the idealized conditions that form the theoretical basis of the heat ratio method, and they are estimated together with wood thermal diffusivity and probe geometry.

4.2 Materials and Methods

4.2.1 Data acquisition

The heat ratio apparatus employed in this study consists of three 3-cm-long hypodermic needles, two of which are temperature probes and one is the heater probe with a resistance around 20 ohms. For each temperature probe, there are two thermocouple junctions in-

stalled at two different depths, 1 cm and 2.5 cm into the sapwood, respectively, to capture the radial variation of sap flow. The upstream and downstream temperature probes were installed to as close to 0.6 cm equidistantly from the central heater probe as possible. Each tree had two sets of sensors, one at breast height (around 1.5 m from the ground) and the other close to ground (around 0.3 m from the ground). Both sets were installed on the north side of the tree when possible to minimize the influence of diurnal bole temperature fluctuation, and all sensors were insulated with aluminum foil.

For each test, a 12-15 V voltage was applied on the heater probe for six seconds to generate the heat pulse. Temperature traces were recorded every two seconds until 100 s after the heat pulse stopped. The temperature increases were calculated by subtracting the initial temperature taken before the onset of the heat pulse from the temperature traces. The test was repeated in different seasons because wood thermal diffusivity may vary throughout the year due to the change of stem water content and ambient temperature.

4.2.2 Parameter Estimation Method

It has been investigated in Chapter 3 that the heat pulse velocity is linearly related to the ratio of temperature increases recorded between 60-100 s following the heat pulse, with the empirical factors determined by the probe geometry. Asymmetry in probe geometry usually results in a shift in the estimation of heat pulse velocity. In addition to such correction for non-ideal probe geometry, flow deformation imposed by the implanted probes is found to underestimate the heat pulse velocity using heat pulse technique [*Burgess et al.*, 2001;

Swanson and Whitfield, 1981]. Empirical factors are thus introduced to correct for the wounding effects as well as the difference in thermal properties of wood and probe material. It is studied in *Burgess et al.* [2001] that a linear correction function performs as well as a polynomial one. Therefore, we adopt a linear correction factor, W, then the corrected heat pulse velocity is $v_{ch} = W v_h$ with v_h determined by equation (3.10).

Reliable sap flow estimation using HRM relies on the determination of appropriate parameter values. Here we discuss how to determine the parameters to calculate v_h: empirical factors (B_0 and B_1), wood matrix thermal diffusivity (κ), and the geometry of probe installation (x_d, x_u, y_d, and y_u), while the estimation of wounding correction factor (W) is not considered. The parameter estimation is conditioned on the heat response curves measured by the downstream and upstream temperature probes following the release of a heat pulse.

Given a set of heat response curves taken downstream and upstream as shown in Figure 3.2, it is assumed that they can be described by the Marshall's analytical solution with the heat pulse velocity determined from Eq. (3.10). The ratio of temperature increases downstream and upstream is calculated from the temperature increases measured over 60-100s following the heat pulse, and a noise is added to simulate the measurement error in practice. Then, the parameters are selected on the basis of model fitting to the time series data.

In order to deal with the uncertainty involved in measured heat response curves and to facilitate the proceeding uncertainty analysis using the derived parameters, Bayesian inversion technique with the Markov Chain Monte Carlo (MCMC) sampling method is

adopted for parameter estimation. This framework is implemented in the WINBUGS software [*Lunn et al.*, 2000], which is a powerful tool for Bayesian inverse modeling with open access. A more detailed description of the estimation procedure can be found in *Chen et al.* [2008b]. Multiple chains of the parameters were simulated in parallel and the modified Gelman-Rubin convergence diagnostic statistics [*Brooks and Gelman*, 1998] were used to test the effective convergence of the samples. Each chain had a sample size of 45,000 parameter sets with the first 40,000 realizations discarded to obtain a stationary distribution. One sample out of every ten was selected to assure the independence among samples. The resulting pool of samples was considered realizations of the joint posterior distribution of the parameters. The marginal distribution of each parameter was approximated from the joint posterior samples by using the kernel density estimator [*Venables and Ripley*, 2003]. Details in MCMC implementation can be found in the appendix.

4.3 Results and Discussions

4.3.1 Model verification

The performance of the proposed parameter estimation framework depends on two important factors: one is whether Marshall's analytical solution is appropriate to describe the heat transport process in sapwood for a specific application; the other is whether the proposed framework is able to find the true parameter values if no model error is present. The latter can be tested using synthetic response curves generated from Eq. (3.3) with known

κ, v_h, x_d, x_u, y_d, and y_u. The parameters estimated using our proposed framework can then be compared to their true values. Furthermore, the sensitivity of estimated parameters to their prior knowledge can be investigated using the synthetic data.

Marshall [1958] mentions that the solution to a given heat response curve may not be unique, i.e., different combinations of κ, v_h and x may produce the identical heat response curves. To overcome this problem, heat response curves from multiple tests are used rather than a single curve. Each test consists of a pair of curves, as shown in Figure 3.2, which share same κ and v_h. All the tests are conducted on the same set of probes, i.e., they have same x_d, x_u, y_d, and y_u. The heat pulse velocity corresponding to each test is determined by κ and x through Eq. (3.10). With these extra constraints, we anticipate to achieve parameter distributions centered around their true values if no model error is present.

The synthetic case to verify the parameter estimation framework contains three tests for a probe set with x_d= 0.5 cm, x_u= -0.7cm, $y_d = 0.1$ cm, and $y_u = 0.2$ cm. The thermal diffusivity for each test is 0.0030, 0.0035, and 0.0028 cm^2/s, and the heat pulse velocity for each test is 30, 15, and 10 cm/hr, respectively. The heat released by the heater is set at 12 J/cm. The density and specific heat capacity of fresh wood are set at 1530 kg/m^3 and 1500 J/(kg$\cdot^o$C), respectively. In this formulation, x_u is negative because the x-coordinate of Eq. (3.3) has an origin at the heater probe and points downstream.

Assuming amount of released heat, wood density, and wood specific heat capacity are known, the inferred posterior distributions of the parameters are presented in Figure 4.1, where the limits of x-axis are the bounds imposed on the parameters as prior distributions,

and the true parameter values and their posterior means are represented by the solid and dashed vertical line, respectively. The results demonstrate that our parameter estimation process significantly reduces the parameter uncertainty after conditioning the parameter values on the observed heat response curves. All the inferred parameters except B_1 are have tight distributions around their true values. For the estimated thermal diffusivities, both the mean and mode of the posterior distributions are close to the true values. Whereas for probe geometries, modes of the posterior distributions are closer to the true values although the mean value still provides a good estimate. Given that only square terms of y_u and y_d are involved in the analytical models of the heat transport process, y_u^2 and y_d^2 are estimated rather than y_u and y_d.

Each set of sampled parameters from the MCMC method yields an estimation of heat pulse velocity using Eq. (3.10), and ultimately, a possible model fit to the data through Eq. (3.3). Inclusion of a large number of alternative parameter sets defines the uncertainty in model fitting as well as the estimated heat pulse velocity, which is a key step in field applications of the heat ratio method. The distribution of estimated heat pulse velocities and uncertainty in model fitting for the test case are shown in Figure 4.2, from which we can observe that the model fittings to the data are with a narrow uncertainty range, and the estimated heat pulse velocities are distributed closely around the true values.

However, it is not surprising that the heat amount, wood density, and wood specific heat capacity are not known exactly in actual applications, because the heat loss may not be easily estimated without detailed analysis of the complete circuit and knowledge of how

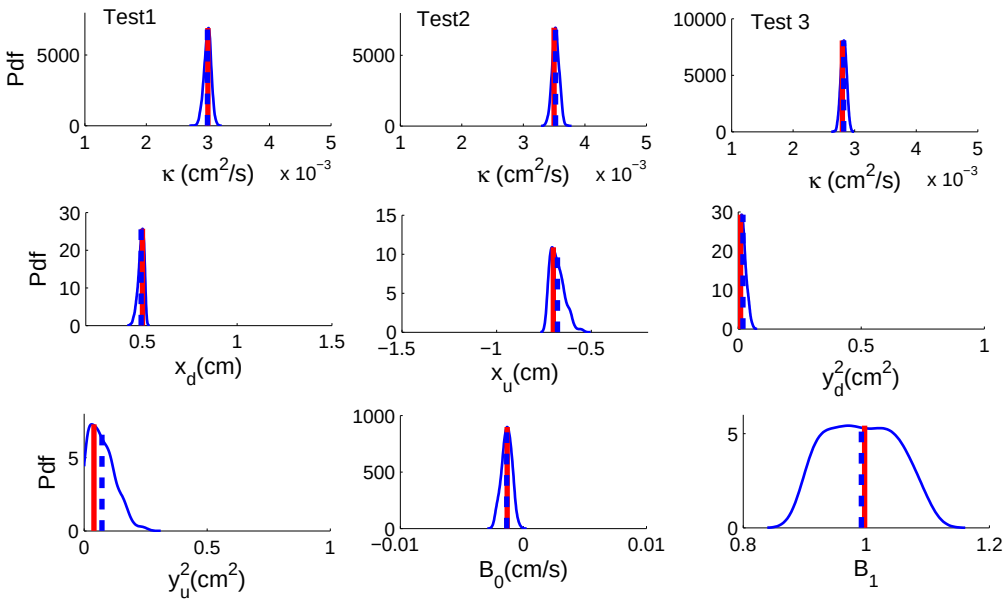

Figure 4.1: Posterior distributions of parameters with known heat amount, wood density and wood specific heat capacity. The limits of x-axis represent the bounds imposed on parameters as prior distributions. The solid vertical lines represent the true parameter values and dashed vertical lines are the mean values calculated from the posterior distributions.

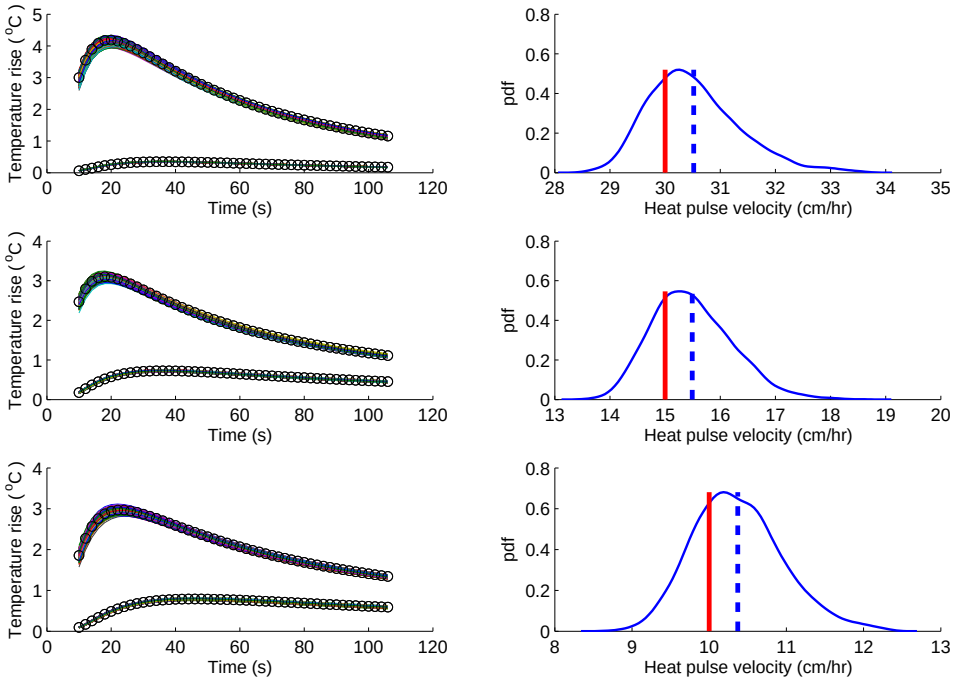

Figure 4.2: Model fitting and statistical distribution of estimated heat pulse velocities for the test case with known heat amount, wood density, and wood specific heat capacity. In the left panel, each solid line represents a model fit to the data by a parameter set from the MCMC method. In the right panel, solid vertical lines represent the true heat pulse velocities and dashed vertical lines are the mean values calculated from the posterior distributions.

wood density and specific heat capacity change with stem moisture content, which is usually not measured in situ. In such case, $q/(\rho c)$ in Eq. (3.3) is defined as another unknown parameter, C, and it can be estimated along with other parameters in our framework.

For the same test case that yield results in Figures 4.1 and 4.2, its counterpart with unknown C lead to the results in Figures 4.3 and 4.4, where the uncertainty levels in estimated parameters and heat pulse velocities, as well as in the model fitting increase by introducing uncertainty into C. The results also show that our framework tends to slightly overestimate C values, which causes overestimation in κ and v_h. Nevertheless, in all three tests the mean values of κ and v_h provide reasonable estimations of their underlying true values.

We also studied the case assuming that the true probe geometry is known, in which very accurate estimates of C, κ, and v_h are obtained as shown in Table 4.1. The estimated parameters are provided as their mean values plus or minus their standard deviations. We can therefore conclude that, provided with the exact probe geometry, the parameters estimated by the proposed method converge to the true values with low uncertainty.

It is worth mentioning that the Least-Square estimator is likely to converge to wrong parameter values when neither C or probe geometry is known, yet provides near perfect model fits to the data. This observation indicates the existence of multiple solutions under such conditions. On the other hand, it shows the necessity of using Bayesian technique to characterize statistical distributions of the parameters rather than an optimized set, which might be biased.

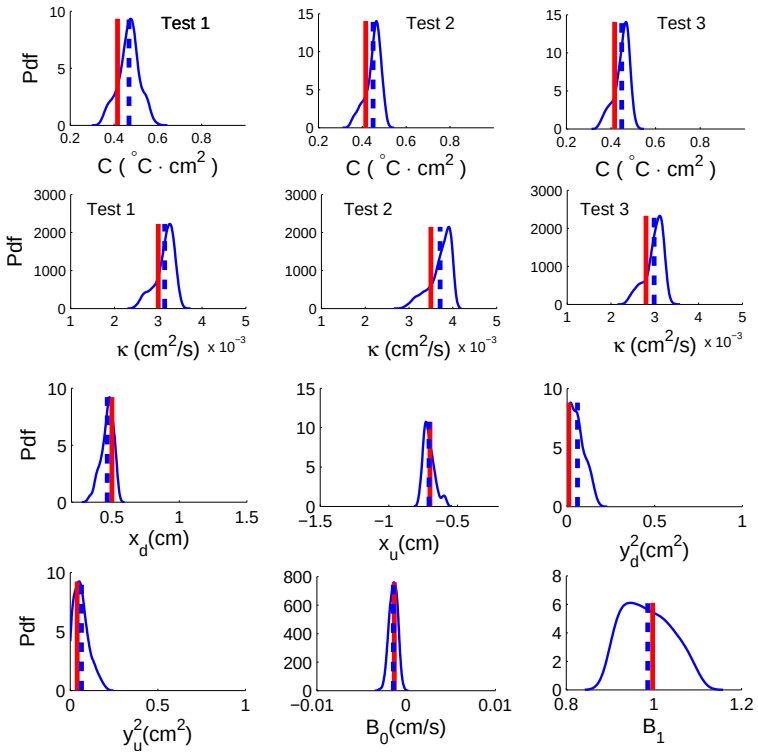

Figure 4.3: Posterior distributions of parameters with unknown heat amount, wood density and wood specific heat capacity. The solid lines represent the true parameter values and dashed vertical lines are the mean values calculated from the posterior distributions.

Table 4.1: Parameters estimated by MCMC method with known probe geometry compared to true values

	Parameter	**True value**	**Estimated**
Test 1	$C(^oC \cdot cm^2)$	0.416	0.412 ± 0.006
	$\kappa(\times 10^{-3} cm^2/s)$	3.0	3.0 ± 0.034
	$v_h(cm/hr)$	30.0	30.0 ± 0.5
Test 2	$C(^oC \cdot cm^2)$	0.416	0.413 ± 0.006
	$\kappa(\times 10^{-3} cm^2/s)$	3.5	3.5 ± 0.054
	$v_h(cm/hr)$	15.0	15.0 ± 0.4
Test 3	$C(^oC \cdot cm^2)$	0.416	0.412 ± 0.005
	$\kappa(\times 10^{-3} cm^2/s)$	2.8	2.8 ± 0.036
	$v_h(cm/hr)$	10.0	10.0 ± 0.4

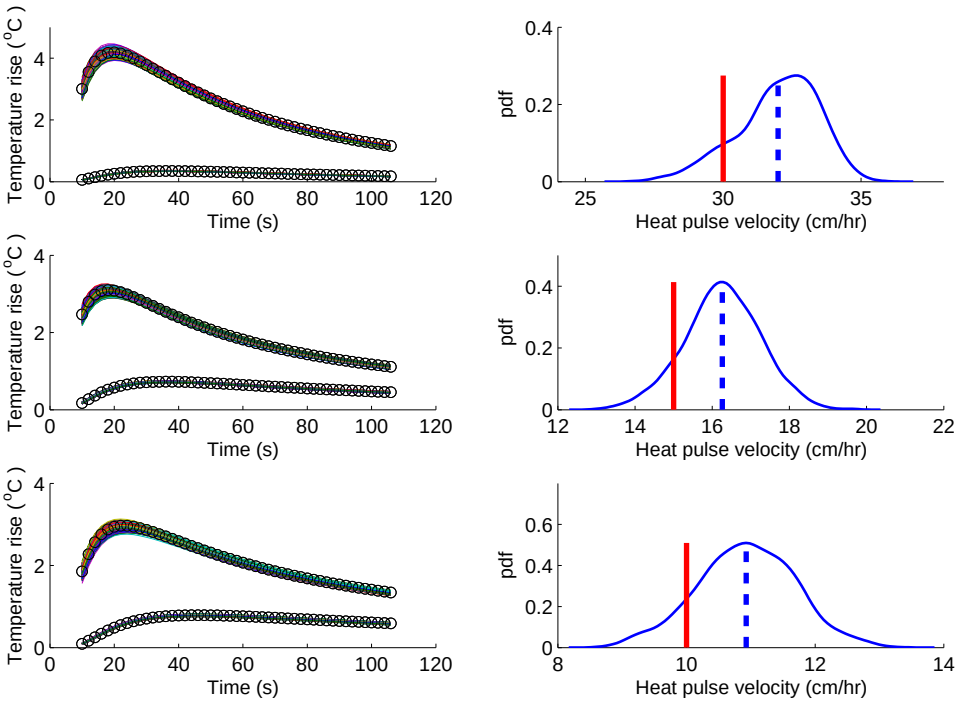

Figure 4.4: Model fitting and statistical distributions of estimated heat pulse velocities for the test case with unknown heat amount, wood density, and wood specific heat capacity. In the left panel, each solid line represents a model fit to the data by a parameter set from the MCMC method. In the right panel, solid vertical lines represent the true heat pulse velocities and dashed vertical lines are the mean values calculated from the posterior distributions.

4.3.2 Applications to field data

Our field tests were conducted on days 221, 234, 251,297, 315 and 329 in year 2007. When the data were used for parameter estimation, Marshall's model was adopted to fit the heat response curves for its simplicity and computational efficiency in repeated sampling required by the MCMC scheme. We accounted for the significant discrepancy between Marshall's idealized model and our more realistic model in calculating early-time temperature increases, by using only the temperature increases measured at times greater than 20s following the heat pulse. The change in mean and standard deviation of the inferred wood thermal diffusivity over test period is shown in Figure 4.3, along with the precipitation and wood temperatures when the tests were conducted. It can be observed that the mean value of wood thermal diffusivity changes over the dry period, while in wet period, it changes only slightly. The uncertainty associated with the inferred thermal diffusivity is steady over the season.

The seasonality of the wood thermal diffusivity can be related to the wood moisture content, wood temperature, and wood porosity [*Steinhagen*, 1977; *Suleiman et al.*, 1999; *Simpson and TenWolde*, 1999]. In general, wood thermal diffusivity decreases with wood moisture content and wood porosity while increases with temperature. The example in Appendix C shows dependence of wood thermal diffusivity on wood moisture content. The temperature effect is found negligible using the calculation procedure outlined in Appendix C. It is demonstrated in Figure 4.5 that wood thermal diffusivity changes more significantly in the dry period than in the wet period, which might be related to shrinkage of tree trunk

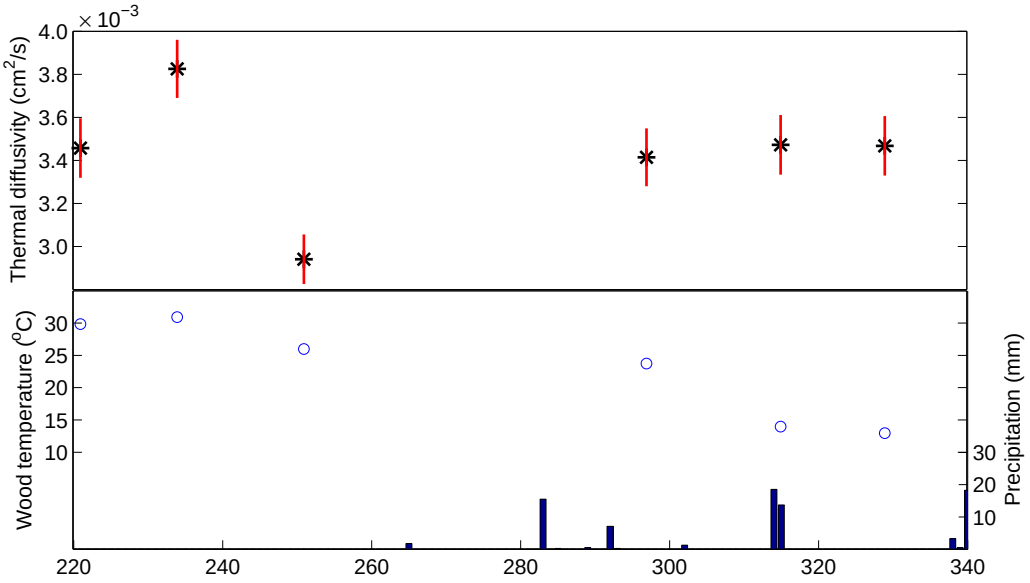

Figure 4.5: Seasonal change of inferred wood thermal diffusivity with precipitation and wood temperature. Means of wood thermal diffusivity are shown in stars and the vertical lines denote the uncertainty range within one standard deviation. Wood temperature is shown in circles and precipitation is shown in bars.

during the prolonged summer drought. However, our data were limited to late growing season and winter, tests covering the entire year may better reveal the complex dependence of wood thermal diffusivity on moisture content and wood temperature. While conducting the heat response experiment, taking core samples of sapwood or recording tree diameters can help to relate the seasonal change of wood thermal diffusivity to those factors. Measuring wood thermal diffusivity on the samples would facilitate model validation as well.

The fitting of the Marshall's model with the calibrated parameters to the data of the first three tests is shown in Figure 4.6. Evidently, the fitting is good despite the discrepancies at the beginning, which is expected because the Marshall's model tends to overestimate the temperature increases at the early times.

Also available in Figure 4.6 are the statistical distributions of the estimated heat pulse velocity associated with each experiment, which show slow flows around 10 cm/hr. Such direct assessment of uncertainties in measured heat pulse velocity by the proposed framework is of great importance in real applications, because it facilitates further uncertainty assessment in applications using the sap flow data, which is discussed in detail in next chapter.

4.4 Conclusions

The heat pulse method is widely used to measure water flux in plants and soil and is valued for its simple instrumentation and easily automated data collection. However, no

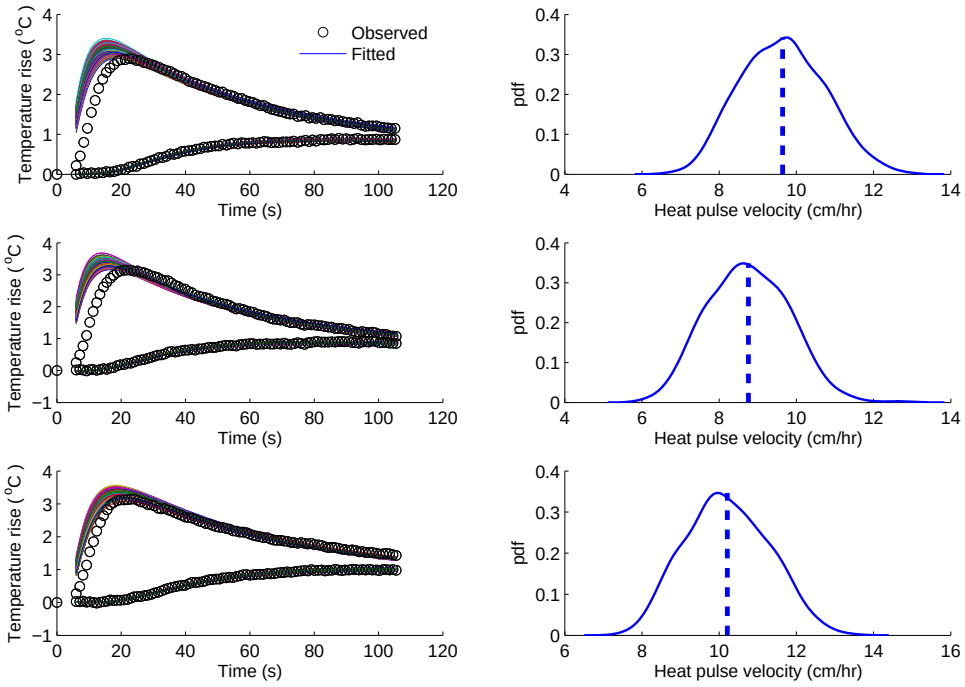

Figure 4.6: Model fitting to data and statistical distributions of estimated heat pulse velocity for the field test.In the left panel, each solid line represents a model fit to the data by a parameter set from the MCMC method. In the right panel, dashed vertical lines are the mean values calculated from the posterior distributions.

systematic, non-destructive calibration procedure has yet been developed to determine the site-specific parameters necessary for calculating sap velocity, i.e., wood thermal diffusivity and probe geometry. In-situ parameter calibration is important in sap flow measurements since the wood diffusivity can be affected by wood moisture content, wood temperature, and wood porosity, and the probes can be misaligned during installation due to drilling difficulties. Such parameter calibration is crucial to obtaining the correct transpiration amount from the sap flow measurements at the plant scale, and consequently affects the up-scaling of water flux modeling of the soil-vegetation-atmosphere continuum.

In this study, we presented a statistical framework to estimate these parameters from in-situ heat response curves collected by the implanted probes of heat ratio apparatus. Conditioned on the heat response data, the parameters were inferred using a Bayesian inversion technique with Markov chain Monte Carlo sampling method. Experiments using synthetic data showed that multiple tests conducted on the same apparatus can be used to obtain reliable statistical distributions of probe geometry as well as wood thermal diffusivity. The uncertainties in the estimated parameters can be reduced by introducing additional knowledge on heat amount input to the system or probe geometry.

The wood thermal diffusivity is known to be affected wood moisture content, wood temperature, and wood porosity. Therefore, addressing seasonality of the wood thermal diffusivity is an important task in sites that experiences contrasting seasons. The parameter estimation framework proposed in this study can be used to obtain such seasonality by conducting heat response experiments over different seasons. In our field site, the wood

thermal diffusivity is found to change more significantly in the dry period than in the wet period. However, the tests were limited to late growing season and winter, we expect that the seasonality of the wood thermal diffusivity can be studied thoroughly by conducting tests over the entire growing season and with complimentary measurements such as taking core samples of sapwood or recording changes in stem diameter.

The primary advantages of the proposed methodology are threefold: (1) it does not require known probe geometry or any further intrusive sampling of sapwood, unlike most other existing work. All the unknown parameters are inverted using the heat response curves collected by the implanted probes. (2) The Bayesian framework enables direct quantification of uncertainty in estimated sap flow velocity, which can further facilitate the uncertainty assessment in water balance study or upscaled water flux involving the sap flow measurements. (3) Empirical factors are used to relate the heat pulse velocity to the ratio of temperature increases under asymmetrical probe alignment and these factors were estimated in this study. With the empirical factors, we were able to model the heat transfer in sapwood with a simple analytical solution derived on the basis of idealized assumptions, which fits the observed heat response curves fairly well.

The proposed methodology is ready to be applied to calibrate existing heat ratio sap flow systems at other sites. It is highly recommended that any study involving sap flow measurements take temperature response curves routinely to improve the data accuracy. It is especially useful when alternative transpiration calibration devices such as lysimeters are not available.

Chapter 5

Monitoring and Modeling Water Dynamics at Plant Scale

5.1 Introduction

Conceptual understanding and mathematical modeling of water dynamics in water-limited ecosystems have been extensively researched in hydrological and meteorological studies. As vegetation plays a critical role in uptaking water from soil and transport it to the atmosphere, many efforts are invested on understanding and modeling the change of water uptake by plant roots subjected to water stress. Hydrological and meteorological studies usually adopt different strategies. Many hydrological studies focus on the root-zone water balance, and the root water uptake is considered as a sink term in water budget [e.g., *Feddes et al.*, 1978, 2001; *Laio et al.*, 2001; *Guswa et al.*, 2002; *Clemente et al.*, 1994;

Feddes and Raats, 2004; *Vrugt et al.*, 2001]. In these studies, a potential transpiration is calculated or specified depending on meteorological conditions and vegetation type, then this amount is distributed to different soil layers based on root density, finally the amount assigned to each layer is modified in presence of water stress, using a piece-wise linear reduction factor similar to Figure 2.1. This approach has also been incorporated into numerical models of soil water and solute transport, such as SWAP [*van Dam et al.*, 2008], and HYDRUS [*Šimünek et al.*, 2005, 2008].

One drawback of the aforementioned approach in hydrological studies is that the calculation of potential ET does not take into account other environmental stresses, such as solar radiation and temperature stresses, even though mechanistic model such as Penman-Monteith (P-M) equation [*Monteith and Unsworth*, 1990] is sometimes implemented (e.g., SWAP model). On the other hand, meteorological studies often assume that plants adjust their transpiration rates under stressed conditions by means of stomatal conductance, and stomata respond to various environmental stresses including solar radiation, temperature, vapor pressure deficit, and soil moisture [*Jones*, 1992]. When P-M equation is applied to a tree canopy or to a larger scale, all the transpiring and non-transpiration leaves are treated as if a big leaf, and the bulk conductance is modeled as a function of environmental stresses, whose effects are assumed to be multiplicative in most empirical studies [*Jarvis and McNaughton*, 1986]. Therefore, there is a need to connect the hydrological studies on soil water dynamics to the meteorological studies on plant transpiration under stressed condition, such that the soil water stress can be distinguished from the other environmental

stresses and the potential plant transpiration can be calculated appropriately.

Another difficulty in soil water dynamics modeling is to specify the boundary conditions. The top boundary condition is relatively easier since it is either infiltration or soil evaporation, which can be measured and modeled. However, the bottom boundary condition is less known due to the difficulty of obtaining measurements. It has been a common practice to assume a free drainage or no flux boundary at bottom [e.g., *Laio et al.*, 2001; *Guswa et al.*, 2002; *Vrugt et al.*, 2001], and these options are provided in models like SWAP and HYDRUS. Nevertheless, the boundary conditions may be more complicated in semi-arid ecosystems as many studies identified groundwater uptake during dry seasons in these ecosystems [*Lubczynski*, 2006; *Lewis and Burgy*, 1964]. The specification of bottom boundary condition should be considered jointly with the way to distribute total potential transpiration to different water sources.

One key to understanding the water dynamics in water-limited is to monitor water use continuously in soil and in plants across different scales. The availability of such data not only helps to understand the mechanisms, but also provides valuable source for developing models and validating them. One primary goal of this study is to present a suite of such water dynamics data, including sap flow, soil moisture, and other auxiliary data, collected over the growing season of 2007 on a single tree in a Californian oak-savanna ecosystem. The concurrent measurements of tree transpiration, root zone soil moisture, and meteorological forcings are used to identify the the functional relations between the tree transpiration and environmental stresses, and to estimate the model parameters using statistical tools. The

comparison of change in soil water volume and tree transpiration amount provides insights to the contribution of soil moisture to tree transpiration over the growing season.

5.2 Materials and Methods

5.2.1 Data acquisition

The specific measurements on an individual tree include multiple soil moisture probes to monitor soil moisture profile vertically and laterally, soil temperature probes for the purpose of energy balance and soil respiration calculations, and sap flow sensors at different tree heights for measuring tree transpiration. A schematic representation of the experimental setup is given in Figure 5.1. The soil moisture in root zone is monitored at depths of 5cm, 20cm and 50cm, respectively, and it is monitored at a depth of 20cm along the dripline and in the open space. Soil temperature is measured at depths of 5cm and 20cm in both the root zone and the open space.

Sap flow probe sets were manufactured following the instructions given in *Burgess et al.* [2001]. We built thermocouple junctions using 36-G copper-constantan wires. They were put inside micro-capillary tubes filled with silicone heat transfer compound and then inserted into capped steel hypodermic needles. Each temperature probe consists of two thermocouple junctions 1.5 cm apart to allow for temperature readings at two radial depths (1.0 and 2.5 cm) into the sapwood. The same type of temperature probes were also used to measure the soil temperature in the root zone and in the open space. The heater probes

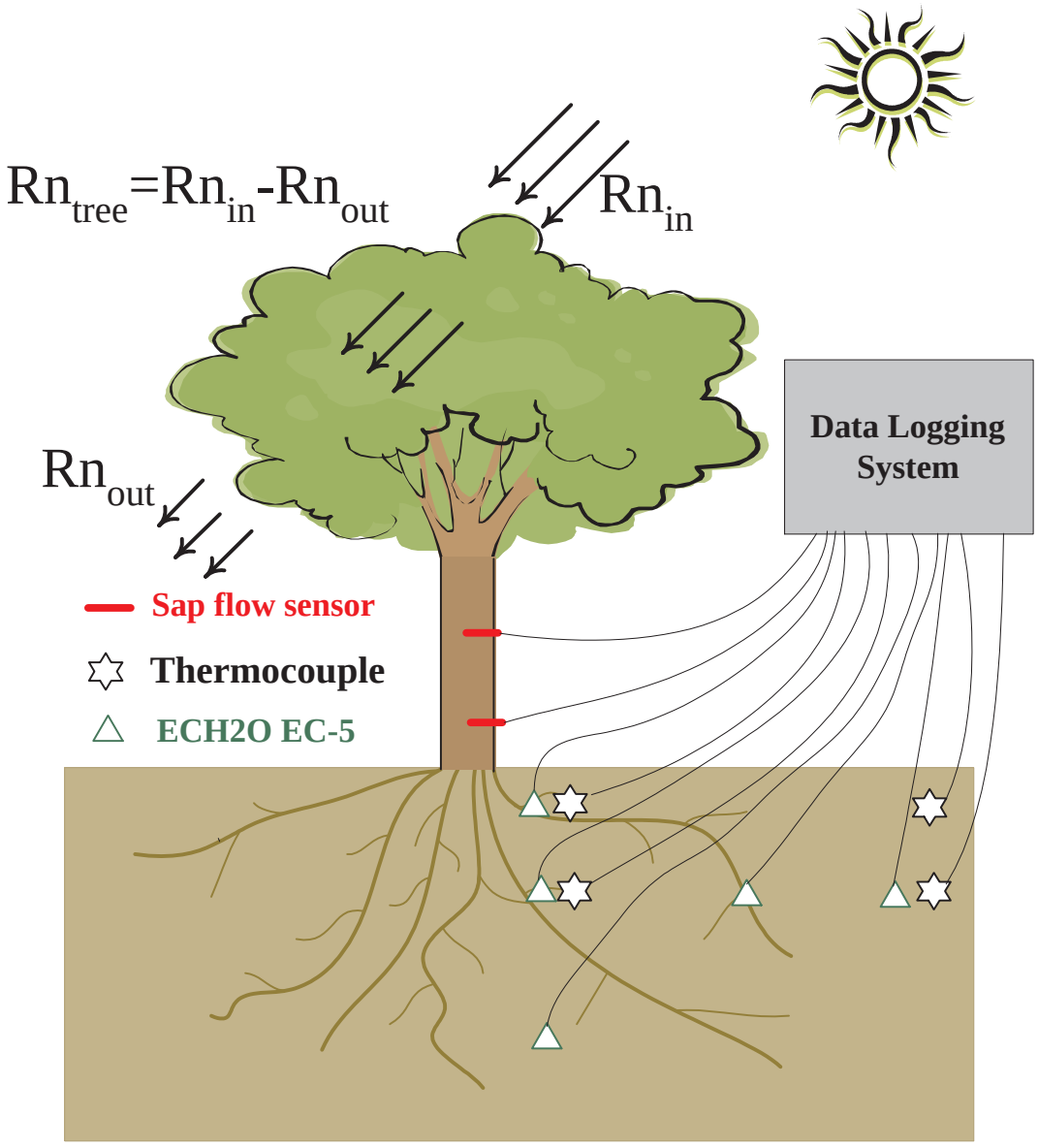

Figure 5.1: Schematic of measurement equipments installed around each experimental tree

were built with coiled 36-G nichrome wire and they were also put inside steel hypodermic needles. All the needle lengths were 3 cm, and the needle hubs for both the thermocouple and heater needle bases were sealed with waterproof epoxy resin.

When installing the sap flow sensors, the outer barks were stripped to ensure xylem contact and a steel drill guide was used to control the distance between probes. The sap flow sensors were installed on the north side of the tree and were insulated with aluminum foil to minimize the influence of diurnal bole temperature fluctuation.

Soil moisture at the site has been monitored using ECH$_2$O EC-5 sensors (Decagon Devices, Inc., Pullman, WA). The sensor measures the dielectric constant of the medium surrounding the probe and outputs a single voltage value, which can be directly related to volumetric soil water content. All the probes were calibrated in our laboratory using soil samples taken from the experimental site. After the samples were dried in oven, they were put into containers with known volume, then different amount of water was added to each container to obtain a range of volumetric soil water contents in field. The soil samples were equilibrated before measurements were taken. For each probe, voltage readings at each soil water content were recorded and a regression analysis were conducted to relate voltage readings and real volumetric soil water content. The calibration curves for the five sensors involved in this study is shown in Figure 5.2, which show linear relationships.

All the sensors were connected to an AM16/32 multiplexer attached to a CR10X data logger (Campbell Scientific Inc., Logan, UT). Data were logged every 30 minutes. A temperature thermistor was attached to the multiplexer for a reference temperature. The

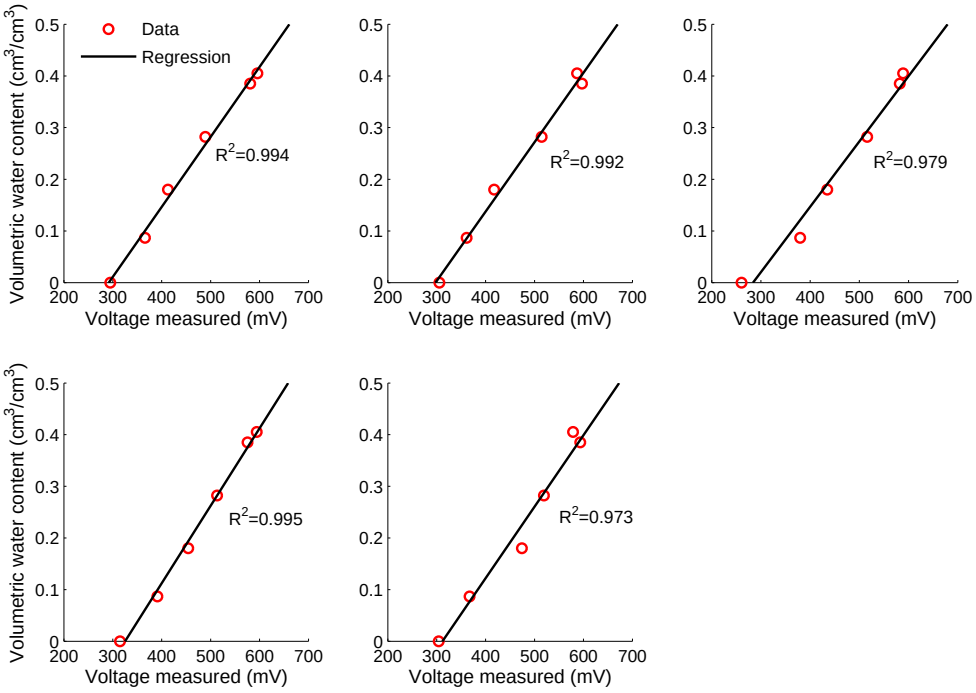

Figure 5.2: Calibration curves for EC-5 sensors

heat pulse was controlled by a relay manufactured at our lab. The program used to collect all the data is attached in Appendix C.

In addition to the continuous measurements taken on the individual tree, predawn(around 5am) and midday(around 2pm) leaf water potentials were measured on two trees on the site in the growing seasons of 2007 and 2008. The measurements were taken every one or two weeks after the last precipitation event in the spring until the trees were dormant. Meteorological measurements (e.g., solar radiation, air temperature, wind speed, precipitation, etc) are available from the overstory eddy covariance tower. The net radiation intercepted by the tree canopy is estimated from the difference between net radiations measured above the tree canopy (by sensors installed on the eddy covariance tower) and under the tree canopy (by sensors installed on a 20-m-long railtrack under tree canopies).

The data of water retention characteristics came from three sources. One of them was estimated from soil texture and bulk density using pedotransfer functions in Rosetta database (USDA, 1999), which adopts van Genuchten model [*van Genuchten*, 1980]. A range of water retention curves was obtained from soil texture and bulk density of 49 samples collected over a 200 m $\times$ 200 m area. Another one was from samples analyzed at the Division of Agriculture and Natural Resources (DANR) Analytical Soils Laboratory, University of California-Davis. The other set of data was obtained by Liukang Xu in 2002, using a WP4 Dewpoint PotentiaMeter (Decagon Devices, Inc., Pullman, WA), which measures water potential of the sample by relating it to the vapor pressure of air in equilibrium with the sample.

5.2.2 Tree transpiration model under water stress

The whole-plant transpiration can be modeled using the following Penman-Monteith equation [*Monteith and Unsworth*, 1990] that assumes the tree canopy as a big leaf,

$$\lambda E = \frac{s(R_n - G) + \rho_a C_p G_a VPD}{s + \gamma(1 + G_a/G_c)} \tag{5.1}$$

where λ is the latent heat of vaporization of water, E is transpiration flux, s is the derivative of the saturated vapor pressure against temperature, R_n is the net radiation intercepted by tree canopy, G is the ground heat flux density, ρ_a is the air density, C_p is the specific heat of air at constant pressure, VPD is the vapor pressure deficit at air temperature, γ is the psychrometric constant, G_a is the bulk aerodynamic conductance for heat and water vapor transfer through the surface layer, and G_c is the bulk canopy conductance for water vapor transfer. G_a can be approximated using friction velocity and wind speed at a reference height, i.e.,

$$G_a = \frac{u_*^2(z)}{u(z)} \tag{5.2}$$

where $u(z)$ and $u_*(z)$ are wind speed and friction velocity at reference height z, respectively.

The bulk canopy conductance (G_c) is generally assumed to be affected by the same factors that control stomatal behavior of a single leaf [*Lhomme*, 2001]. While the mechanistic modeling of stomatal functioning is extremely difficult, empirical models are often adopted to relate stomatal conductance to environmental or physiological factors. One of the most widely used approaches is the Jarvis-type [*Jarvis*, 1976; *Jarvis and McNaughton*, 1986; *Jones*, 1992], which uses a multiplicative form to describe the response of stomata

to environmental factors

$$G_c = G_{cmax} f_1(VPD) \cdot f_2(T_a) \cdot f_3(R_g) \cdot f_4(\theta) \cdots \tag{5.3}$$

where G_{cmax} represents the maximum canopy conductance when none of the controlling factors is limiting. Although the selection of controlling factors may vary among sites, the most extensive collection may be incoming solar radiation (R_g), vapor pressure deficit (VPD), air temperature (T_a), CO_2 concentration and soil water status (volumetric soil water content θ , soil water potential or leaf water potential) [*Lhomme*, 2001]. The forms of controlling functions can be obtained from controlled environmental experiments [*Jones*, 1992], and some examples of typical functions are available in *Jones* [1992] and *Lhomme* [2001].

The empirical form as shown in 5.3 is not accepted as *a priori* in this study. Rather, a statistical approach, alternating conditional expectation (ACE) algorithm [*Breiman and Friedman*, 1985], is adopted to identify the optimal functional dependence of bulk canopy conductance on the environmental factors. ACE identifies the optimal transformation of both dependent and independent variables in multiple regression by maximizing the linear correlation between the transformed dependent and independent variables. The ACE algorithm was first adopted in identifying stress functions at a stand level using eddy covariance measurements by *Kiang* [2002]. Its primary advantage is that it is totally data-driven and does not assume parametric functional forms. More details on this method are available in Appendix E. ACE algorithm enables us to investigate whether a multiplicative form of stress functions as suggested in 5.3 applies to the tree on which data were collected,

and the functional forms can be determined from the transformed variables. Furthermore, ACE identifies if a variable is statistically significant in the regression after transformation, which enables us to decide whether to include a variable in the regression equation.

Once the transformations of the variables are determined, the parameters involved can be estimated through Bayesian inversion technique with MCMC sampling method, as described in Chapter 2 and Chapter 4. This framework was again implemented in the WINBUGS software [*Lunn et al.*, 2000]. More details on the Bayesian inference and MCMC sampling can be found in the Appendix A. Multiple chains of the parameters were simulated in parallel and the modified Gelman-Rubin convergence diagnostic statistics [*Brooks and Gelman*, 1998] were used to test the effective convergence of the samples. Each chain had a sample size of 60,000 parameter sets with the first 50,000 realizations discarded to obtain a stationary distribution. One sample out of every twenty was selected to assure the independence among samples. The resulting pool of samples was used to derive the joint posterior distribution of the parameters, as well as the marginal distribution of each parameter.

5.3 Results and Discussions

5.3.1 Meteorological and water status observations

The continuous measurements on the tree started in March of 2007. Soil moisture data collected since then are presented in Figure 5.3 along with leaf water potential, air

temperature, and precipitation observations in 2007 and 2008. Soil moisture data and air temperature data are averaged values during daytime (8am-6pm). These two years are relatively dry years with below-average precipitation: 403 mm for 2007 and 257 mm for the first 10 months of 2008. Major rainfall events stopped early in 2008 (day 50 compared to day 100-150 in a normal year). The seasonal pattern of air temperature is representative for other meteorological variables, such as solar radiation and vapor pressure deficit. In general, the summer is characterized by high solar radiation, high temperature, and high vapor pressure deficit with essentially no precipitation.The results from two typical days with full leaf foliage during the growing season of 2007 yield an estimation of 50% of net radiation intercepted by the tree canopy during the course of day, and this value is used through the growing season.

The dynamics of soil moisture in wet seasons are mainly controlled by the rainfall events. The magnitude of soil moisture pulse responding to rainfall is damped with depth as expected. Soil moisture at all depths started to decline rapidly right after the rainfall stopped, followed by a slowdown of depletion, which may indicate the onset of soil water stress. In contrast, the decrease in leaf water potential seems to accelerate in summer. This can be explained by the high non-linearity of soil water retention characteristics when soil is getting progressively drier, as shown in Figure 5.4. It is found in 2007 that the soil is wetter in deeper root zone or in places further away from the center of the tree. However, in the summer of 2008, the soil moisture at 50 cm in the root zone is significantly drier than it was in 2007, which might imply change in root water uptake strategy in dry years.

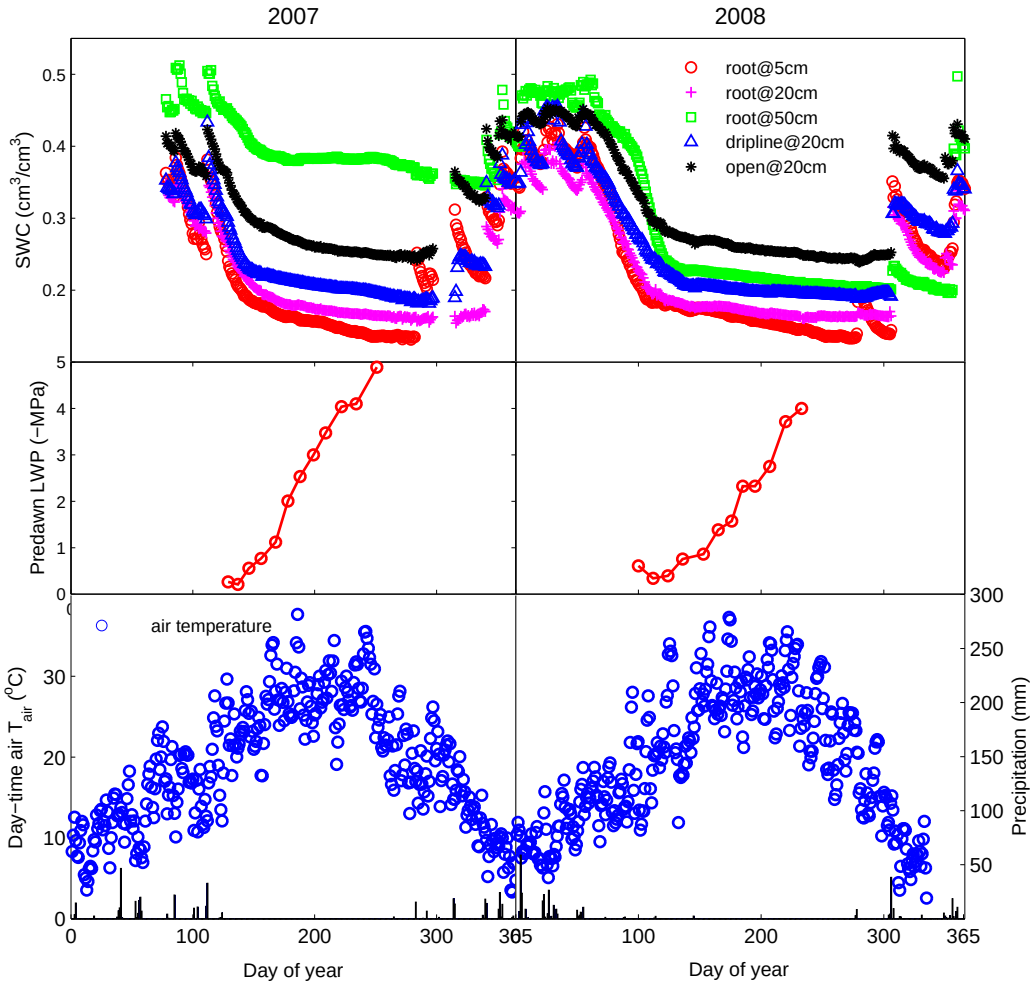

Figure 5.3: Meteorological and water status observations in 2007 and 2008. Soil moisture data and air temperature data are averaged values during daytime (8am-6pm). Predawn leaf water potential (LWP) were averaged from measurements taken at two other trees within the footprint of the overstory eddy covariance tower.

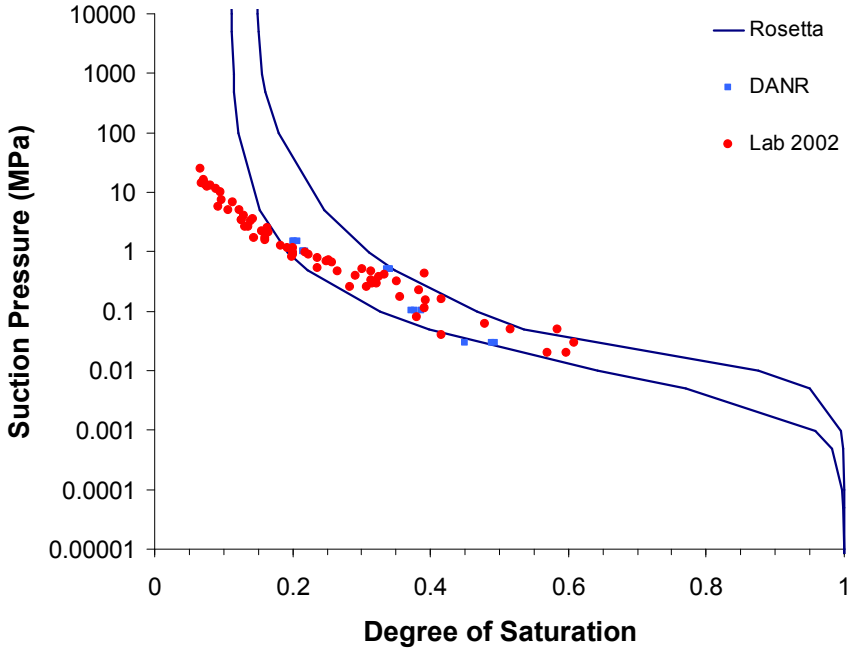

Figure 5.4: Soil water retention curve at experimental site. The range of water retention curves (in solid lines) were obtained from soil texture and bulk density using pedotransfer functions in Rosetta database (USDA, 1999), which adopts van Genuchten model [*van Genuchten*, 1980]. Data points in squares were from samples analyzed at the DANR Analytical Soils Laboratory, University of California-Davis. Data shown in dots were obtained by Liukang Xu in 2002, using a WP4 Dewpoint PotentiaMeter.

5.3.2 Sap flow observations

The heat pulse velocities were calculated from the ratio of temperature increases following the procedures outlined in the previous chapter, with parameters calibrated using heat response curves collected on this specific tree. The data points fluctuate beyond three standard deviations from daily mean were regarded random spikes and were removed from the time series. A snapshot of heat pulse velocities between day 150 and day 160 of 2007 from the bottom set of probes is given in Figure 5.5. The results show that uncertainty in estimated heat pulse velocities increases with velocity magnitude, and the velocities measured at outer section are higher than those measured deeper into the trunk. The data also show non-zero transpiration at night-time, which was also found in another independent study at the site [*Fisher et al.*, 2007].

The heat pulse velocities were corrected for wounding effect with a linear factor adopted from *Burgess et al.* [2001]. The corrected heat pulse velocities were then converted to sap flux density following *Marshall* [1958] and *Burgess et al.* [2001]. The conversion factor is dependent on wood moisture content, which is assumed to vary from 0.5 in wet season to 0.25 in dry season. A detailed description of wood moisture relations of sap flux calculation is given in Appendix D.

Sapwood area is an essential parameter to calculate sap fluxes from the sap flux density. A power-law equation is fitted on sapwood area and tree diameter based on data collected from fresh tree samples cut down by the ranch owner occasionally. The boundary between sapwood and heartwood was identified from the change of color. The data and the regres-

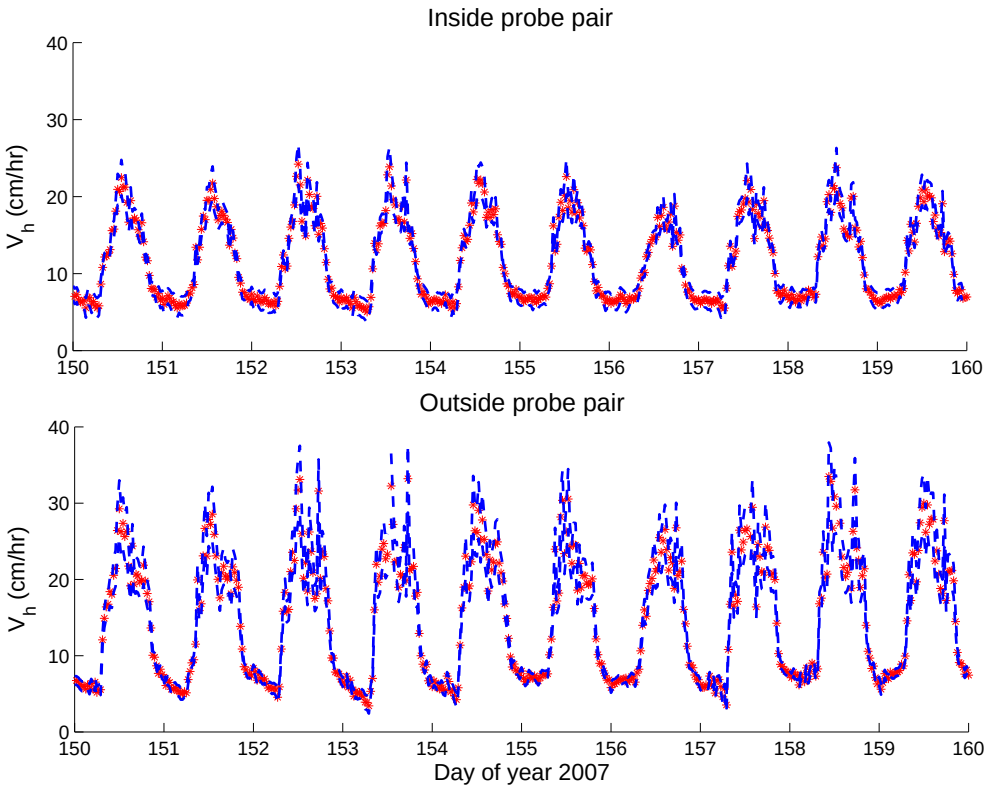

Figure 5.5: Heat pulse velocities measured from the bottom set of sap flow sensors. Inside and outside probe pairs are 2.5 cm and 1 cm into the tree sapwood, respectively. The scatters are mean values calculated from MCMC samples and dashed lines are plus minus two standard deviations from the mean value.

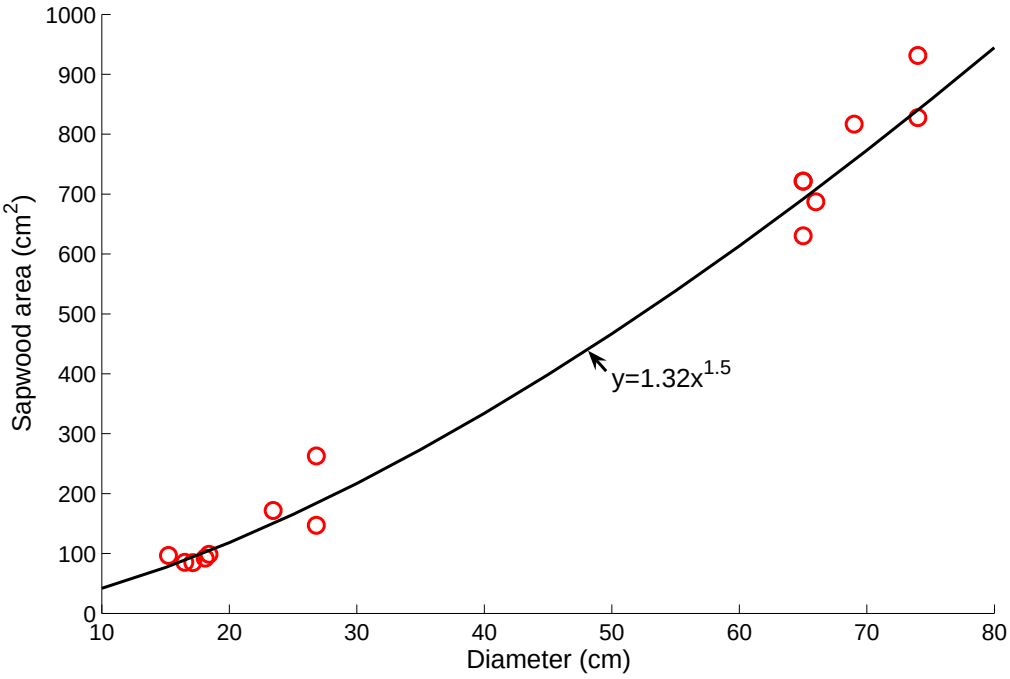

Figure 5.6: Relation between tree diameter and sapwood area. Measurements of diameter and sapwood area were conducted on fresh tree samples cut down by the ranch owner occasionally. The boundary between sapwood and heartwood was identified from the change of color.

sion equation are given in Figure 5.6.

The half-hour sap fluxes were added up during day-time (8am to 6pm) as the daily amount. The night-time transpiration was removed from the study because the mechanism of night-time transpiration is different from that controls day-time transpiration, and P-M equation is not suitable for the conditions with low available energy. Figure 5.7 shows the daily transpiration on leaf area basis in the growing season of 2007. An increasing trend in the early growing season and declining trend in the summer is clearly observed from the data. The transpiration data also responds well to the leaf-out date, around day

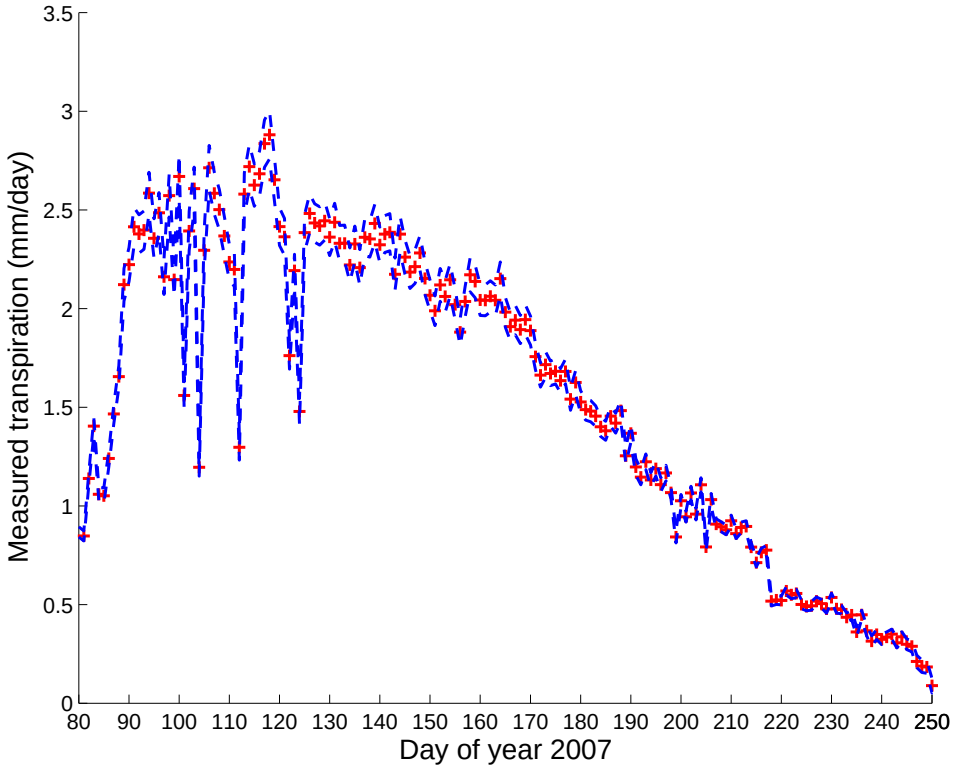

Figure 5.7: Daily transpiration measured from bottom set of sap flow sensors. The scatters are mean values calculated from MCMC samples and dashed lines are two standard deviations from the mean value.

83, in 2007. The total mean transpiration from day 80 to day 250 adds up to 250mm. The uncertainty range is two standard deviations below or above the mean value. The sap flow measurements on the same tree seem problematic in 2008, which may be due to the growing wound effect to the tree. Therefore, these data in 2008 are not used in this study.

5.3.3 Water balance calculation

The total transpiration amount during day-time is compared to the total change in soil water volume on daily and weekly basis in Figure 5.8 and Figure 5.9, respectively. The negative change in soil water volume indicates infiltration during rainfall events. It is observed that after large rainfall events, the depletion in soil water is more than the amount of transpiration, which may be a result of water leakage to the deeper soils and loss through soil evaporation. However, tree transpires much more water than the depletion of soil water during the dry season, which is a strong evidence of tree tapping water from deeper soil and groundwater. This factor must be appropriately accounted for in future soil moisture dynamics modeling work.

5.3.4 Parameter estimation results for bulk canopy conductance

The data used in this study were those collected in water-stressed period (normally includes late spring and entire summer) since the goal is to investigate the effects of soil water stress. Root-density weighted soil moisture was calculated from the vertical profile of soil moisture in the root zone using Eq. (2.5). The soil moisture at the depth of 20 cm was averaged from the two measurements at the same depth in root zone and at the dripline. The exponential model for cumulative distribution of root biomass [*Jackson et al.*, 1996] was again adopted, $P(z)=1-\beta^z$, with z being the depth in centimeters and β value is chosen to be 0.976 for the oak trees. Bulk canopy conductances were inverted from the P-M equation, and ACE transformation were conducted on the inverted G_c on net radiation,

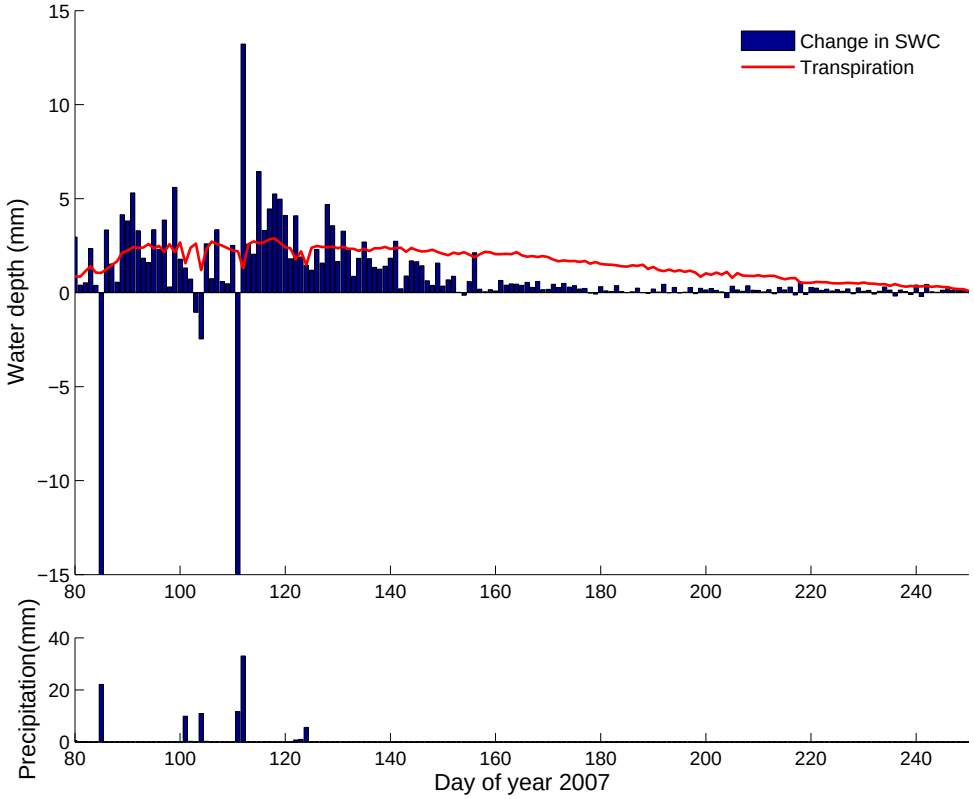

Figure 5.8: Daily water balance. The range of negative change in soil water is cut to enlarge the scale of the plot. The actual values for the two large negative changes are -28mm and -60mm, respectively.

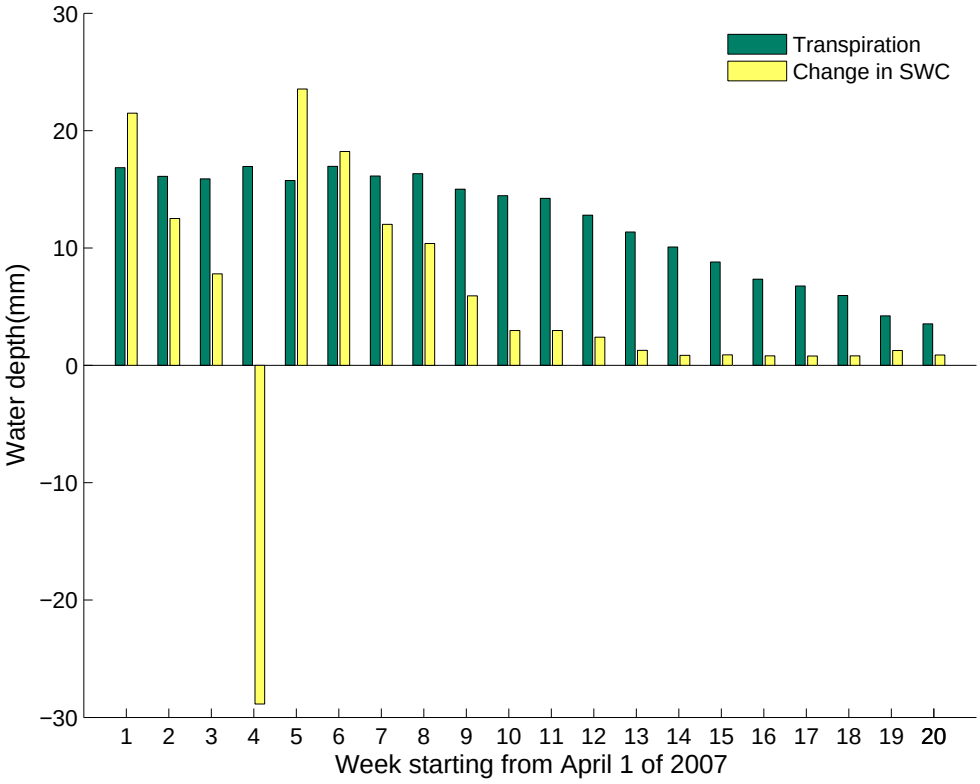

Figure 5.9: Weekly water balance.

air temperature, vapor pressure deficit and soil moisture, using free statistical software R (http://cran.r-project.org/). Effect of CO_2 concentration was omitted since the fluctuation of CO_2 concentration within a year or two may not cause significant change in stomatal functioning. The ACE algorithm identified significant variables to be net radiation, vapor pressure deficit, and soil moisture. The air temperature is not significant mostly because it is closely related to vapor pressure deficit and therefore its effect can be represented by the vapor pressure deficit.

After trying both original and log-transformed variables in ACE procedure, the one with log-transformed G_c and VPD resulted in the highest correlation (R^2 =0.99) between transformed dependent variable and transformed independent variables. The optimal transformations in this case are shown in Figure 5.10. It can be observed that no further transformation is needed for G_c and VPD, and a piece-wise linear transformation works well for the net radiation. As for the soil moisture, the optimal transformation appears to be non-linear. However, a piece-wise linear function can work well for it since identifying the non-linear form is not easy and it may not perform better than the piece-wise linear relation. Therefore, a piece-wise linear function is adopted for the transformations of both net radiation and soil moisture.

The high R^2 value indicates a strong linear relationship between the transformed G_c and transformed VPD, R_n, and SWC. It is also evident in the plot of transformed $\log(G_C)$ on summation of transformed log(VPD), SWC, and R_n. These results imply that a multiplicative form of stress functions on bulk canopy conductance is applicable at the tree level,

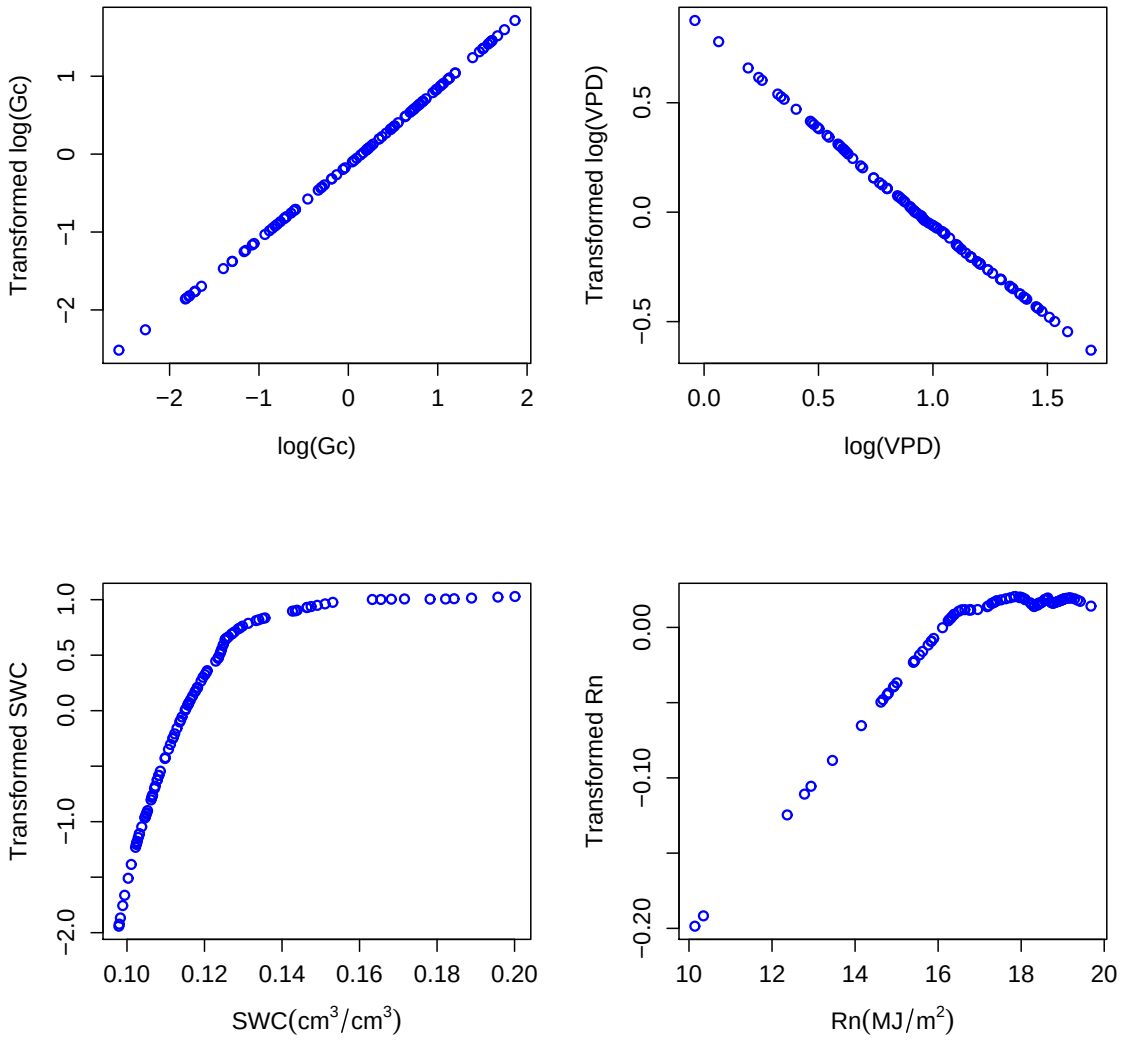

Figure 5.10: Optimal transformations as determined by ACE. The multiple R^2=0.99. The units of G_c and VPD are mm/s and kPa, respectively.

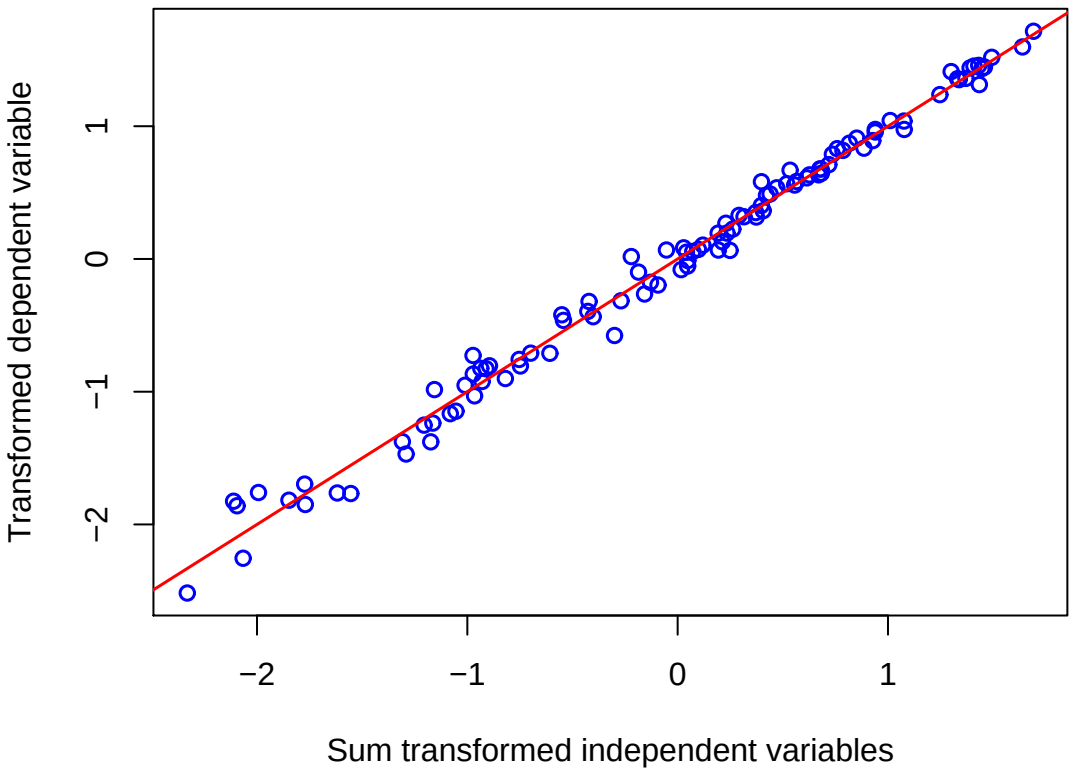

Figure 5.11: Optimal transformation of $\log(G_c)$ vs the sum of the optimal transformations of log(VPD), SWC, and R_n. The solid line is the 1:1 line.

although it is found not appropriate at the stand level [*Kiang*, 2002].

In summary, the following equation can be applied to describe the dependence of G_c on VPD, SWC and R_n,

$$\log(G_c) = b_0 + k_{VPD}\log(VPD) + k_\theta(\theta^* - \theta) + k_R(R_n^* - R_n). \tag{5.4}$$

The parameters in Eq. 5.4 are statistically inverted conditioned on day-time tree transpiration measurements deduced from sap flow method, soil moisture measurements, and

meteorological measurements. The prior distributions assigned to the parameters are

$$
\begin{aligned}
b_0 &\sim \text{uniform}\,(0,\ 2.2) \\
k_{VPD} &\sim \text{uniform}\,(\text{-}1,\ -0.3) \\
\theta^* &\sim \text{uniform}\,(0.12,\ 0.15) \\
k_\theta &\sim \text{uniform}\,(2,\ 100) \\
R_n^* &\sim \text{uniform}\,(15,\ 18) \\
k_R &\sim \text{uniform}\,(\text{-}0.06,\ -0.005)
\end{aligned}
\tag{5.5}
$$

where the unit of G_{cmax} is mm/s and the unit of VPD is kPa. The posterior marginal distributions of the parameters are given in Figure 5.12. Compared to their uniform prior distributions, the posterior distributions are bounded by much narrower ranges with well-defined peak densities, which implies a reduction in uncertainty and the parameters were successfully inferred with the Bayesian framework.

The mean values of fitted transpiration and fitted bulk canopy conductance based on the parameters estimated from the MCMC method are compared to the mean values of observed transpiration and inverted bulk canopy conductance in Figure 5.13. The scatters are observed to distribute closely around the 1:1 line, which indicate good model fitting. Further diagnosis plots in Figure 5.14 show that residuals, which are defined as the difference between the fitted values and observed values, appear to be independent on SWC, net radiation, VPD and air temperature. This suggests a good fitting to the model and there is no other significant factors left out.

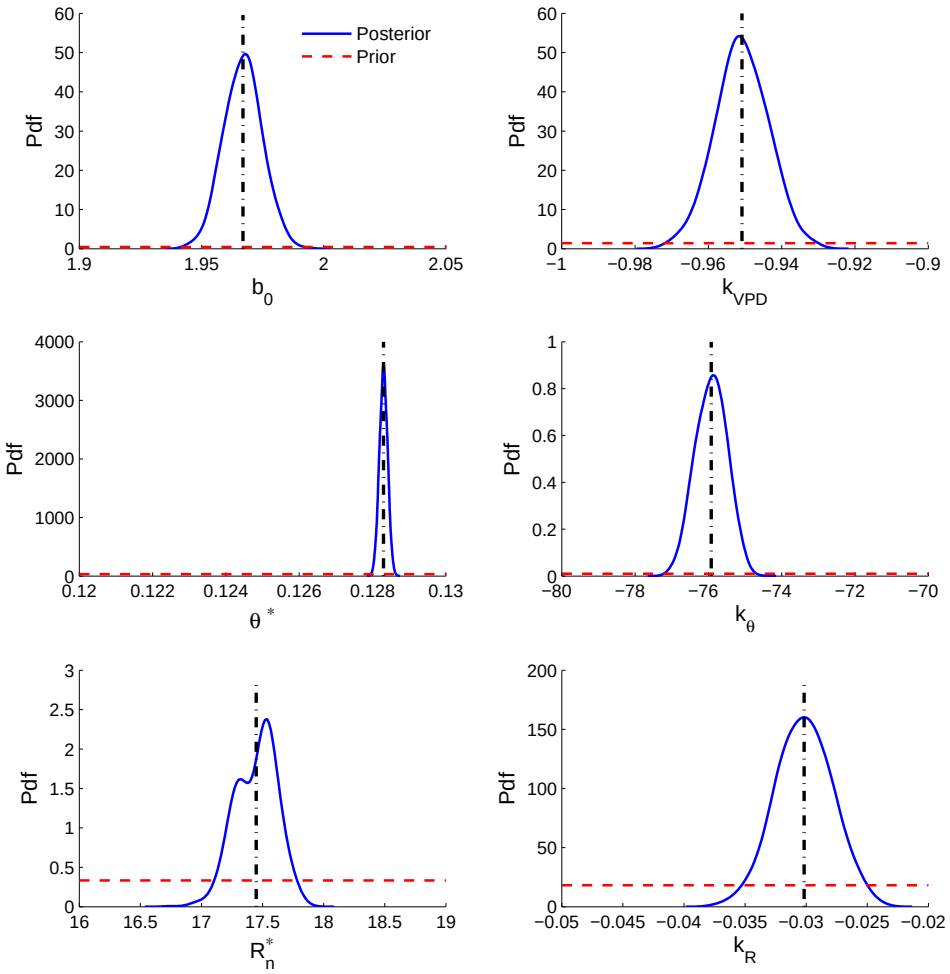

Figure 5.12: Posterior marginal distributions of the G_c stress function parameters. The vertical dashed lines are the mean values calculated from the posterior samples.

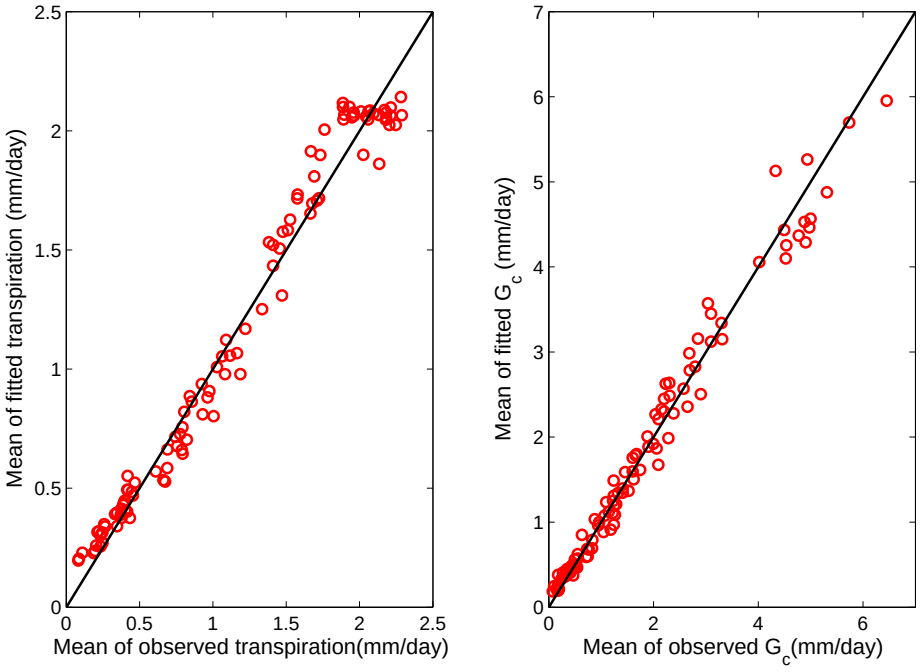

Figure 5.13: Model fitting to observed transpiration and bulk canopy conductance. The solid lines are 1:1 line

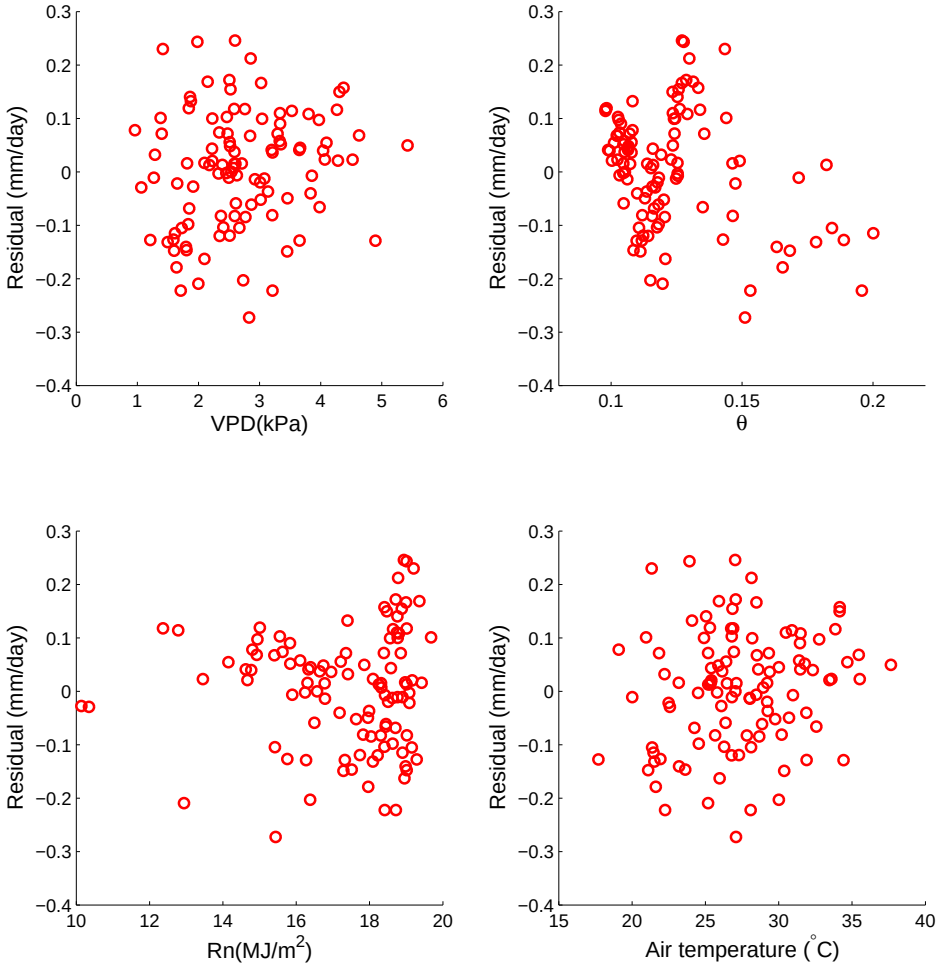

Figure 5.14: Diagnosis plots of residuals versus dependent variables.

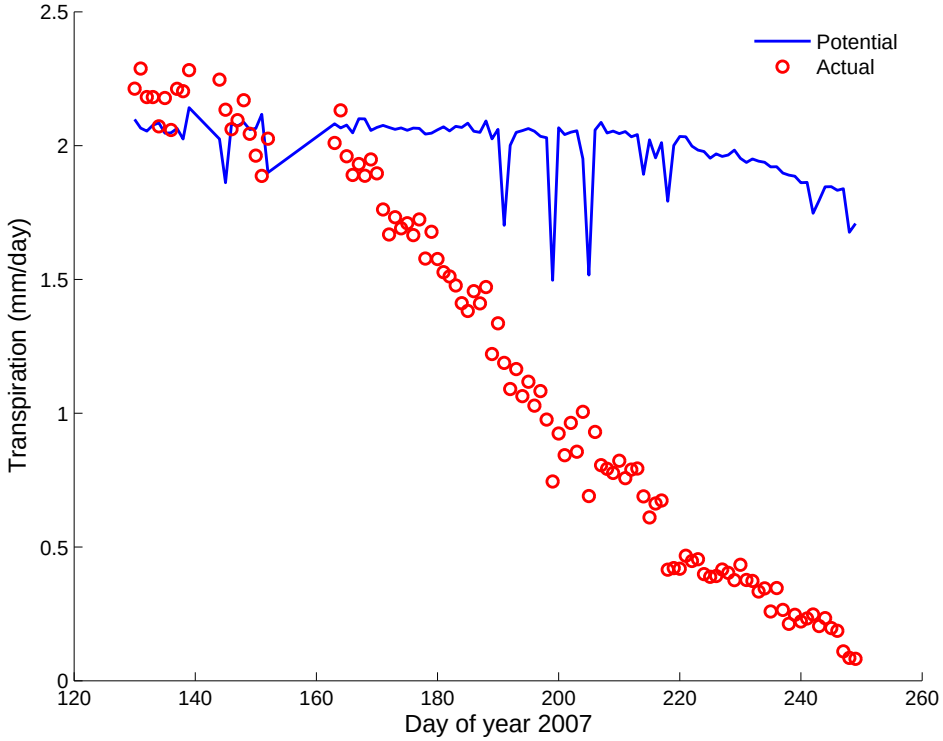

Figure 5.15: Potential transpiration calculated in 2007 compared to measured actual transpiration

With Eq.5.4, the potential tree transpiration can be calculated by setting soil moisture to be θ^* in Eq. 5.4 and then substitute the G_c values into the P-M equation. The potential transpiration calculated for the growing season of 2007 is given in Figure 5.15 for illustration. It is clearly shown in the plot that soil moisture controls the actual tree transpiration in the summer time. This calculated potential transpiration can be incorporated in further soil water dynamics modeling.

5.4 Conclusions

Understanding water dynamics under water stress is important for water resources management in the arid and semi-arid areas. We discussed in this study how plant adjusts transpiration under the stressed conditions, using continuous transpiration and soil moisture data collected at the plant scale in a Californian oak-savanna. The primary goal of this study was to connect the soil water dynamics modeling work in hydrological studies to meteorological studies on tree transpiration responding to environmental stresses including water stress.

The influence of soil and atmospheric water stresses on plant-scale transpiration was investigated through inverting bulk canopy conductance from the Penman-Monteith equation. The functional dependence of bulk canopy conductance on environmental stresses was identified using the ACE algorithm, which is a non-parametric data-driven statistical tool. A multiplicative form of stress functions on tree transpiration is suggested by the data. The parameters involved in the stress functions were inferred using a Bayesian framework with the MCMC sampling method. The calibrated model can then be used to estimate the potential transpiration of a tree, which can be incorporated into future soil dynamics models. The advantages of this procedure are that it accounts for the effects of other environmental stresses, such as vapor pressure deficit and net radiation, on the calculation of potential transpiration, and the parameters inferred using MCMC enables further quantification of uncertainties involved in the calculated potential transpiration.

A water budget calculation at the plant scale was conducted by comparing the tree

transpiration amount with the change in soil water volume in the root zone. It is found that most water transpired in summer comes from deeper soil or groundwater. This is a strong evidence showing the groundwater dependence of the semi-arid ecosystem, and it is an important fact to be considered in further soil water dynamics modeling by specifying appropriate bottom boundary conditions in dry seasons.

This study can improve further root-zone soil dynamics modeling in semi-arid ecosystems by providing a prototype to include environmental stresses in mechanistic calculation of potential tree transpiration rate and by showing evidence of tree tapping water from the deeper soil and groundwater in dry season. Although this study only included data from a single tree, the fundamental methodology can be applied to data collected on other single trees and at larger scales. It is also useful for upscaling tree transpiration and soil water dynamics to larger scales.

Chapter 6

Summary

The purpose of this dissertation work was to improve the conceptual understanding and mathematical modeling of water transport in the soil-plant-atmospheric continuum under drought conditions, from a plant scale to a stand scale. The particular focus was on investigating the regulation of soil moisture on plant water use at both scales, for which models of water stress function were examined and calibrated using water exchange data acquired in a Californian oak-savanna ecosystem.

With the recognition that successful model development and calibration relies on field data, part of the dissertation work was to acquire water use data at plant scale, in addition to on-going data acquisition efforts at the study site, which included water fluxes and meteorological variables measured by the eddy covariance tower and soil moisture measured within the tower footprint. Root zone soil moisture at the plant scale was monitored at various depths and tree transpiration was monitored using sap flow measurements. The

availability of such continuous data sets an example for acquiring water use data at consistent scales and enables the study on how water dynamics at a plant scale respond to water stress. Furthermore, a network of such measurements on representative trees within the ecosystem provides valuable information on upscaling water fluxes in heterogeneous environment.

The amount of transpiration by individual trees were monitored by installing sap flow sensors in the tree trunks. The sapflow velocity was inferred from the ratio of temperature changes measured downstream and upstream of a heating element following the release of a heat pulse. The theoretical basis of sap flow measurements using the heat ratio method was reevaluated in this dissertation. An improved solution to the heat transport process in sapwood was derived by replacing idealized assumptions in Marshall's classic solution with more realistic ones. More specifically, the sapwood was considered bounded porous medium, the line source had finite length, which may or may not extend through the entire sapwood depth, and the heat was released from the line source over a duration. Extensive comparisons on the difference of calculated temperature fields by Marshall's solution and the improved solution revealed that most significant discrepancy occurs around the early times, whereas the difference is negligible at later times. It is therefore recommended that, when employing the heat ratio method, the temperature increases should be measured in late time windows.

Numerical experiments based on the improved analytical solution to the heat transport process in sapwood discovered that the original fundamental equation of the heat ratio

method may result in a significant bias in estimated heat pulse velocity, if the temperature probes are not installed symmetrically around the heating element. Nevertheless, simple modifications to the intercept and slope of original fundamental equation can account for the departure of field experimental setup from the ideal setup. Such modification can also be accurately determined by the probe geometry. This revised equation was adopted in this dissertation to calculate sapflow velocities.

The successful application of heat ratio method depends on obtaining reliable estimation of sapwood thermal diffusivity and probe geometry. To assure the quality of the sap flow measurements acquired from the experimental site, this dissertation study also provided a systematic, non-destructive, and replicable methodology to determine wood thermal diffusivity and probe geometry for the sap flow measurements using the heat ratio apparatus. The estimation of these parameters was conditioned on the time series of temperature increases, i.e., temperature response curves, monitored by the downstream and upstream temperature probes after a heat pulse was released by the central heating probe. The primary advantage of the methodology is that it relies on the information that can be obtained using the installed probes without any further disturbance to the tree. It can also be used to obtain seasonality of wood thermal properties by conducting heat response experiments over different seasons. The proposed methodology is ready to be applied to calibrate existing heat ratio sap flow systems at other sites. It is highly recommended that any study involving sap flow measurements take temperature response curves routinely to improve the data accuracy. It is especially useful when alternative transpiration calibration

devices such as lysimeters are not available.

It was discussed in this dissertation how soil moisture controls actual evapotranspiration at the stand scale using multi-year field observations at the daily time step. The influence of soil moisture on actual ET was investigated through the dependence of the ratio between ET, as measured by the eddy covariance towers, and the potential ET, as approximated by the Priestley-Taylor equation, on the representative soil moisture. The Feddes Model was found to be in agreement with the observed patterns of soil moisture effects on ET regardless of whether the heterogeneous environment of trees and grasses was homogenized or treated as the sum of its individual components. However, the parameters of the Feddes Model varied with time. Grasses have lower θ_2^* and higher θ_1^* during wetter years, whereas trees have the opposite trend, i.e., they start to control ET under moister soil (higher θ_2^*) during wetter years so that their ET persists into drier soil conditions (i.e., lower θ_1^*). This inter-annual variability is primarily driven by variations in the seasonal precipitation distribution pattern from year to year, as well as the responses of various plant functional types to changes in soil water availability. Grasses tend to rapidly use up the available water resources during the wetter years because they have little control over the evaporation, whereas trees are able to control water loss by limiting the xylem hydraulic conductance and by controlling their stomata. This difference in responses can also be a result of change in fine root distributions due to water availability in early seasons.

The selection of representative soil moisture led to considerable difference in the inter-annual variability of model parameters. Among the various averaging schemes tried in

this study, including (1) the arithmetic average of soil moisture measurements at different depths obtained at one location, (2) the arithmetic average of the spatially distributed soil moisture measurements at different depths and (3) the root density weighted average of the distributed soil moisture measurements at different depths, the last scheme yielded the most consistent behavior of the Feddes Model over time. The study demonstrated that distributed sampling of soil moisture is necessary to study the effects of soil moisture availability on ET in open canopy ecosystems. Furthermore, the soil water availability at different depths has a different influence on the total ET depending on the fraction of root biomass present at the corresponding depths. This difference can be accounted for by using the root density weighted average of the vertical soil moisture profile to produce representative soil moisture.

The influence of soil and atmospheric water stresses on plant-scale transpiration was investigated through inverting bulk canopy conductance from Penman-Monteith equation. The functional dependence of bulk canopy conductance on environmental stresses was identified using a non-parametric data-driven statistical tool, ACE method. A multiplicative form of stress functions of tree transpiration was suggested by the data. This form can be used to separate soil water stress from other environmental stresses so that the potential tree transpiration can be appropriately calculated. A water budget calculation at the plant scale found that most water transpired in summer comes from deeper soil or groundwater. This is a strong evidence showing the groundwater dependence of the semi-arid ecosystem, and it is an important fact to be considered in further soil water dynamics modeling by specifying

appropriate boundary conditions in dry seasons. This part of study demonstrated the importance to connect water dynamics studies in both hydrology and meteorology societies. Although both communities are interested in water transport from soil to the atmosphere through plant regulation, hydrology community mostly focuses on the root zone soil water dynamics under drought conditions, whereas the meteorology community is more focused on studying the mechanisms of plants adapting to changing climate. It is beneficial to look into the efforts in both sides in order to better understand and model the water transport process along the soil-plant-atmospheric continuum under drought conditions.

This dissertation also demonstrated the strength of Bayesian inverse modeling technique in dealing with uncertainties arising from various sources in model calibration. This parameter estimation methodology provided a systematic tool to quantify the parameter uncertainties conditioned on field observations. Adopting MCMC sampling scheme enables direct assessment of uncertainties in predictions that use the parameters or any functions of the parameters. The improved ability in model calibration along with the availability of new observations can improve our understanding of the complex mechanisms related to water dynamics under drought conditions and thus enables newer model development in water-controlled ecosystems.

Bibliography

Andrieu, C., N. Freitas, A. Doucet, and J. M. (2003), An introduction to MCMC for machine learning, *Machine Learning*, *50*, 5–43.

Baldocchi, D. (1997), Flux footprints within and over forest canopies, *Boundary-Layer Meteorology*, *85*(2), 273–292.

Baldocchi, D., and T. Meyers (1998), On using eco-physiological, micrometeorological and biogeochemical theory to evaluate carbon dioxide, water vapor and trace gas fluxes over vegetation: A perspective, *Agricultural and Forest Meteorology*, *90*(1-2), 1–25.

Baldocchi, D., et al. (2001), Fluxnet: A new tool to study the temporal and spatial variability of ecosystem-scale carbon dioxide, water vapor, and energy flux densities, *Bulletin of the American Meteorological Society*, *82*(11), 2415–2434.

Baldocchi, D. D., and L. Xu (2007), what limits evaporation from mediterranean oak woodlands - the supply of moisture in the soil, physiological control by plants or the demand by the atmosphere?, *Advances in Water Resources*, *30*(10), 2113–2122.

Baldocchi, D. D., L. K. Xu, and N. Kiang (2004), How plant functional-type, weather, seasonal drought, and soil physical properties alter water and energy fluxes of an oak-grass savanna and an annual grassland, *Agricultural and Forest Meteorology*, *123*(1-2), 13–39.

Barrett, D. J., T. J. Hatton, J. E. Ash, and M. C. Ball (1995), Evaluation of the heat pulse velocity technique for measurement of sap flow in rainforest and eucalypt forest species of south-eastern australia, *Plant Cell and Environment*, *18*(4), 463–469, 0140-7791.

Bell, J. L., L. C. Sloan, and M. A. Snyder (2004), Regional changes in extreme climatic events: A future climate scenario, *Journal of Climate*, *17*(1), 81–87, 23.

Blonquist, J. M., S. B. Jones, and D. A. Robinson (2005), Standardizing characterization of electromagnetic water content sensors: Part 2. evaluation of seven sensing systems, *Vadose Zone Journal*, *4*(4), 1059–1069.

Botter, G., A. Porporato, I. Rodriguez-Iturbe, and A. Rinaldo (2007), Basin-scale soil moisture dynamics and the probabilistic characterization of carrier hydrologic flows: Slow, leaching-prone components of the hydrologic response, *Water Resources Research*, *43*, W02417, doi:10.1029/2006WR005043.

Breiman, L., and J. Friedman (1985), Estimating optimal transformations for multiple regression and correlation, *Journal of the Americal Statistical Association*, *80*(391), 580–598.

Bristow, K. L., G. J. Kluitenberg, and R. Horton (1994), Measurement of soil thermal properties aith a dual-probe heat-pulse technique, *Soil Science Society of America Journal*, *58*(5), 1288–1294.

Bristow, K. L., G. J. Kluitenberg, C. J. Goding, and T. S. Fitzgerald (2001), A small multi-needle probe for measuring soil thermal properties, water content and electrical conductivity, *Computers and Electronics in Agriculture*, *31*(3), 265–280.

Brooks, S. P., and A. Gelman (1998), General methods for monitoring convergence of iterative simulations, *Journal of Computational and Graphical Statistics*, *7*(4), 434–455.

Burgess, S. (2008), Sixth international workshop on xylem sap flow, perth, australia, november 2006, *Plant and Soil*, *305*(1/2), 144 pp.

Burgess, S. S. O. (2006), Measuring transpiration responses to summer precipitation in a mediterranean climate: a simple screening tool for identifying plant water-use strategies, *Physiologia Plantarum*, *127*(3), 404–412.

Burgess, S. S. O., M. A. Adams, N. C. Turner, and C. K. Ong (1998), The redistribution of soil water by tree root systems, *Oecologia*, *115*(3), 306–311, doi: 10.1007/s004420050521.

Burgess, S. S. O., M. A. Adams, and T. M. Bleby (2000), Measurement of sap flow in roots of woody plants: a commentary, *Tree Physiology*, *20*(13), 909–913.

Burgess, S. S. O., M. A. Adams, N. C. Turner, C. R. Beverly, C. K. Ong, A. A. H. Khan,

and T. M. Bleby (2001), An improved heat pulse method to measure low and reverse rates of sap flow in woody plants, *Tree Physiology*, *21*(9), 589–598.

Campbell, G. S., C. Calissendorff, and J. H. Williams (1991), Probe for measuring soil specific heat using a heat-pulse method, *Soil Science of America Journal*, *55*(1), 291–293.

Carslaw, H., and J. Jaeger (1959), *Conduction of Heat in Solids*, 2nd ed., Clarendon Press, Oxford.

Casper, B. B., H. J. Schenk, and R. B. Jackson (2003), Defining a plant's belowground zone of influence, *Ecology*, *84*(9), 2313–2321.

Cermak, J., M. Deml, and M. Penka (1973), New method of sap flow rate determination in trees, *Biologia Plantarum*, *15*(3), 171–178.

Cermak, J., R. Matyssek, and J. Kucera (1993), Rapid response of large, drought-stressed beech trees to irrigation, *Tree Physiology*, *12*(3), 281–290.

Cermak, J., J. Kucera, and N. Nadezhdina (2004), Sap flow measurements with some thermodynamic methods, flow integration within trees and scaling up from sample trees to entire forest stands, *Trees: Structure and Function*, *18*(5), 529–546.

Chandra, S., P. A. Lindsey, and N. L. Bassuk (1994), A gauge to measure the mass flow rate of water in trees, *Plant Cell and Environment*, *17*(7), 867–874.

Chen, Q., D. Baldocchi, P. Gong, and T. Dawson (2008a), Modeling radiation and photosynthesis of a heterogeneous savanna woodland landscape with a hierarchy of model complexity, *Agricultural and Forest Meteorology*, *148*, 1005–1020.

Chen, X., Y. Rubin, S. Ma, and D. Baldocchi (2008b), Observations and stochastic modeling of soil moisture control on evapotranspiration in a californian oak savanna, *Water Resources Research*, *44*, W08409, doi:10.1029/2007WR006646.

Cienciala, E., J. Kucera, and A. Lindroth (1999), Long-term measurements of stand water uptake in swedish boreal forest, *Agricultural and Forest Meteorology*, *98-9*, 547–554, sp. Iss. SI.

Clark, J. S. (2005), Why environmental scientists are becoming bayesians, *Ecology Letters*, *8*(1), 2–14.

Clark, J. S., and A. E. Gelfand (2006), A future for models and data in environmental science, *Trends in Ecology & Evolution*, *21*(7), 375–380.

Clemente, R. S., R. De Jong, H. N. Hayhoe, R. W. D., and M. Hares (1994), Testing and comparison of three unsaturated soil water flow models, *Agricultural Water Management*, *25*(2), 135 – 152, doi:10.1016/0378-3774(94)90041-8.

Cohen, Y., and Y. Li (1996), Validating sap flow measurement in field-grown sunflower and corn, *Journal of Experimental Botany*, *47*(304), 1699–1707.

Cohen, Y., M. Fuchs, and G. C. Green (1981), Improvement of the heat pulse method for determining sap flow in trees, *Plant Cell and Environment*, *4*(5), 391–397.

Cohen, Y., M. Fuchs, V. Falkenflug, and S. Moreshet (1988), Calibrated heat pulse method for determining water uptake in cotton, *Agronomy Journal*, *80*(3), 398–402.

Crainiceanu, C. M., J. R. Stedinger, D. Ruppert, and C. T. Behr (2003), Modeling the us national distribution of waterborne pathogen concentrations with application to cryptosporidium parvum, *Water Resources Research*, *39*(9), 1235, doi: 10.1029/2002WR001664.

Crosbie, R. S., B. Wilson, J. D. Hughes, and C. McCulloch (2007), The upscaling of transpiration from individual trees to areal transpiration in tree belts, *Plant and Soil*, *297*, 223–232.

Dawson, T. E., S. S. O. Burgess, K. P. Tu, R. S. Oliveira, L. S. Santiago, J. B. Fisher, K. A. Simonin, and A. R. Ambrose (2007), Nighttime transpiration in woody plants from contrasting ecosystems, *Tree Physiology*, *27*(4), 561–575.

de Bruin, H. (1983), A model for the priestley-taylor parameter, *Journal of Applied Meteorology*, *22*(4), 572–578.

de Bruin, H. A. R., and J. Q. Keijman (1979), Priestley-taylor evaporation model applied to a large, shallow lake in the netherlands, *Journal of Applied Meteorology*, *18*(7), 898–903.

Detto, M., N. Montaldo, J. D. Albertson, M. Mancini, and G. Katul (2006), Soil

moisture and vegetation controls on evapotranspiration in a heterogeneous mediterranean ecosystem on sardinia, italy, *Water Resources Research*, *42*(8), W08419, doi: 10.1029/2005WR004693.

Dewar, R. C. (2002), The ball-berry-leuning and tardieu-davies stomatal models: synthesis and extension within a spatially aggregated picture of guard cell function, *Plant Cell and Environment*, *25*(11), 1383–1398.

D'Odorico, P., F. Laio, A. Porporato, and I. Rodriguez-Iturbe (2003), Hydrologic controls on soil carbon and nitrogen cycles. ii. a case study, *Advances in Water Resources*, *26*(1), 59–70, doi:10.1016/S0309-1708(02)00095-7.

Duursma, R. A., et al. (2008), Predicting the decline in daily maximum transpiration rate of two pine stands during drought based on constant minimum leaf water potential and plant hydraulic conductance, *Tree Physiology*, *28*(2), 265–276.

Dye, P. J. (1996), Response of eucalyptus grandis trees to soil water deficits, *Tree Physiology*, *16*(1-2), 233–238.

Eamus, D., A. P. O'Grady, and L. Hutley (2000), Dry season conditions determine wet season water use in the wet-dry tropical savannas of northern australia, *Tree Physiology*, *20*(18), 1219–1226.

Eastham, J., and S. A. Gray (1998), A preliminary evaluation of the suitability of sap

flow sensors for use in scheduling vineyard irrigation, *American Journal of Enology and Viticulture*, *49*(2), 171–176.

Esterling, D. R., G. A. Meehl, C. Parmesan, S. A. Changnon, T. R. Karl, and L. O. Mearns (2000), Climate extremes: Observations, modeling, and impacts, *Science*, *289*(5487), 2068–2074, doi:10.1126/science.289.5487.2068.

Feddes, R., and P. Raats (2004), Parameterizing the soil-water-plant root system, in *Unsaturated-zone Modeling - Progress, Challenges and Applications*, edited by R. A. Feddes, G. H. d. Rooij, and J. C. v. Dam, Wageningen UR Frontis Series, pp. 95–141, Kluwer Academic Publishers, Dordrecht, The Netherlands.

Feddes, R., P. Kowalik, , and H. Zaradny (1978), *Simulation of field water use and cropyield: Simulation Monograph*, John Wiley & Sons Inc, New York, USA.

Feddes, R. A., et al. (2001), Modeling root water uptake in hydrological and climate models, *Bulletin of the American Meteorological Society*, *82*(12), 2797–2809.

Federer, C. A. (1979), Soil-plant-atmosphere model for transpiration and availability of soil-water, *Water Resources Research*, *15*(3), 555–562.

Fernandez, J. E., M. J. Palomo, A. Diaz-Espejo, B. E. Clothier, S. R. Green, I. F. Giron, and F. Moreno (2001), Heat-pulse measurements of sap flow in olives for automating irrigation: tests, root flow and diagnostics of water stress, *Agricultural Water Management*, *51*(2), 99–123, 0378-3774.

Fisher, J. B., D. D. Baldocchi, L. Misson, T. E. Dawson, and A. H. Goldstein (2007), What the towers don't see at night: nocturnal sap flow in trees and shrubs at two ameriflux sites in california, *Tree Physiology*, *27*(4), 597–610.

Gelfand, A. E., and A. F. M. Smith (1990), Sampling-based approaches to calculating marginal densities, *Journal of the American Statistical Association*, *85*(410), 398–409.

Gelman, A., J. Carlin, H. Stern, and D. Rubin (1995), *Bayesian Data Analysis*, Texts in Statistical Science, CRC Press, Boca Raton, Fla.

Gemand, S., and D. Gemand (1984), Stochastic relaxation, gibbs distributions and the bayesian restoration of images, *IEEE Transactions on Pattern Analysis and Machine Intelligence*, *6*, 721–741.

Geweke, J. (1989), Bayesian inference in econometric models using monte carlo integration, *Econometrica*, *24*, 1317–1399.

Gollan, T., N. C. Turner, and E. D. Schulze (1985), The responses of stomata and leaf gas-exchange to vapor pressure deficits and soil water content.3. in the sclerophyllous woody species nerium-oleander, *Oecologia*, *65*(3), 356–362.

Granier, A. (1985), Une nouvelle methode pour la mesure du flux de seve brute dans le tronc des arbres, *Annales des Sciences Forestieres*, *42*, 193–200.

Granier, A., P. Biron, N. Breda, J. Pontailler, and B. Saugier (1996), Transpiration of

trees and forest stands: short and long-term monitoring using sapflow methods, *Global Change Biology*, *2*, 265–274.

Green, S., B. Clothier, and B. Jardine (2003), Theory and practical application of heat pulse to measure sap flow, *Agronomy Journal*, *95*(6), 1371–1379.

Green, S. R., M. B. Kirkham, and B. E. Clothier (2006), Root uptake and transpiration: From measurements and models to sustainable irrigation, *Agricultural Water Management*, *86*(1-2), 165–176.

Gribben, R. (1999), On the heat impulse method for deducing sap flow, *Journal of Applied Mathematics & Decision Sciences*, *3*(2), 171–187.

Guswa, A. J., M. A. Celia, and I. Rodriguez-Iturbe (2002), Models of soil moisture dynamics in ecohydrology: A comparative study, *Water Resources Research*, *38*(9), 1166, doi:10.1029/2001WR000826.

Hastings, W. K. (1970), Monte carlo sampling mehtods using markov chains and their applications, *Biometrika*, *87*, 97–109.

Hikaru, K. (2005), Forest categorization according to dry-canopy evaporation rates in the growing season: comparison of the priestley-taylor coefficient values from various observation sites, *Hydrological Processes*, *19*(19), 3873–3896, doi:10.1002/hyp.5987.

Hopmans, J., and K. Bristow (2002), Current capabilities and future needs of root water

and nutrient uptake modeling, in *ADVANCES IN AGRONOMY*, vol. 77, pp. 103–183, Elsevier.

Hou, Z. S., and Y. Rubin (2005), On minimum relative entropy concepts and prior compatibility issues in vadose zone inverse and forward modeling, *Water Resources Research*, *41*(12), W12425, doi:10.1029/2005WR004082.

Ishikawa, C. M., and C. S. Bledsoe (2000), Seasonal and diurnal patterns of soil water potential in the rhizosphere of blue oaks: evidence for hydraulic lift, *Oecologia*, *125*(4), 459–465, doi:10.1007/s004420000470.

Jackson, R. B., J. Canadell, J. R. Ehleringer, H. A. Mooney, O. E. Sala, and E. D. Schulze (1996), A global analysis of root distributions for terrestrial biomes, *Oecologia*, *108*(3), 389–411.

Jarvis, P. (1976), The interpretation of the variations in leaf water potential and stomatal conductance found in canopies in the field, *Philosophical Transactions of the Royal Society, London B*, *273*, 593–610.

Jarvis, P., and K. McNaughton (1986), Stomatal control of transpiration: Scaling up from leaf to region, pp. 1 – 49, Academic Press, doi:10.1016/S0065-2504(08)60119-1.

Jones, H. G. (1992), *Plants and Microclimate: A Quantitative Approach to Environmental Plant Physiology*, 2nd ed., Cambridge University Press, Cambridge, UK.

Katul, G., R. Leuning, and R. Oren (2003”), Relationship between plant hydraulic and

biochemical properties derived from a steady-state coupled water and carbon transport model, *Plant Cell and Environment*, *26*(3), 339–350.

Kiang, N. (2002), Savannas and seasonal drought: the landscape-leaf connection through optimal stomatal control, Ph.D. thesis, University of California, Berkeley, California.

Kim, J., Q. Guo, D. D. Baldocchi, M. Y. Leclerc, L. Xu, and H. P. Schmid (2006), Upscaling fluxes from tower to landscape: Overlaying flux footprints on high-resolution (ikonos) images of vegetation cover, *Agricultural and Forest Meteorology*, *136*(3-4), 132–146.

Kluitenberg, G. J., and J. M. Ham (2004), Improved theory for calculating sap flow with the heat pulse method, *Agricultural and Forest Meteorology*, *126*(1-2), 169–173.

Knapp, A. K., et al. (2002), Rainfall variability, carbon cycling, and plant species diversity in a mesic grassland, *Science*, *298*(5601), 2202–2205, doi:10.1126/science.1076347.

Kurz-Besson, C., et al. (2006), Hydraulic lift in cork oak trees in a savannah-type mediterranean ecosystem and its contribution to the local water balance, *Plant and Soil*, *282*(1-2), 361–378.

Lagergren, F., and A. Lindroth (2002), Transpiration response to soil moisture in pine and spruce trees in sweden, *Agricultural and Forest Meteorology*, *112*(2), 67–85.

Laio, F., A. Porporato, L. Ridolfi, and I. Rodriguez-Iturbe (2001), Plants in water-controlled ecosystems: active role in hydrologic processes and response to water stress: II. probabilistic soil moisture dynamics, *Advances in Water Resources*, *24*(7), 707–723.

Lefever, R., and O. Lejeune (1997), On the origin of tiger bush, *Bulletin of Mathematical Biology*, *59*(2), 263–294.

Lejeune, O., P. Courteron, and R. Lefever (1999), Short range co-operativity competing with long range inhibition explains vegetation patterns, acta oecol, *Journal of International Ecology*, *20*(3), 171–183.

Lewis, D. C., and R. H. Burgy (1964), Relationship between aak tree roots and groundwater in fractured rock as determined by tritium tracing, *Journal of Geophysical Research*, *69*(12), 2579–2588.

Lhomme, J.-P. (2001), Stomatal control of transpiration: Examination of the jarvis-type representation of canopy resistance in relation to humidity, *Water Resources Research*, *37*(3), 689–699.

Lubczynski, M. (2006), Groundwater fluxes in arid and semi-arid environments, in *Groundwater and Ecosystems*, p. 225.

Lunn, D., A. Thomas, N. Best, and D. Spiegelhalter (2000), Winbugs – a bayesian modelling framework: concepts, structure, and extensibility, *Statistics and Computing, 10:325–337.*, *10*, 325–337.

Ma, S., D. D. Baldocchi, L. Xu, and T. Hehn (2007), Inter-annual variability in carbon dioxide exchange of an oak/grass savanna and open grassland in california, *Agricultural and Forest Meteorology*, *147*(3-4), 157–171, doi:10.1016/j.agrformet.2007.07.008.

Mahfouf, J. F., C. Ciret, A. Ducharne, P. Irannejad, J. Noilhan, Y. Shao, P. Thornton, Y. Xue, and Z. L. Yang (1996), Analysis of transpiration results from the rice and pilps workshop, *Global and Planetary Change*, *13*(1-4), 73–88.

Marshall, D. C. (1958), Measurement of sap flow in conifers by heat transport, *Plant Physiology*, *33*(6), 385–396.

McNaughton, K. G., and T. W. Spriggs (1986), A mixed-layer model for regional evaporation, *Boundary-Layer Meteorology*, *34*(3), 243–262.

Metropolis, N., A. W. Rosenbluth, A. H. Teller, and E. Teller (1953), Equations of state calculations by fast computating machine, *Journal of Chemical Physics*, *21*, 1087–1091.

Miller, G. R., D. D. Baldocchi, B. E. Law, and M. T. (2007), An analysis of soil moisture dynamics using multi-year data from a network of micrometeorological observation sites, *Advances in Water Resources*, *30*(5), 1065–1081, doi: 10.1016/j.advwatres.2006.10.002.

Milly, P. C. D. (1993), An analytical solution of the stochastic storage problem applicable to soil water, *Water Resources Research*, *29*(11), 3755–3758.

Monteith, J., and M. Unsworth (1990), *Principles of Environmental Physics*, 2nd ed., Butterworth-Heinemann, Oxford, UK.

Nadezhdina, N., J. Cermak, J. Gasparek, V. Nadezhdin, and A. Prax (2006), Vertical and

horizontal water redistribution in norway spruce (picea abies) roots in the moravian upland, *Tree Physiology*, *26*(10), 1277–1288.

National Research Council (NRC) (2008), *Integrating Multiscale Observations of U.S. Waters*, National Academies Press, Washington, D.C.

Oren, R., N. Phillips, B. E. Ewers, D. E. Pataki, and J. P. Megonigal (1999), Sap-flux-scaled transpiration responses to light, vapor pressure deficit, and leaf area reduction in a flooded taxodium distichum forest, *Tree Physiology*, *19*(6), 337–347.

Paruelo, J. M., and O. E. Sala (1995), Water losses in the patagonian steppe - a modeling approach, *Ecology*, *76*(2), 510–520.

Porporato, A., P. D'Odorico, F. Laio, and I. Rodriguez-Iturbe (2003), Hydrologic controls on soil carbon and nitrogen cycles. i. modeling scheme, *Advances in Water Resources*, *26*(1), 45–58, doi:10.1016/S0309-1708(02)00094-5.

Porporato, A., E. Daly, and I. Rodriguez-Iturbe (2004), Soil water balance and ecosystem response to climate change, *American Naturalist*, *164*(5), 625–632, 35.

Poyatos, R., P. Llorens, J. Pinol, and C. Rubio (2008), Response of scots pine (pinus sylvestris l.) and pubescent oak (quercus pubescens willd.) to soil and atmospheric water deficits under mediterranean mountain climate, *Annals of Forest Science*, *65*(3), 306p1–306p13.

Priestley, C., and R. J. Taylor (1972), On the assessment of surface heat-flux and evaporation using large-scale parameters, *Monthly Weather Review*, *100*(2), 81–92.

Rana, G., and N. Katerji (2000), Measurement and estimation of actual evapotranspiration in the field under mediterranean climate: a review, *European Journal of Agronomy*, *13*(2-3), 125–153.

Reis, D. S., and J. R. Stedinger (2005), Bayesian MCMC flood frequency analysis with historical information, *Journal of Hydrology*, *313*(1-2), 97–116, sp. Iss. SI.

Ren, T., G. J. Kluitenberg, and R. Horton (2000), Determining soil water flux and pore water velocity by a heat pulse technique, *Soil Science Society of America Journal*, *64*(2), 552–560.

Rietkerk, M., S. C. Dekker, P. C. de Ruiter, and J. van de Koppel (2004), Self-organized patchiness and catastrophic shifts in ecosystems, *Science*, *305*(5692), 1926–1929, doi: 10.1126/science.1101867.

Rodriguez-Iturbe, I. (2000), Ecohydrology: A hydrologic perspective of climate-soil-vegetation dynamics, *Water Resources Research*, *36*(1), 3–10.

Rodriguez-Iturbe, I., P. A., F. Laio, and L. Ridolfi (2001a), Intensive or extensive use of soil moisture: plant strategies to cope with stochastic water availability, *Geophysical Research Letter*, *28*(23), 2295–4498.

Rodriguez-Iturbe, I., A. Porporato, F. Laio, and L. Ridolfi (2001b), Plants in water-controlled ecosystems: active role in hydrologic processes and response to water stress - I. scope and general outline, *Advances in Water Resources*, *24*(7), 695–705.

Rubin, Y. (2003), *Applied Stochastic Hydrogeology*, Oxford University Press, Oxford, UK.

Saugier, B., A. Granier, J. Pontailler, E. Dufrene, and D. Baldocchi (1997), Transpiration of a boreal pine forest measured by branch bag, sap flow and micrometeorological methods, *Tree Physiology*, *17*, 511–519.

Scales, J. A., and R. Snieder (1997), To bayes or not to bayes, *Geophysics*, *62*(4), 1045–1046.

Scholes, R. J., and S. R. Archer (1997), Tree-grass interactions in savannas, *Annual Review of Ecology and Systematics*, *28*(1), 517–544.

Scott, R. L., W. L. Cable, and K. R. Hultine (2008), The ecohydrologic significance of hydraulic redistribution in a semiarid savanna, *Water Resources Research*, *44*(2), W02440, doi:10.1029/2007WR006149.

Service, R. F. (2004), Water resources: As the West goes dry, *Science*, *303*(5661), 1124–1127, doi:10.1126/science.303.5661.1124.

Settin, T., G. Botter, I. Rodriguez-Iturbe, and A. Rinaldo (2007), Numerical studies on soil moisture distributions in heterogeneous catchments, *Water Resources Research*, *43*, W05425, doi:10.1029/2006WR005737.

Simpson, W., and A. TenWolde (1999), Physical properties and moisture relations of wood wood handbook : wood as an engineering material, *General technical report FPL GTR-113*, USDA Forest Service, Forest Products Laboratory, Madison, WI.

Sketchley, H. R. (1965), Soil survey of the amador area, California, *Tech. rep.*, Soil Conservation Service, Department of Agriculture.

Smith, A. F. M., and G. O. Roberts (1993), Bayesian computation via the gibbs sampler and related markov chain monte carlo methods, *Journal of the Royal Statistical Society*, *55*(1), 3–23.

Smith, D. M., and S. J. Allen (1996), Measurement of sap flow in plant stems, *Journal of Experimental Botany*, *47*(305), 1833–1844.

Smith, T. J., and L. A. Marshall (2008), Bayesian methods in hydrologic modeling: A study of recent advancements in markov chain monte carlo techniques, *Water Resources Research*, *44*, W00B05, doi:10.1029/2007WR006705.

Spittlehouse, D. L., and T. A. Black (1981), A growing-season water-balance model applied to 2 douglas-fir stands, *Water Resources Research*, *17*(6), 1651–1656.

Steinhagen, H. P. (1977), Thermal conductive properties of wood, green or dry, from $-40^o c$ to $100^o c$: a literature review, *Tech. Rep. FPL-9*, USDA Forest Service, Madison, WI.

Suleiman, B. M., J. Larfeldt, L. B., and M. Gustavsson (1999), Thermal conductiv-

ity and diffusivity of wood, *Wood Science and Technology*, *33*(6), 465–473, doi: 10.1007/s002260050130.

Swanson, R. H. (1994), Significant historical developments in thermal methods for measuring sap flow in trees, *Agricultural and Forest Meteorology*, *72*(1-2), 113–132.

Swanson, R. H., and R. Lee (1966), Measurement of water movement from and through shrubs and trees, *Journal of Forestry*, *64*(3), 187–190, 0022-1201.

Swanson, R. H., and D. W. A. Whitfield (1981), A numerical analysis of heat pulse velocity: Theory and practice, *Journal of Experimental Botany*, *32*(126), 221–239.

Tang, J., and D. D. Baldocchi (2005), Spatial-temporal variation in soil respiration in an oak-grass savanna ecosystem in california and its partitioning into autotrophic and heterotrophic components, *Biogeochemistry*, *73*(1), 183–207.

Teuling, A. J., S. I. Seneviratne, C. Williams, and P. A. Troch (2006), Observed timescales of evapotranspiration response to soil moisture, *Geophysical Research Letters*, *33*(23), 5.

Tierney, L., and A. Mira (1999), Some adaptive monte carlo methods for bayesian inference, *Statistics in Medicine*, *18*, 2507–2515.

Tuzet, A., A. Perrier, and R. Leuning (2003), A coupled model of stomatal conductance, photosynthesis and transpiration, *Plant Cell and Environment*, *26*(7), 1097–1116.

Tyree, M. T., S. D. Davis, and H. Cochard (1994), Biophysical perspectives of xylem evolution - is there a tradeoff of hydraulic efficiency for vulnerability to dysfunction, *Iawa Journal*, *15*(4), 335–360.

van Dam, J. C., P. Groenendijk, R. F. Hendriks, and J. G. Kroes (2008), Advances of Modeling Water Flow in Variably Saturated Soils with SWAP, *Vadose Zone Journal*, *7*(2), 640–653, doi:10.2136/vzj2007.0060.

van Genuchten, M. (1980), A closed-form equation for predicting the hydraulic conductivity of unsaturated soils, *Soil Science Society of America Journal*, *44*, 892–898.

Venables, W., and B. Ripley (2003), *Modern Applied Statistics with S*, 4th ed., Springer, Heidelberg, Germany.

Vrugt, J. A., J. W. Hopmans, and J. Šimünek (2001), Calibration of a two-dimensional root water uptake model, *Soil Sci Soc Am J*, *65*(4), 1027–1037.

Šimünek, J., M. T. van Genuchten, and M. Sejna (2005), The HYDRUS-1D software package for simulating the one-dimensional movement of water, heat, and multiple solutes in variably-saturated media. Version 3.0, HYDRUS Software Series 1, *Tech. rep.*, Department of Environmental Sciences,University of California Riverside, Riverside.

Šimünek, J., M. T. van Genuchten, and M. Sejna (2008), Development and applications of the HYDRUS and STANMOD software packages and related codes, *Vadose Zone Journal*, *7*(2), 587–600, doi:10.2136/vzj2007.0077.

Wan, C., I. Yilmaz, and R. E. Sosebee (2002), Seasonal soil-water availability influences snakeweed root dynamics, *Journal of Arid Environments*, *51*(2), 255.

Wang, Q. J., T. E. Ochsner, and R. Horton (2002), Mathematical analysis of heat pulse signals for soil water flux determination, *Water Resources Research*, *38*(6), doi: 10.1029/2001WR001089, 1091.

West, A. G., K. R. Hultine, J. S. Sperry, S. E. Bush, and J. R. Ehleringer (2008), Transpiration and hydraulic strategies in a pinon-juniper woodland, *Ecological Applications*, *18*(4), 911–927.

Whitley, R., M. Zeppel, N. Armstrong, C. Macinnis-Ng, I. Yunusa, and D. Eamus (2008), A modified jarvis-stewart model for predicting stand-scale transpiration of an australian native forest, *Plant and Soil*, *305*(1-2), 35–47.

Williams, C. A., and J. D. Albertson (2004), Soil moisture controls on canopy-scale water and carbon fluxes in an african savanna, *Water Resources Research*, *40*(9), W09302, doi:10.1029/2004WR003208.

Williams, C. A., and J. D. Albertson (2005), Contrasting short- and long-timescale effects of vegetation dynamics on water and carbon fluxes in water-limited ecosystems, *Water Resources Research*, *41*(6), W06005, doi:10.1029/2004WR003750.

Wilson, K. B., P. J. Hanson, P. J. Mulholland, D. D. Baldocchi, and S. D. Wullschleger (2001), A comparison of methods for determining forest evapotranspiration and its com-

ponents: sap-flow, soil water budget, eddy covariance and catchment water balance, *Agricultural and Forest Meteorology*, *106*(2), 153–168.

Woodbury, A. D., and Y. Rubin (2000), A full-bayesian approach to parameter inference from tracer travel time moments and investigation of scale effects at the cape cod experimental site, *Water Resources Research*, *36*(1), 159–171.

Woodbury, A. D., and T. J. Ulrych (1993), Minimum relative entropy - forward probabilistic modeling, *Water Resources Research*, *29*(8), 2847–2860.

Xu, L., and D. Baldocchi (2003), Seasonal trends in photosynthetic parameters and stomatal conductance of blue oak (quercus douglasii) under prolonged summer drought and high temperature, *Tree Physiology*, *23*, 865–877.

Yokozawa, M., Y. Kubota, and T. Hara (1998), Effects of competition mode on spatial pattern dynamics in plant communities, *Ecological Modelling*, *106*(1), 1–16.

Appendix A

Parameter estimation for the Feddes Model

A.1 Parameter Estimation Method

The basis of our parameter estimation approach is the Bayes' Theorem given by:

$$f_{\mathbf{M}|\mathbf{D}}(\mathbf{m}|\mathbf{d}^*) = \frac{f_{\mathbf{D}|\mathbf{M}}(\mathbf{d}^*|\mathbf{m})\, f_{\mathbf{M}}(\mathbf{m})}{f_{\mathbf{D}}(\mathbf{d}^*)} = \frac{f_{\mathbf{D}|\mathbf{M}}(\mathbf{d}^*|\mathbf{m})\, f_{\mathbf{M}}(\mathbf{m})}{\int\limits_{\mathbf{m}} f_{\mathbf{D}|\mathbf{M}}(\mathbf{d}^*|\mathbf{m})\, f_{\mathbf{M}}(\mathbf{m})\, d^p\mathbf{m}} \tag{A.1}$$

where the boldfaced fonts represent vectors, upper-case letters represent random variables, and lower-case ones represent realizations of random variables. $\mathbf{M}$ is a vector of unknown parameters with dimension p and $\mathbf{d}^*$ is a vector or matrix of observed data. $f_{\mathbf{M}}(\mathbf{m})$ denotes the prior probability density function (pdf) of $\mathbf{M}$, which reflects our knowledge of model

parameters before observing $\mathbf{d}^*$, $f_{\mathbf{D}|\mathbf{M}}(\mathbf{d}^*|\mathbf{m})$ is the likelihood of observing $\mathbf{d}^*$ given model parameters, and $f_{\mathbf{M}|\mathbf{D}}(\mathbf{m}|\mathbf{d}^*)$ is the posterior pdf of $\mathbf{M}$ after the observations are taken into account. The major advantage of Bayesian parameter estimation is that it enables us to incorporate the prior knowledge about the model parameters into the learning process through the prior distributions.

Specifically, the parameters involved in this study are $\mathbf{m} = \{\beta, \theta_1^*, \theta_2^*\}$. The observations are $\mathbf{R} = \{R_i(\theta_i)\}$ with the subscript i being the i-th observation. The representative soil moisture values are taken as observed inputs.

A.1.1 Principle of Minimum Relative Entropy

The selection of prior distributions is critical in the Bayesian approach [*Scales and Snieder*, 1997] because the posterior distribution is dependent on the prior distribution as evident in Eq. (A.1). Instead of choosing arbitrary prior distributions, we adopted a systematic approach based on the principle of Minimum Relative Entropy (MRE) [*Hou and Rubin*, 2005; *Rubin*, 2003; *Woodbury and Rubin*, 2000; *Woodbury and Ulrych*, 1993], which states that of all the probabilities that satisfy the given constraints, such as average or higher-order moments, choose the one that has the highest entropy with respect to a known prior. Since entropy represents the amount of uncertainty associated with a probability distribution, the principle of MRE favors distribution that is the most uncommitted or the least subjective with respect to the constraints.

Assume $f_{\mathbf{M}}^0(\mathbf{m})$ is an initial estimate of the prior distribution $f_{\mathbf{M}}(\mathbf{m})$, the principle of

MRE obtains the optimal estimation of $f_{\mathbf{M}}(\mathbf{m})$ by minimizing its negative entropy with respect to the initial estimate subject to known constraints. Its mathematical form is

$$\min \int_{\mathbf{m}} f_{\mathbf{M}}(\mathbf{m}) \ln \left(\frac{f_{\mathbf{M}}(\mathbf{m})}{f_{\mathbf{M}}^{0}(\mathbf{m})} \right) d^{p}\mathbf{m} \tag{A.2}$$

The optimal solution, $f_{\mathbf{M}}^{*}(\mathbf{m})$, has to satisfy the following constraints,

$$\int_{\mathbf{m}} f_{\mathbf{M}}^{*}(\mathbf{m})\, r_i(\mathbf{m})\, d^{p}\mathbf{m} = \bar{r}_i, fori = 1, \cdots, N \tag{A.3}$$

$$\int_{\mathbf{m}} f_{\mathbf{M}}^{*}(\mathbf{m})\, d^{p}\mathbf{m} = 1 \tag{A.4}$$

where r_i is some known functional forms, such as the moments of the data, with $\bar{r}_i$ being the corresponding prior knowledge, and N is the number of constraints in addition to Eq. (A.4).

For the parameters engaged in the Feddes Model, only their physical bounds are known as *a priori*. Their prior distributions are therefore assigned as uniform between the lower and upper bounds.

A.1.2 Markov Chain Monte Carlo Method

Given the likelihood of data and the prior distributions of the parameters, the inference of the posterior distribution based on Eq. (A1) is often not tractable, mainly due to the

multidimensional integration in the denominator. Sampling or Monte Carlo method has been extensively used for exploring posterior distribution, one of which is the well-known importance sampling. However, importance sampling [*Geweke*, 1989] is of limited use in high-dimension case because it requires an importance sampling density that has a tail at least as heavy as the target distribution [*Tierney and Mira*, 1999]. Markov chain Monte Carlo (MCMC) method provides an effective alternative sampling strategy in a wide variety of problems [*Gelfand and Smith*, 1990; *Tierney and Mira*, 1999; *Andrieu et al.*, 2003; *Smith and Roberts*, 1993], and it has become a widespread tool for Bayesian inference.

The underlying rationale of the MCMC method is to construct a Markov chain in the parameter space that converges to a stationary distribution, which is the desired posterior distribution. The chain is constructed such that the next state is only dependent on the current state according to a transitional probability. There are two general algorithms for the MCMC method, Metropolis-Hastings algorithm based on the idea of proposal and rejection [*Metropolis et al.*, 1953; *Hastings*, 1970] and Gibbs sampler [*Gemand and Gemand*, 1984; *Gelfand and Smith*, 1990] by breaking the joint distribution into a series of conditional probabilities that are easier to sample. We adopted the latter algorithm because the full conditional probabilities can be specified for sampling. The samples generated from the joint posterior distribution allow direct assessment of uncertainty in predictions, using the parameters or any functions of the parameters.

A.1.3 Inference Using WinBUGS

In this study, the MCMC method was implemented using the software package WinBUGS [*Lunn et al.*, 2000]. The statistical inference using WinBUGS is based on prior distributions and a series of conditional probabilities as shown in the following:

$$
\begin{aligned}
R_i|\alpha_i,\beta &\sim \text{lognormal}\left(\alpha_i\beta,\sigma_R\right)\\
\alpha_i|\theta_i,\theta_1^*,\theta_2^* &= \max\left(1,\min\left(0,\frac{\theta_i-\theta_1^*}{\theta_2^*-\theta_1^*}\right)\right)\\
\theta_i|\theta_{\text{obs},i},\sigma_\theta &\sim \text{normal}\left(\theta_{\text{obs},i},\,\sigma_\theta\right)\\
\theta_1^*|\theta_2^* &\sim \text{uniform}\left(0,\,\theta_2^*\right)\\
\theta_2^* &\sim \text{uniform}\left(0,\,0.5\right)\\
\beta &\sim \text{uniform}\left(0.1,\,2.0\right)\\
\log\left(\sigma_R\right) &\sim \text{uniform}\left(\text{-}5.0,\,2.0\right)\\
\log\left(\sigma_\theta\right) &\sim \text{uniform}\left(-7.0,\,-1.0\right),
\end{aligned}
\tag{A.5}
$$

where R_i is assumed to be lognormally-distributed for its non-negative restriction, with mean $\alpha_i\beta$ and standard deviation σ_R. The uncertainty of R_i arises from the measurement errors in the variables involved in the calculation as well as the model uncertainty to estimate the potential ET. Representative soil moisture is modeled as a random variable for its errors in measurements, interpolation, and aggregation from point measurements to a representative value at the stand scale. The standard deviations of both R_i and θ_i are assigned

as hyper-parameters that are parameters of unknown parameters. The connection between θ_1^* and θ_2^* is due to the constraint that θ_1^* cannot exceed θ_2^*.

The uniform prior distributions, $f(\theta_2)$, $f(\theta_1|\theta_2)$, $f(\beta)$, $f(\sigma_\theta)$ and $f(\sigma_R)$ were selected based on the principle of MRE and their product constitutes the combined prior of model parameters and hyper-parameters. It is assumed in the inference that R_i's are independent given α_i and β, the likelihood is therefore $f_{\mathbf{D}|\mathbf{M}}(\mathbf{d}*|\mathbf{m}) \equiv f(\mathbf{R}|\theta, \theta_1^*, \theta_2^*, \beta, \sigma_R, \sigma_\theta) = \prod_{i=1}^{N} LN(\alpha_i\beta, \sigma_R)$.

Appendix B

Regression Relations used to Extend TDR Measurements in 2003-2005 at Tonzi Site

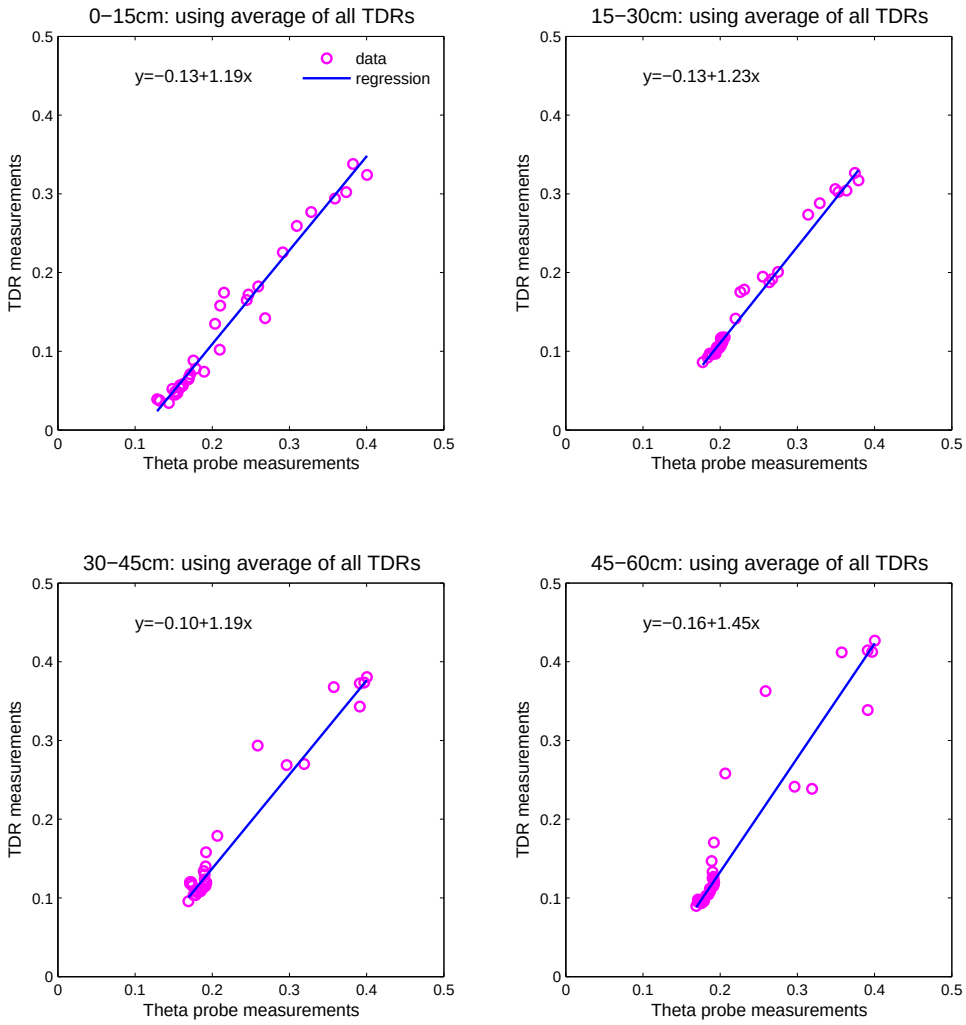

Figure B.1: Regression of average TDR measurements on the Theta probe measurements in 2003. Theta probe measurements are daily averages calculated from continuous data on half-hour basis. TDR measurements are averages calculated from all TDRs located in the site. The regression equations are shown along with the regression lines.

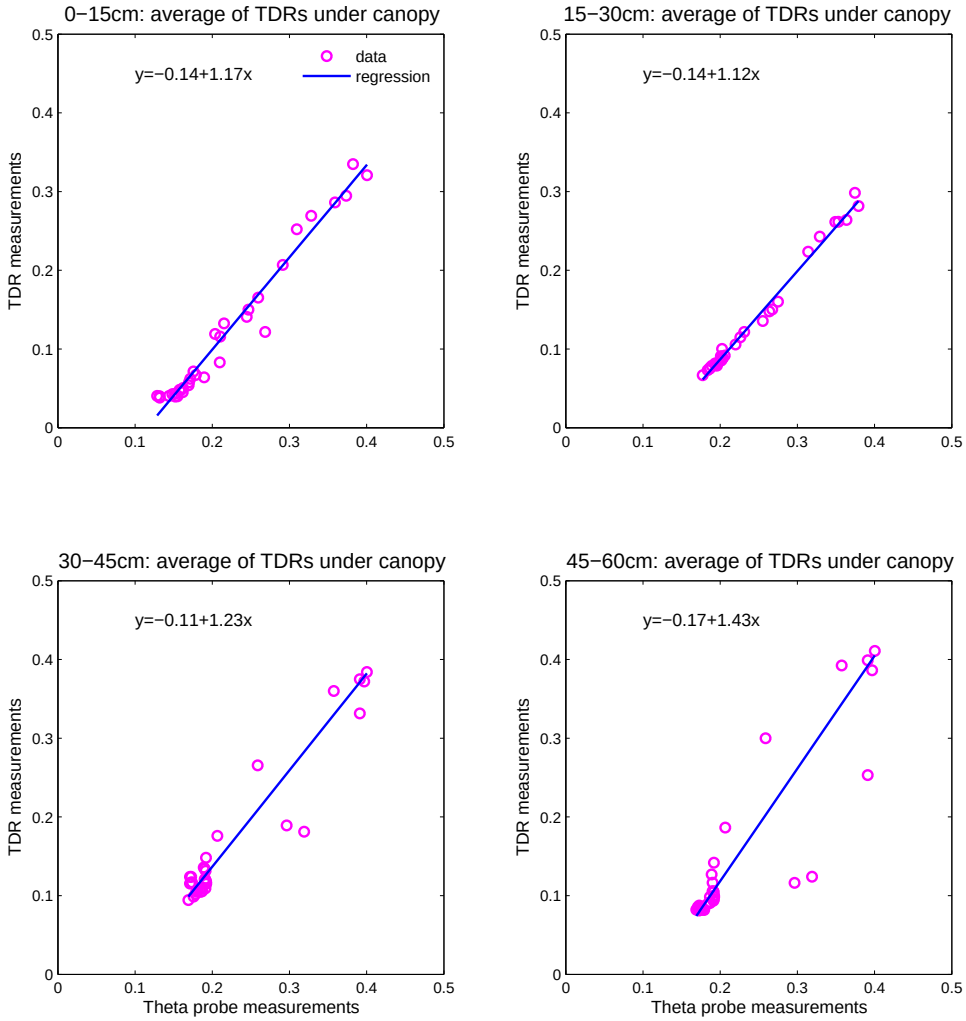

Figure B.2: Regression of TDR measurements under tree canopies on the Theta probe measurements in 2003. Theta probe measurements are daily averages calculated from continuous data on half-hour basis. TDR measurements are averages calculated from TDRs located under tree canopies. The regression equations are shown along with the regression lines.

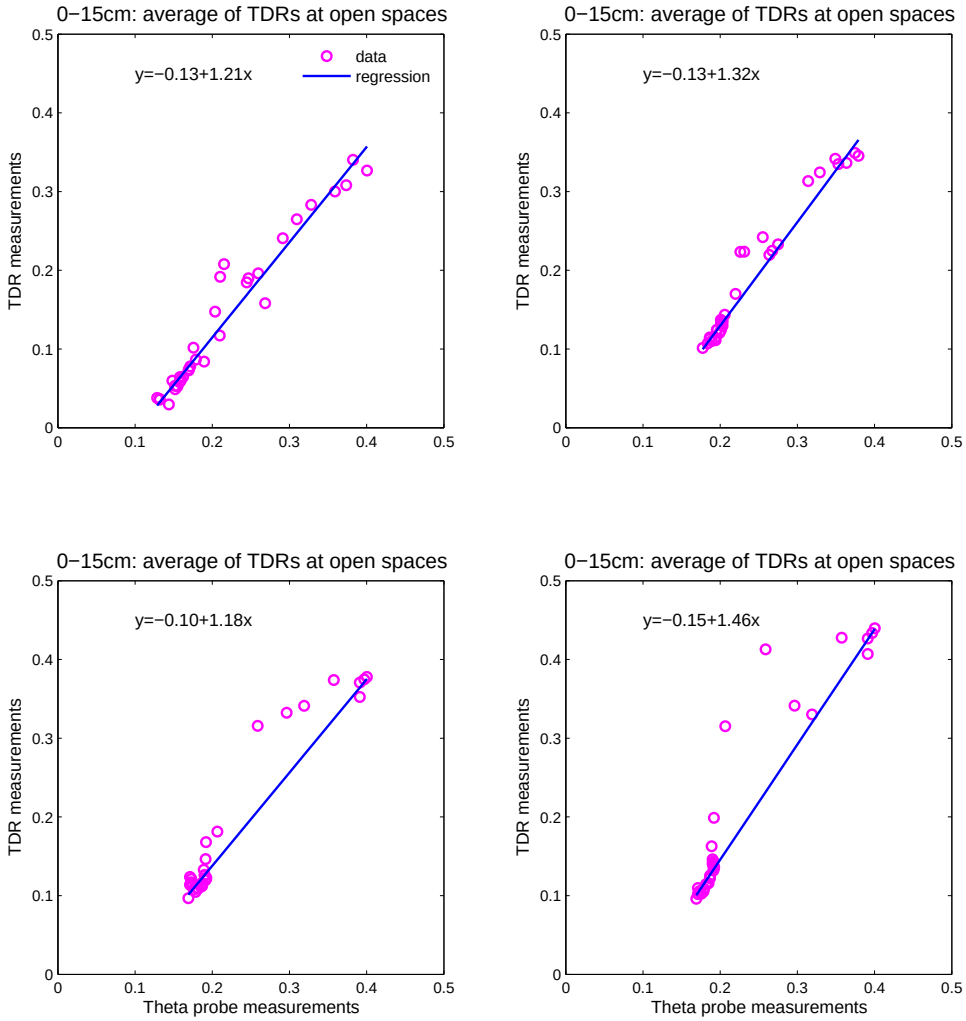

Figure B.3: Regression of TDR measurements in open spaces on the Theta probe measurements in 2003. Theta probe measurements are daily averages calculated from continuous data on half-hour basis. TDR measurements are averages calculated from TDRs located in the open spaces (not covered by tree canopy). The regression equations are shown along with the regression lines.

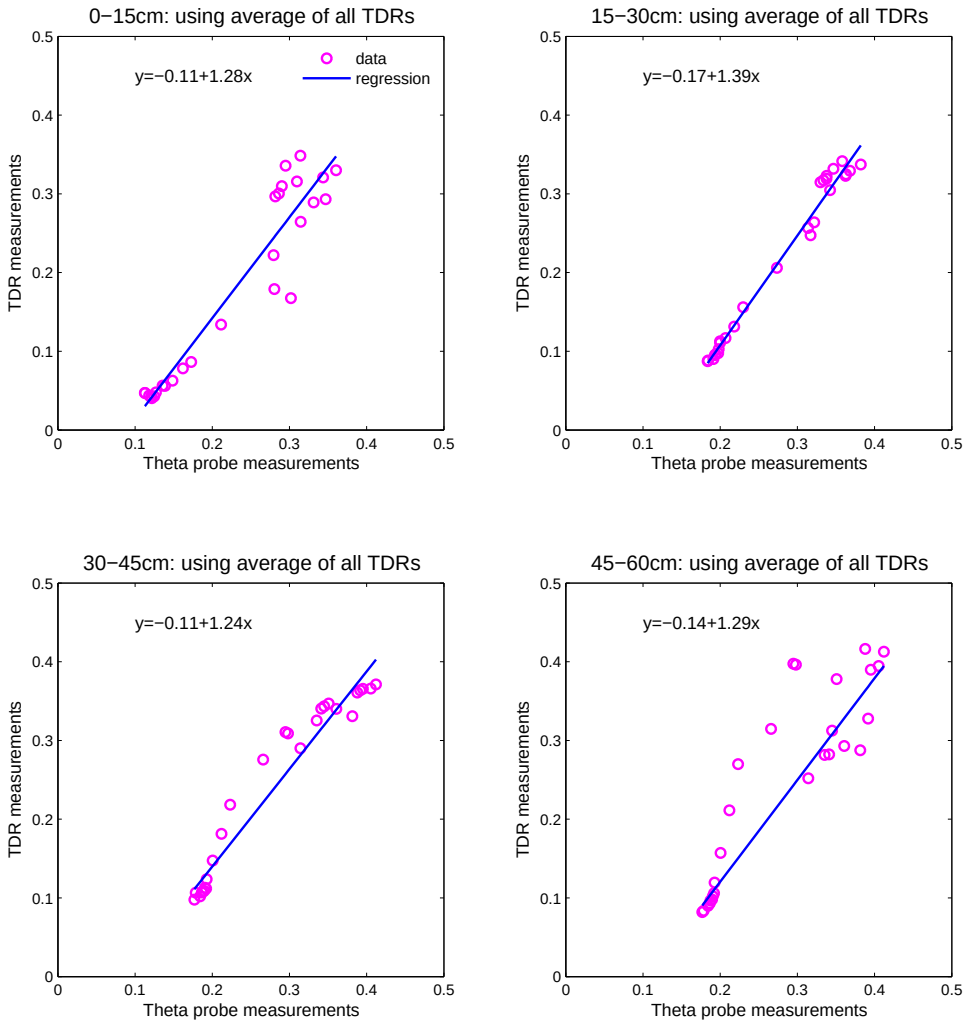

Figure B.4: Regression of average TDR measurements on the Theta probe measurements in 2004. Theta probe measurements are daily averages calculated from continuous data on half-hour basis. TDR measurements are averages calculated from all TDRs located in the site. The regression equations are shown along with the regression lines.

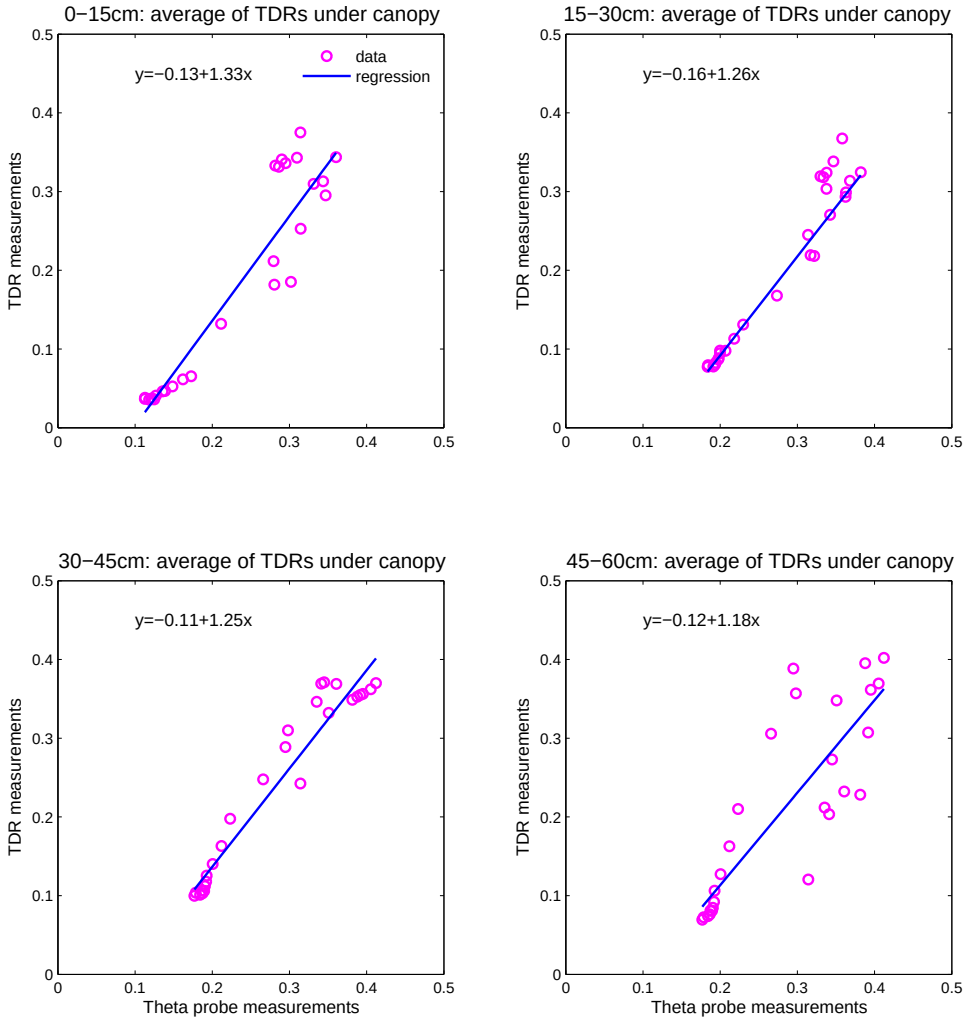

Figure B.5: Regression of TDR measurements under tree canopies on the Theta probe measurements in 2004. Theta probe measurements are daily averages calculated from continuous data on half-hour basis. TDR measurements are averages calculated from TDRs located under tree canopies. The regression equations are shown along with the regression lines.

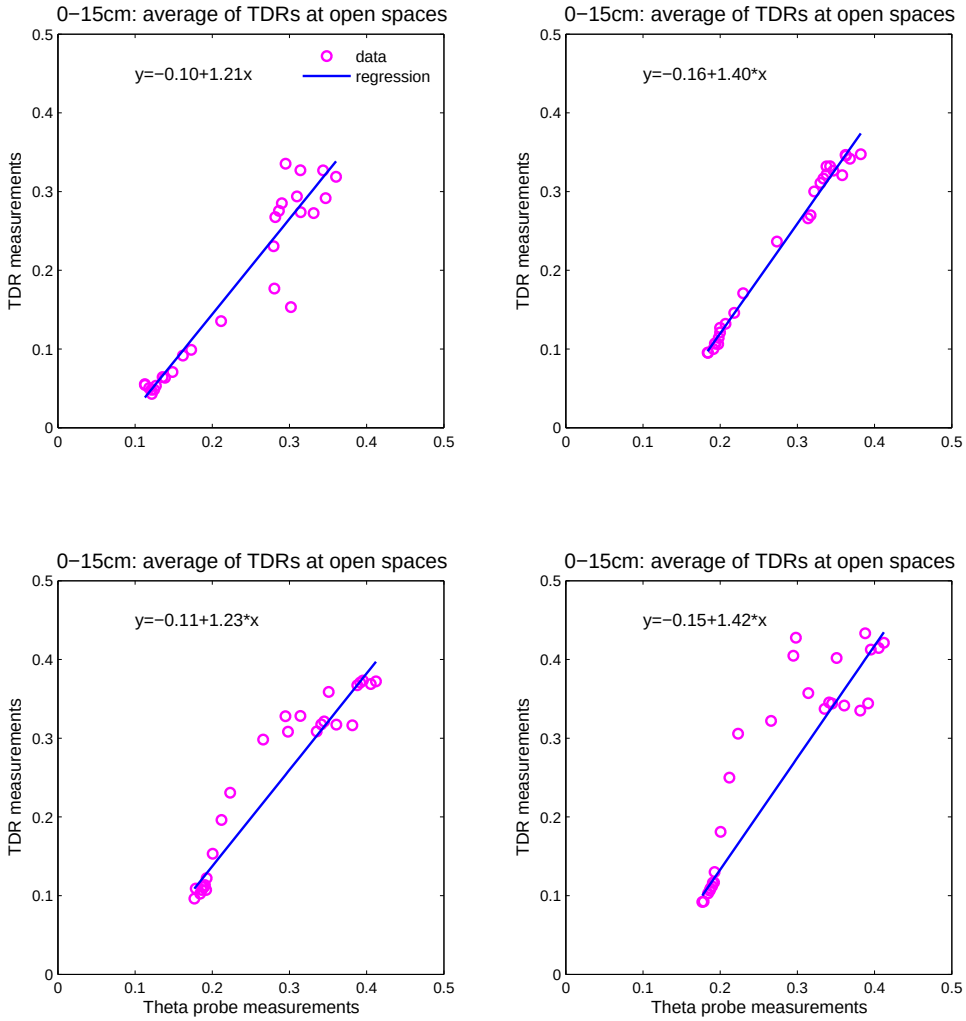

Figure B.6: Regression of TDR measurements in open spaces on the Theta probe measurements in 2004. Theta probe measurements are daily averages calculated from continuous data on half-hour basis. TDR measurements are averages calculated from TDRs located in the open spaces (not covered by tree canopy). The regression equations are shown along with the regression lines.

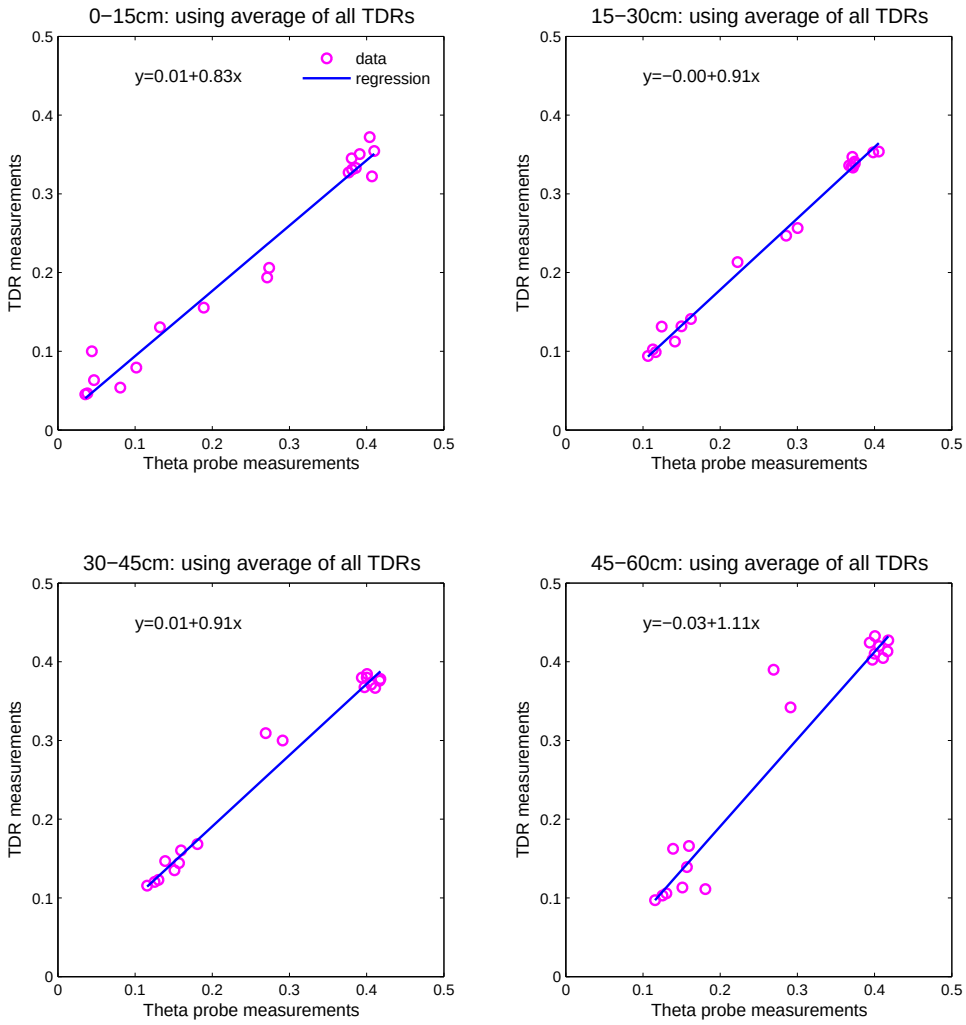

Figure B.7: Regression of average TDR measurements on the Theta probe measurements in 2005. Theta probe measurements are daily averages calculated from continuous data on half-hour basis. TDR measurements are averages calculated from all TDRs located in the site. The regression equations are shown along with the regression lines.

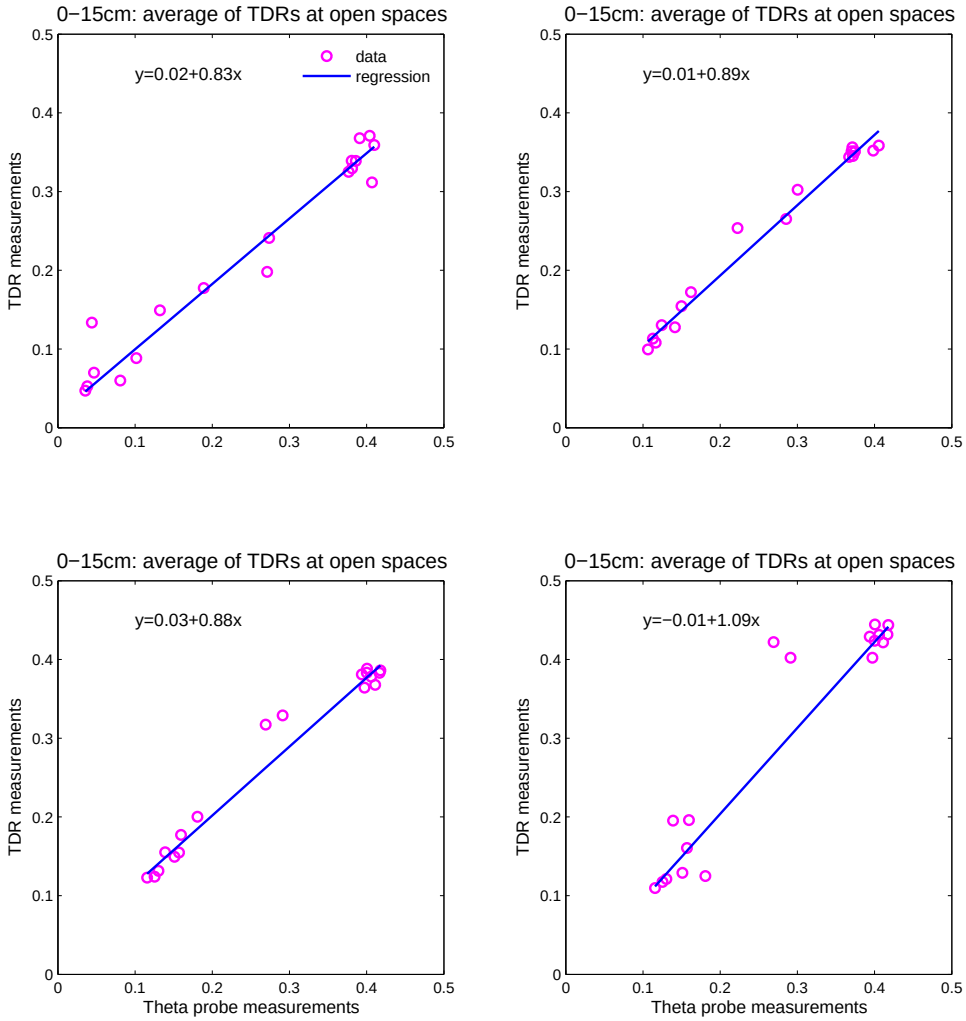

Figure B.8: Regression of TDR measurements in open spaces on the Theta probe measurements in 2005. Theta probe measurements are daily averages calculated from continuous data on half-hour basis. TDR measurements are averages calculated from TDRs located in the open spaces (not covered by tree canopy). The regression equations are shown along with the regression lines.

Appendix C

Data Logger Program for Data Collection

```
;{CR10X}
; data logger program modified from Josh Fisher's code
; for Cluster 1
;AM16/32 is running in 2*32 mode

; Take the measurements every half an hour
*Table 1 Program
  01: 1800    Execution Interval (seconds)

; Check the battery voltage
1:  Batt Voltage (P10)
 1: 1        Loc [ Batt_Volt ]

; Check the circuit everyday
2:  If time is (P92)
 1: 0        Minutes (Seconds --) into a
 2: 1440     Interval (same units as above)
 3: 30       Then Do

     3:  Signature (P19)
      1: 2        Loc [ Prog_Sig  ]
```

```
4:  End (P95)

; Check the panel temp

6:  Temp (107) (P11)
 1: 1        Reps
 2: 12       SE Channel
 3: 3        Excite all reps w/E3
 4: 3        Loc [ PTemp_C   ]
 5: 1.0      Mult
 6: 0.0      Offset

; Turn on the multiplexor
7:  Do (P86)
 1: 41       Set Port 1 High

; Take initial temperatures from the thermocouples
; including sap flow sensors and soil temperature
8:  Beginning of Loop (P87)
 1: 0        Delay
 2: 16       Loop Count

; Clock through the multiplexor
     9:  Do (P86)
      1: 72       Pulse Port 2

; Delay to give enough responding time
    10:  Excitation with Delay (P22)
      1: 1        Ex Channel
      2: 0        Delay W/Ex (units = 0.01 sec)
      3: 1        Delay After Ex (units = 0.01 sec)
      4: 0        mV Excitation

; Each measurement is repeated 10 times
     11:  Beginning of Loop (P87)
      1: 0        Delay
      2: 10       Loop Count

          12:  Thermocouple Temp (DIFF) (P14)
           1: 1        Reps
           2: 1        2.5 mV Slow Range
```

```
           3: 1        DIFF Channel
           4: 1        Type T (Copper-Constantan)
           5: 3        Ref Temp (Deg. C) Loc [ PTemp_C   ]
           6: 65    -- Loc [ tempiT_1  ]
           7: 1        Mult
           8: 0        Offset

     13:  End (P95)

; Average 10 TC measurements!
     14:  Spatial Average (P51)
      1: 10       Swath
      2: 65       First Loc [ tempiT_1  ]
      3: 44    -- Avg Loc [ ainitT_1  ]
15:  End (P95)

; skip the empty channels
16:  Beginning of Loop (P87)
 1: 0        Delay
 2: 4        Loop Count

     17:  Do (P86)
      1: 72       Pulse Port 2

     18:  Excitation with Delay (P22)
      1: 1        Ex Channel
      2: 0        Delay W/Ex (units = 0.01 sec)
      3: 1        Delay After Ex (units = 0.01 sec)
      4: 0        mV Excitation

19:  End (P95)

; take soil moisture measurements
     20:  Beginning of Loop (P87)
      1: 0        Delay
      2: 5        Loop Count

; clock the multiplexor!
          21:  Do (P86)
           1: 72       Pulse Port 2

; Delay
```

```
          22:  Excitation with Delay (P22)
           1: 1        Ex Channel
           2: 0        Delay W/Ex (units = 0.01 sec)
           3: 1        Delay After Ex (units = 0.01 sec)
           4: 0        mV Excitation

; Measure every EC-5 probe 10 times
          23:  Beginning of Loop (P87)
           1: 0        Delay
           2: 10       Loop Count

               24:  Ex-Del-Diff (P8)
                1: 1        Reps
                2: 5        2500 mV Slow Range
                3: 1        DIFF Channel
                4: 1        Excite all reps w/Exchan 1
                5: 1        Delay (units 0.01 sec)
                6: 2500     mV Excitation
                7: 65    -- Loc [ tempiT_1  ]
                8: 1.0      Mult
                9: 0.0      Offset

          25:  End (P95)

; Average the 10 soil moisture measurements!
          26:  Spatial Average (P51)
           1: 10       Swath
           2: 65       First Loc [ tempiT_1  ]
           3: 101   -- Avg Loc [ VWC_1     ]

     27:  End (P95)

; Turn off the multiplexor!
     28:  Do (P86)
      1: 51       Set Port 1 Low

; Reset the HRdivisor to 0
5:  Z=X*F (P37)
 1: 77       X Loc [ HRdivisor ]
 2: 0        F
 3: 77       Z Loc [ HRdivisor ]
```

```
;Turn on the heater and last for 6 seconds
     29:  Do (P86)
      1: 43       Set Port 3 High

     30:  Excitation with Delay (P22)
      1: 1        Ex Channel
      2: 0        Delay W/Ex (units = 0.01 sec)
      3: 600      Delay After Ex (units = 0.01 sec)
      4: 0        mV Excitation

     31:  Do (P86)
      1: 53       Set Port 3 Low

; Set a timer
     32:  Timer (P26)
      1: 0000     Reset Timer

; Measure the temperatures between 60-100s following the heat pulse
     33:  Beginning of Loop (P87)
      1: 0        Delay
      2: 0        Loop Count

          34:  Timer (P26)
           1: 76       Loc [ timer     ]

; Start the loop when t>60s
          35:  IF (X<=>F) (P89)
           1: 76       X Loc [ timer     ]
           2: 3        >=
           3: 60       F
           4: 30       Then Do

; Exit the loop at 100s following the heat pulse
               36:  IF (X<=>F) (P89)
                1: 76       X Loc [ timer     ]
                2: 3        >=
                3: 100      F
                4: 31       Exit Loop if True

;Turn on the multiplexor
               37:  Do (P86)
                1: 41       Set Port 1 High
```

```
;Measure the temperatures from TCs with sap flow sensors
               38:  Beginning of Loop (P87)
                1: 0        Delay
                2: 8        Loop Count

                    39:  Do (P86)
                     1: 72       Pulse Port 2

                    40:  Excitation with Delay (P22)
                     1: 1        Ex Channel
                     2: 0        Delay W/Ex (units = 0.01 sec)
                     3: 1        Delay After Ex (units = 0.01 sec)
                     4: 0        mV Excitation

                    41:  Thermocouple Temp (DIFF) (P14)
                     1: 1        Reps
                     2: 1        2.5 mV Slow Range
                     3: 1        DIFF Channel
                     4: 1        Type T (Copper-Constantan)
                     5: 3        Ref Temp Loc [ PTemp_C   ]
                     6: 24    -- Loc [ postT_1   ]
                     7: 1.0      Mult
                     8: 0.0      Offset

               42:  End (P95)

; Record how many times temperatures are measured on each TC during 60-100s
               43:  Z=Z+1 (P32)
                1: 77       Z Loc [ HRdivisor ]

          44:  End (P95)

; Turn off Multiplexor
          45:  Do (P86)
           1: 51       Set Port 1 Low

     46:  End (P95)

; Output data

     47:  Do (P86)
```

```
      1: 10       Set Output Flag High (Flag 0)

          48:  Set Active Storage Area (P80)^30133
           1: 1        Final Storage Area 1
           2: 100      Array ID

; Time when outputting data
          49:  Real Time (P77)^26495
           1: 1221     Year,Day,Hour/Minute,Seconds (midnight = 2400)

; Battery voltage
          50:  Average (P71)^15633
           1: 1        Reps
           2: 1        Loc [ Batt_Volt ]

; Panel Temp
          51:  Average (P71)^19815
           1: 1        Reps
           2: 3        Loc [ PTemp_C   ]

; Average initial temperature
          52:  Average (P71)^24723
           1: 16       Reps
           2: 44       Loc [ ainitT_1  ]

; Average temperature following heat pulse
          53:  Average (P71)^7966
           1: 8        Reps
           2: 24       Loc [ postT_1   ]

; Soil moisture data
          54:  Sample (P70)
           1: 5        Reps
           2: 101      Loc [ VWC_1     ]

*Table 2 Program
  01: 0.0000    Execution Interval (seconds)

*Table 3 Subroutines

End Program
```

Appendix D

Sapwood Moisture Relations of Sap Flow Measurements

The impact of sapwood moisture content on sap flow measurements are reflected by its influence on thermal diffusivity of fresh wood matrix and the conversion factor from heat pulse velocity to sap velocity. This investigation is based on the previous work by *Burgess et al.* [2001] and *Simpson and TenWolde* [1999]. The citations are not repeated in the discussion hereafter. Some definitions of concepts that are related to this discussion are listed in Table D.1.

Maximum moisture content can be calculated from specific gravity as

$$M_{max} = \frac{1}{G_b} - \frac{1}{1.54} \tag{D.1}$$

where 1.54 is the specific gravity of wood cell walls. Typical values of G_b in oaks are around 0.7. Therefore, the corresponding M_{max} is around 0.78.

Table D.1: Definitions of some concepts related to wood moisture content

Concepts	Symbol	Definition
green wood		wood in which cell walls are completely saturated with water
specific gravity	G_b	$\frac{\text{ovendry weight of wood/green volume of wood}}{\text{Density of water}}$
moisture content	M	$\frac{\text{weight of fresh wood - ovendry weight of wood}}{\text{ovendry weight of wood}}$
fiber saturation point		moisture content at which only the cell walls are completely saturated while no water exists in cell lumens

D.1 Moisture Dependence of Thermal Diffusivity

The thermal diffusivity is defined as the ratio of thermal diffusivity to the product of specific heat capacity and density as the following:

$$\kappa = \frac{K_{gw}}{\rho_{gw} c_{gw}} \tag{D.2}$$

where K_{gw}, ρ_{gw} and c_{gw} are thermal conductivity, density, and specific heat of green wood, respectively. Therefore, the effect of wood moisture content on wood thermal diffusivity is based on its effect on K_{gw}, ρ_{gw} and c_{gw}. The properties of green wood and ovendry wood are distinguished with subscripts gw and dw, respectively.

Density of green wood can be calculated as

$$\rho_{gw} = G_b(1+M) \tag{D.3}$$

where the unit of ρ_{gw} is g/cm^3 and the density of sap water is assumed same as that of pure water.

The heat capacity of green wood is the combination of the heat capacity of dry wood and sap water. Heat capacity of dry wood is temperature-dependent as

$$c_{dw} = 0.1031 + 0.003867T \tag{D.4}$$

where T is wood temperature in kelvin.

For moisture content above fiber saturation point, heat capacity of green wood can be calculated from

$$c_{gw} = \frac{c_{dw} + Mc_s}{1+M}. \tag{D.5}$$

Moreover, when the moisture content falls below the fiber saturation point, there is an additional term to account for extra energy in the wood-water bond, and Eq.(D.5) becomes

$$c_{gw} = \frac{c_{dw} + Mc_s}{1+M} + M(-6.191 + 0.0236T - 1.33M). \tag{D.6}$$

In Eqs.(D.5) and (D.6), heat capacity of sap is taken as 4.182 J/(g.^{o}K).

K_{gw} is calculated from the following equations:

$$K_{gw} = K_s M G_b + K_{dw}(1 - MG_b) \tag{D.7}$$

$$K_{dw} = 0.04182(21 - 20F_v) \tag{D.8}$$

where F_v is the void fraction of wood defined as $F_v = 1 - G_b(0.6494 + M)$, and heat conductivity of sap water is selected as K_s=0.5984 W/(m.^{o}K).

D.2 Moisture Dependence of Conversion from Heat Pulse Velocity to Sap Flux Density

The conversion from heat pulse velocity to sap flux density is given as

$$J_s = \frac{\rho_{gw} c_{gw}}{\rho_s c_s} v_h = F v_h. \tag{D.9}$$

For moisture contents above the fiber saturation point, the conversion factor F can be rewritten by substituting Eqs. (D.5) and (D.3) into ρ_{gw} and c_{gw}, and the following equation is resulted:

$$F = \frac{G_b(c_{dw} + M c_s)}{c_s} \tag{D.10}$$

where the dependence of F on M is linear.

D.3 An Example

For the blue oaks at our experimental site, we assume that the wood moisture content may vary between 0.6 to 0.25, then the dependence of thermal diffusivity of green wood and conversion factor F on wood moisture content is provided in Figure D.1 for three values of G_b : 0.6, 0.7 or 0.8. This example demonstrates that thermal diffusivity of green wood increases with the specific gravity while it decreases with wood moisture content. Furthermore, the dependence is nonlinear. On the other hand, the conversion factor from heat pulse velocity to sap flux density linearly increases with both wood moisture content and wood specific gravity.

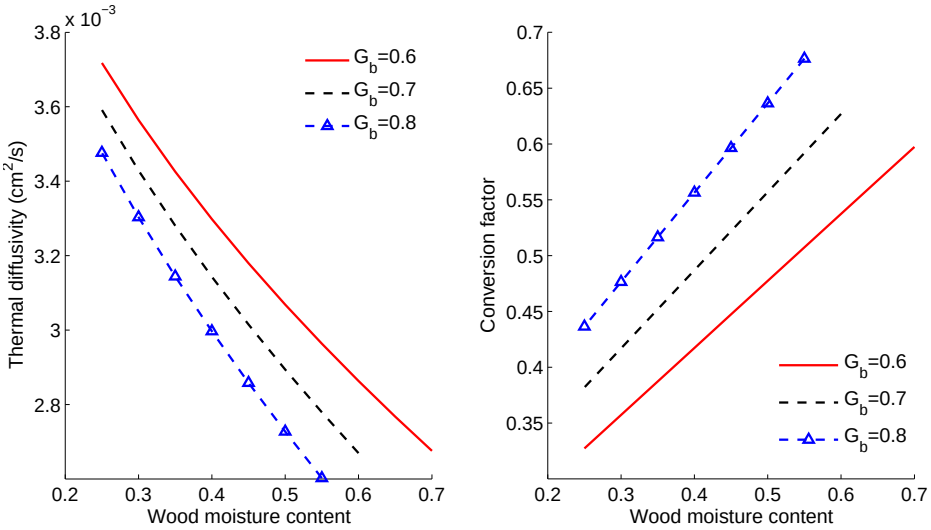

Figure D.1: Dependence of wood thermal diffusivity and conversion factor on wood moisture content

Appendix E

Alternating Conditional Expectation Algorithm

The alternating conditional expectation (ACE) algorithm was introduced by *Breiman and Friedman* [1985] to identify the optimal transformations of dependent and independent variables in multiple regression that produce the maximum linear correlation between the transformed dependent and independent variables. Such optimal transformations can be derived by minimizing the unexplained variance of a linear relationship between the transformed dependent variable and the sum of transformed independent variables.

Consider a given set of dependent variable Y and independent variables $X_1, ..., X_n$, the general form of regression equation in ACE algorithm is

$$\phi_0(Y) = \sum_{i=1}^{p} \phi_i(X_i) + \varepsilon \tag{E.1}$$

where ϕ_0 and ϕ_i represent transformations of the dependent and independent variables, respectively, and p is the dimension of the independent variables. The ACE algorithm starts with arbitrary transformations with zero mean and unit variance. The unexplained variance by the regression is defined as

$$\varepsilon^2(\phi_0, \phi_1, ..., \phi_p) = E\left[\phi_0(Y) - \sum_{i=1}^{p} \phi_i(X_i)\right]^2 \tag{E.2}$$

subject to the constraint $E[\phi_0(Y)] = 1$. The minimization of ε^2 with respect to $\phi_0(Y)$ and $\phi_i(X_i)$ is accomplished through a series of single-function minimizations, which result in the following equations:

$$\phi_i(X_i) = E\left[\phi_0(Y) - \sum_{j \neq i} \phi_j(X_j) \mid X_i\right] \tag{E.3}$$

$$\phi_0(Y) = \frac{E\left[\sum_{i=1}^{p} \phi_i(X_i) \mid Y\right]}{\| E\left[\sum_{i=1}^{p} \phi_i(X_i) \mid Y\right] \|} \tag{E.4}$$

The equations E.3 and E.4 represent two fundamental steps involved in the ACE algorithm: conditional expectations and iterative minimization, and therefore, the name alternating conditional expectation. The optimal transformations are obtained after the minimization operations, and the transformed dependent and independent variables are related as follows:

$$\phi_0^*(Y) = \sum_{i=1}^{p} \phi_i^*(X_i) + \varepsilon^* \tag{E.5}$$

where the minimum regression error, ε^*, is related to the maximum correlation coefficient, ρ^*, by $\varepsilon^{*2} = 1 - \rho^{*2}$.

The optimal ACE transformations are derived on the basis of the given data and do not require *a priori* assumptions of the functional forms of the dependent and independent variables. The ACE algorithm can be used to identify the nonlinearity in the original data and thus provides a powerful tool for exploratory data analysis.